COGEAR

MODULE 3:

Array - measurements in the area of Visp and St. Niklaus

Del. No.: 3.1.2

Authors: Burjanek, J., Gassner-Stamm, G., and Fäh, D.

Swiss Seismological Service

SED/COGEAR/R/003/20100226
February 26, 2010

Array - measurements in the area of Visp and St. Niklaus

Jan Burjánek, Gabriela Gassner-Stamm, Donat Fäh

1. Introduction

In the surrounding area of Visp, a total of ten arrays were measured (Figure 1). In the area of St. Niklaus and Grächen, a total of 7 arrays (one of them linear) were measured (Figure 2), most of them were set up on the slope between St. Niklaus and Grächen. All arrays were conducted with Quanterra Q330 dataloggers and three-component velocity sensors (Lennartz, LE3D-5s).

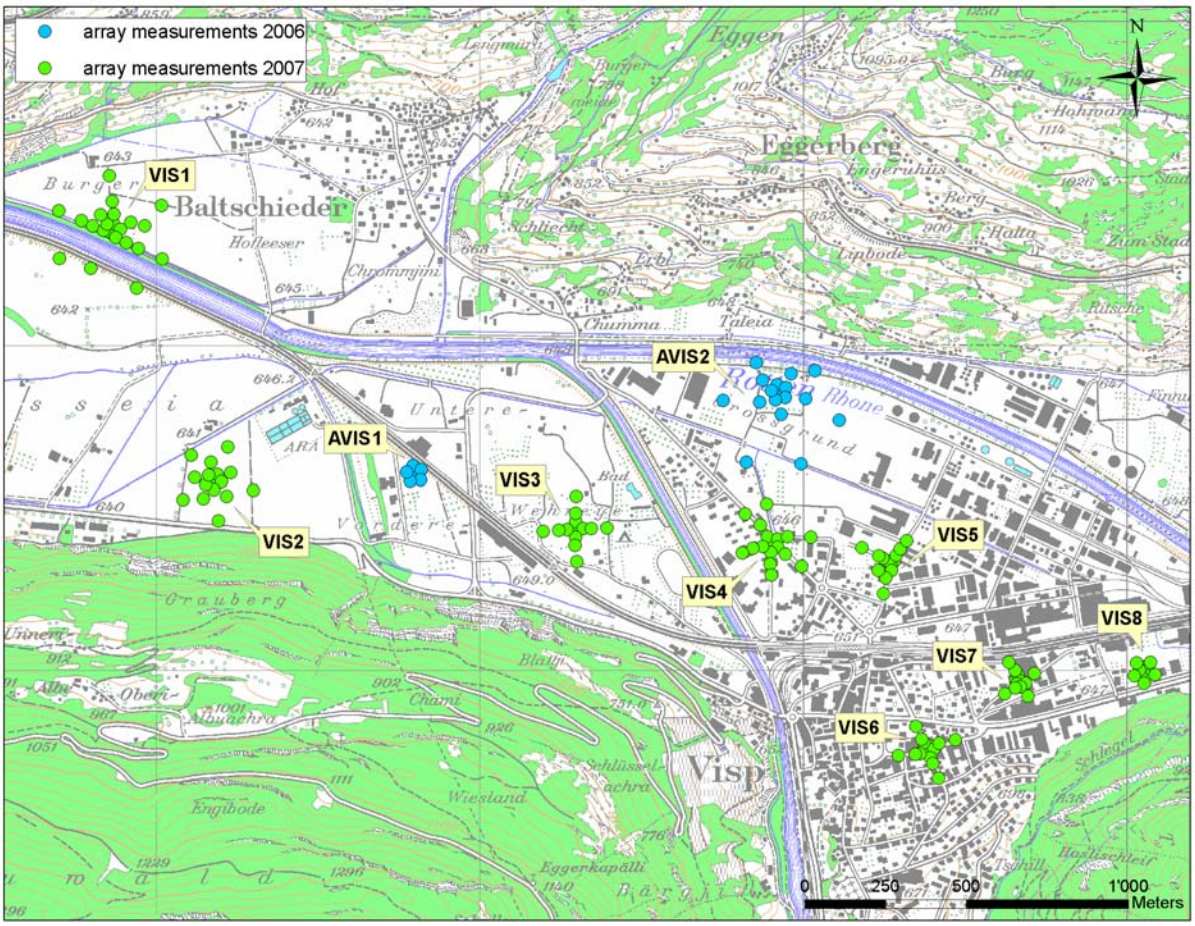

Figure 1: *Overview on the array-measurements done in the area of Visp.*

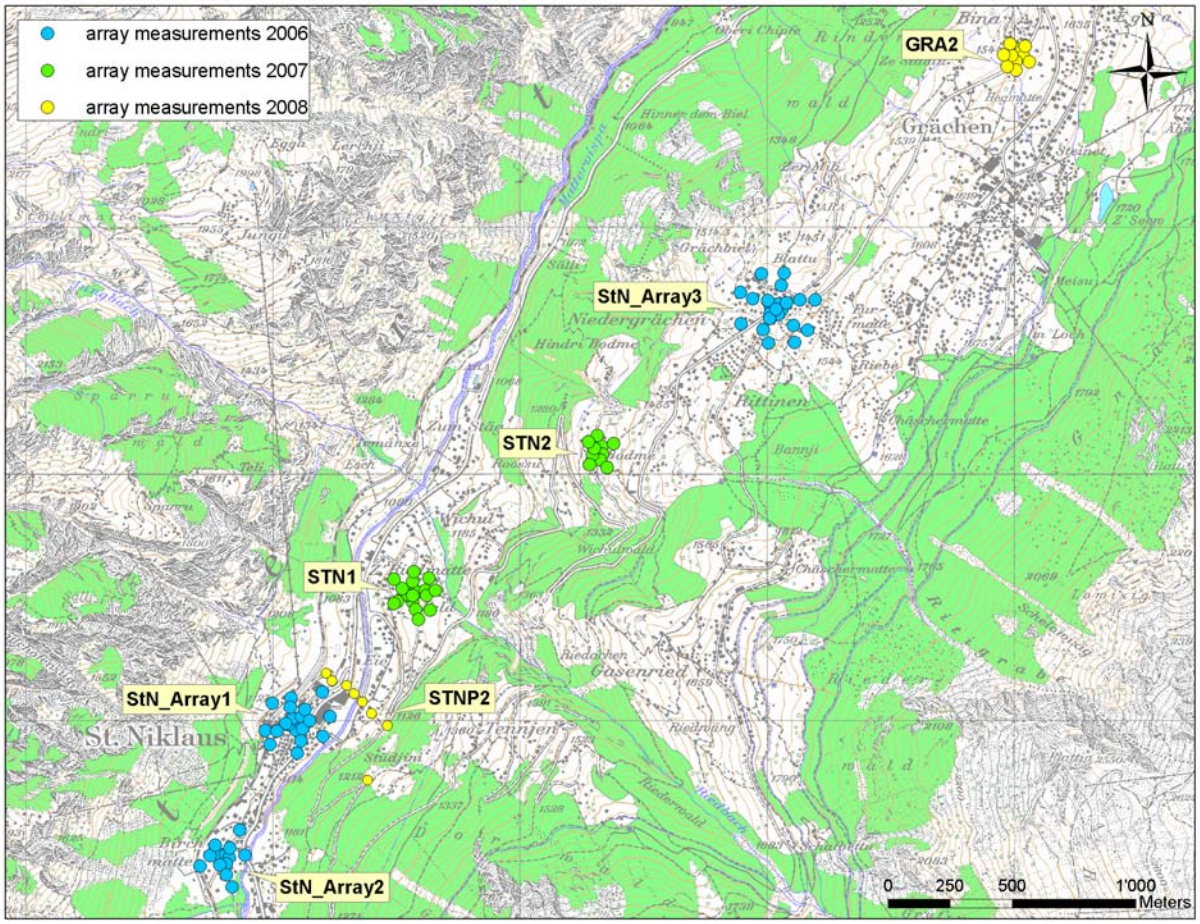

Figure 2: *Overview on the array-measurements done in St. Niklaus and on the slope up to Grächen.*

2. Methods to analyse ambient vibration data

Different methods and algorithms were tested and compared.

Array-processing with f-k method

The first array method we used is based on the high-resolution beam-forming (HRBF). It was originally proposed by Capon (1969) but developed and applied to vertical recordings of ambient vibrations by Kind et al. (2005). We have extended this method to analyse also the horizontal components (Fäh et al., 2008).
Ambient noise consists mostly of surface-waves, and surface-waves are behaving dispersive. This means that wave-packages with different frequency content are propagating with different velocities.
In general, subarrays with different apertures are set up for the measurement to optimise the resolution in a certain frequency band. Small apertures are used to resolve the shallow part of a structure, and by increasing the aperture, deeper and deeper structures can be investigated. The final dispersion curve over a wide frequency-range is then composed of the parts obtained by the different subarrays. The limits of each subarray are given by the aliasing at high frequencies and the loss of resolution at low frequencies.

Array-processing with SPAC method

In a second step the SPAC method was applied. The Spatial Autocorrelation method is another class of array processing techniques of ambient noise vibrations introduced by Aki (1957). Where both HRBF and SPAC methods have been applied successfully to the same data, SPAC methods have been found to yield higher resolution at lower frequencies (Asten, 2006, and references therein). Thus it gives a possibility to increase a bandwidth of the dispersion curves. We use a modified SPAC method for non-circular arrays (Bettig et al., 2001) implemented within GEOPSY software package by Wathelet et al. (2005). Pairs of stations in the array are grouped along rings of finite thickness (the choice of the rings is upon the user). The spatial autocorrelation function is then evaluated for each ring and transformed to the frequency-velocity domain. So called dispersion density is then generated by stacking SPAC functions in frequency-velocity domain. High density regions should then correspond to dispersion curves.

Rayleigh wave ellipticity estimation with f-k method

Ellipticity of Rayleigh waves was shown to be useful additional constrain for the inversion of dispersion curves (Fäh et al., 2003). The estimate of ellipticity by f-k method (array method) was introduced by Poggi and Fäh (2010). It is based on the assumption that a peak in the f-k cross-spectrum obtained from horizontal (radial-polarized) and vertical components of motion must be representative of the signal power of a particular Rayleigh wave mode. Thus the relative frequency-dependent surface displacement ratio can be calculated for each mode separately, once the mode-correspondent dispersion curve is identified on the f-k plane.

Ellipticity estimation with wavelet-based method

In the wavelet-based method of ellipticity estimation, the time-frequency representations of the vertical and both horizontal components are computed using continuous wavelet transform (CWT). In contrast to Love waves, Rayleigh waves will have an energy maximum on the vertical component. Therefore, to extract mostly Rayleigh waves, the absolute value of the CWT for the vertical component is scanned for all maxima. For each maximum identified on the time axis, the value of horizontal component wavelet coefficient is picked with a delay of one quarter of period. That is the theoretical delay between vertical and horizontal components for a Rayleigh wave. It can be positive (prograde particle motion) or negative (retrograde particle motion). The ratio between horizontal and vertical values is saved for each maximum found on the vertical component. Ratios are analyzed statistically, and the whole process is repeated for all frequencies, so the ellipticity of fundamental Rayleigh wave is estimated. We apply a method that was developed during the European project NERIES (Network of Research Infrastructures for European Seismology) joint research activity JRA4.

Inversion

For the inversion we used “dinver”, implemented within the GEOPSY software package from Wathelet et al. (2005) (http://www.geopsy.org). Dinver is using the Conditional Neighbourhood Algorithm or Monte Carlo technique for solving inversion problems (Wathelet, 2008).

3. Measurements and Results

3.1 Site AVIS1

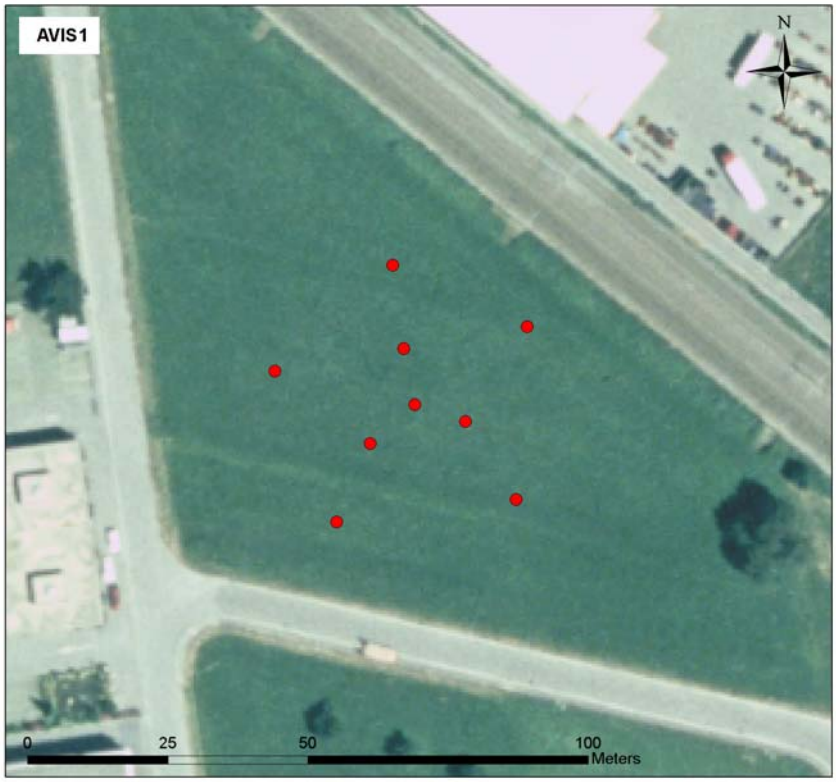

AVIS1 has a maximal diameter of 50 m and consists of 9 stations, all set up simultaneously. It was located on grassland near the SED Strong Motion Station SVIP (Visp-Pomona).

Figure 3.1.1: *Sensor setup for array "AVIS1" in Visp.*

Array processing

Recordings of vertical components were processed by several different high-resolution FK methods and SPAC method. Although the aperture of the array was quite small (50m), it was possible to follow the dispersion curve of the fundamental mode of Rayleigh wave down to 2Hz with both SPAC and FK method (Figure 3.1.2 and Figure 3.1.3). This is far behind the resolution limits defined for FK analysis from the theoretical array response. The spatial correlation ratios (shortly SPAC curves) are depicted in Figure 3.1.4. Note the SPAC curves follow the shape of Bessel functions very well in this case. The dispersion curves obtained with SPAC and FK are in good agreement. As SPAC is assumed to have higher resolution in low frequency range, we prefer the dispersion curve picked from SPAC (bold dashed line in Figures 3.1.2 and 3.1.3).

It was also possible to pick possible higher modes (see Figure 3.1.2). However, an assignment of particular mode number to these modes is very uncertain. This is discussed further in the following section related to inversion.

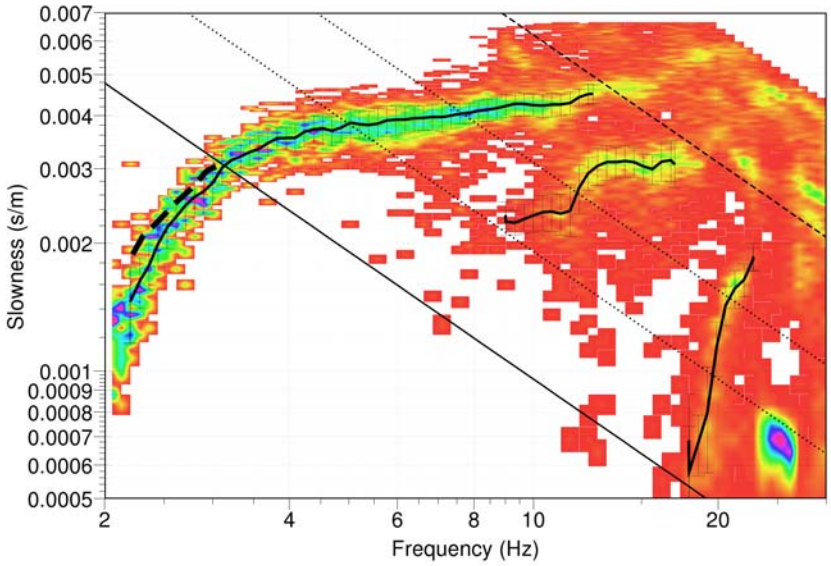

Figure 3.1.2: *Result of array processing using GEOPSY, vertical component: Rayleigh dispersion curve obtained by SPAC method (bold dashed lines), dispersion curves picked from FK plane (solid bold lines), frequency of occurrence of picked peaks in FK plane (colorful background), resolution limits calculated from array response (kmin/2 – solid, kmin & kmax/2 – dotted, kmax - dashed thin lines).*

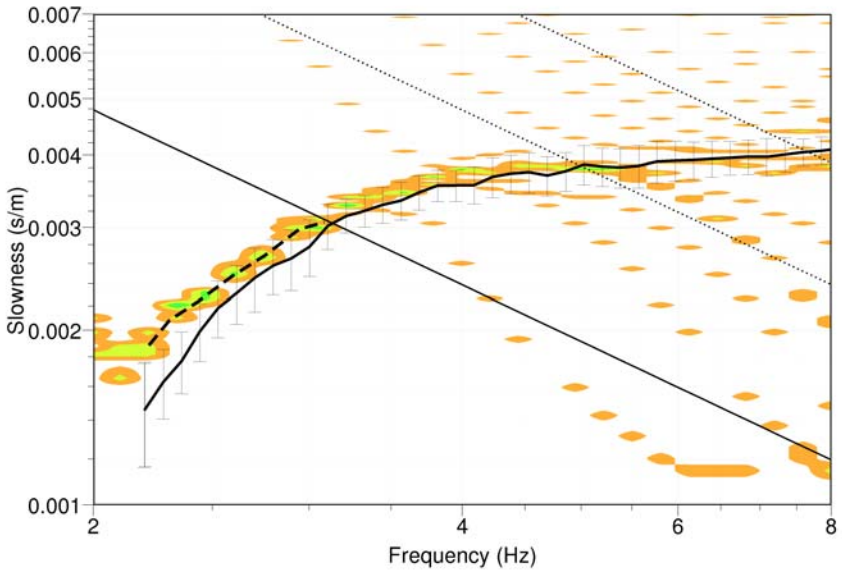

Figure 3.1.3: *Result of SPAC method, vertical component: dispersion curve picked from stacked SPAC curves (bold dashed line), dispersion curve picked from FK plane (solid bold lines, see Figure 3.1.2), resolution limits calculated from array response (kmin/2 – solid, kmin & kmax/2 – dotted thin lines).*

Recordings of horizontal components were processed by high-resolution and classical FK methods, all giving consistent dispersion curve of Love fundamental mode. All picked dispersion curves for both Love and Rayleigh waves are plotted in Figure 3.1.5. Note the remarkable agreement between different codes and methods.
Ellipticity of Rayleigh waves was estimated for each station of the array using wavelet-based method. All ellipticity curves are depicted in Figure 3.1.6. Ellipticity curves are in good agreement across the array in the frequency range of 0.8 - 4 Hz.

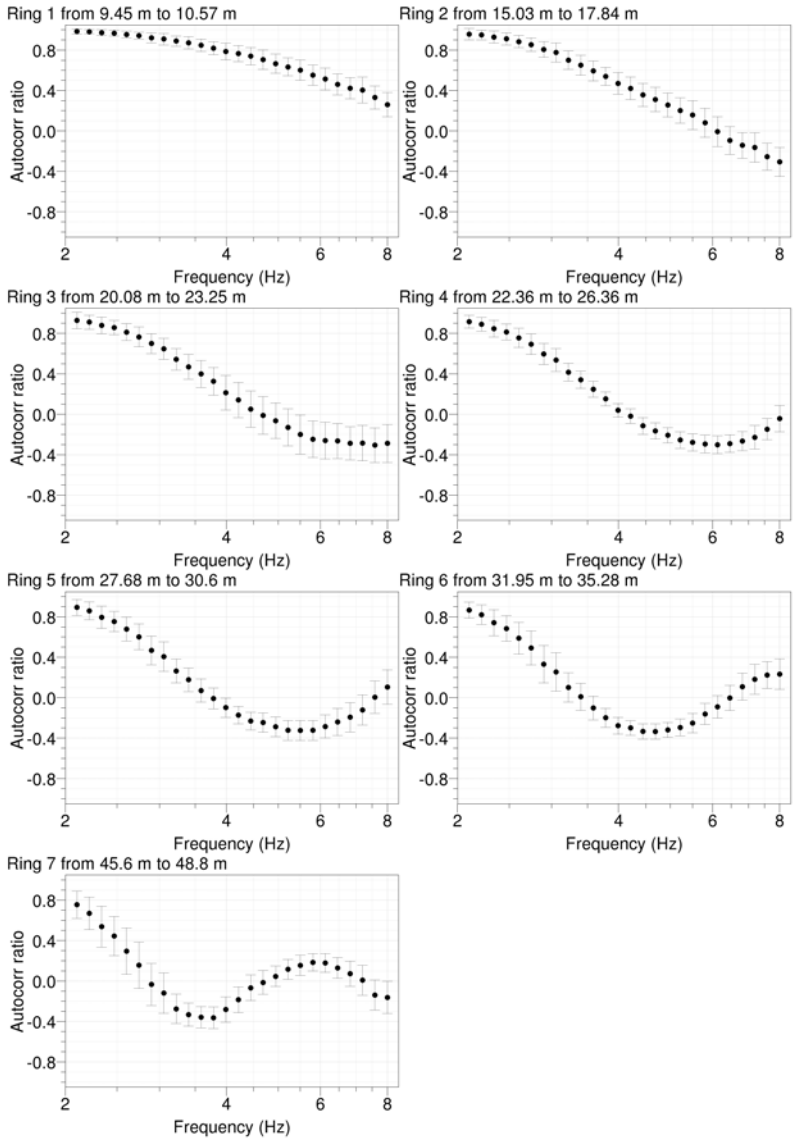

Figure 3.1.4: *Result of SPAC method, vertical component: SPAC functions for different rings.*

Inversion

Models are parametrized by 18 layers of fixed thickness. A constant density of 2100kg/m^3 was used for the final inversion. Several other parametrizations were tested with less success. It was not possible to fit simultaneously Love and Rayleigh fundamental mode dispersion curves (DC) for any parametrization (allowing for low velocity zones, fine layering close to surface etc.). Also joint inversion of Love fundamental mode dispersion curve (DC) and ellipticity (ELL) of Rayleigh fundamental mode did not lead to meaningful result. On the other hand results of the joint inversion of DC and ellipticity of fundamental Rayleigh mode were stable (see Figures: 3.1.7, 3.1.8). A Love-Rayleigh incompatibility is well known issue which could be explained by presence of an anisotropic material (e.g. Babuska and Cara, 1991).

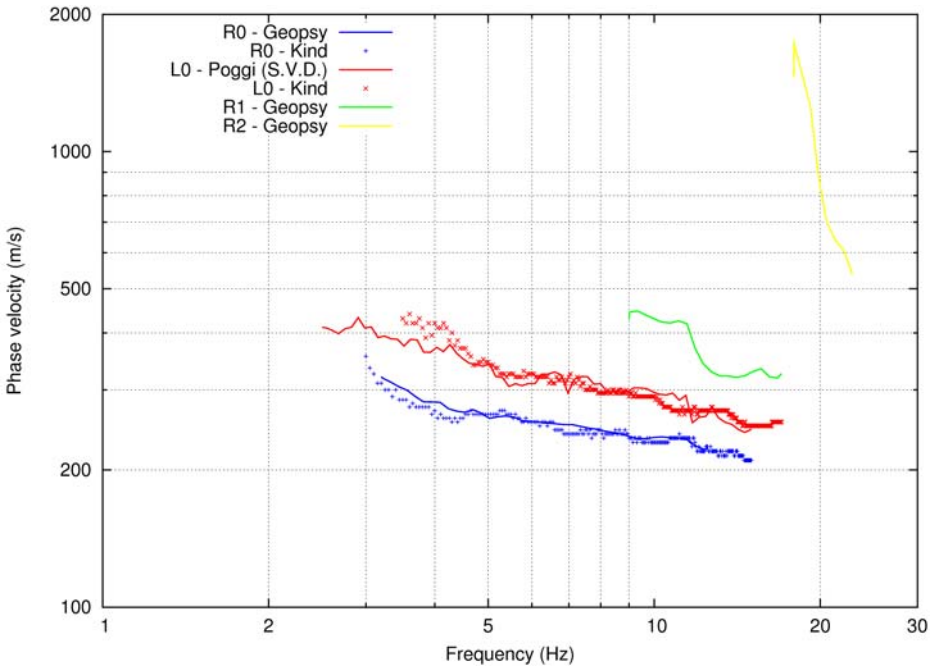

Figure 3.1.5: *Dispersion curves for AVIS1 array: R0 stands for fundamental mode of Rayleigh waves, L0 stands for fundamental mode of Love waves, R1 and R2 denote higher modes of Rayleigh waves.*

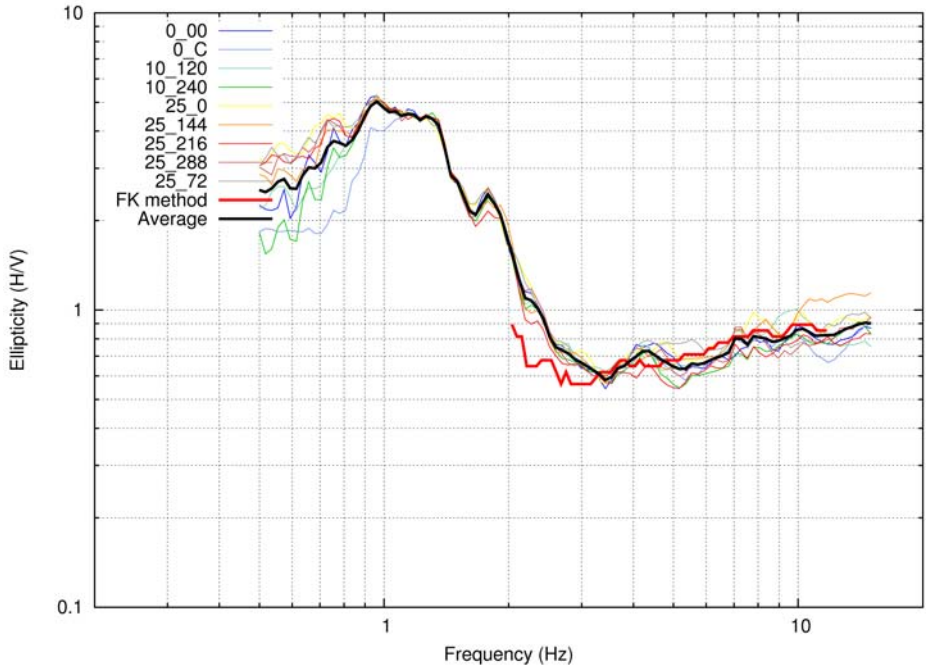

Figure 3.1.6: *Ellipticity curves for AVIS1 array obtained by wavelet and FK method*.

However, we propose a different explanation in this case. A Love fundamental and first higher mode DC were calculated for an ensemble of best models retrieved by joint inversion of ELL and DC of Rayleigh fundamental mode and compared with DC picked on the transversal component (see Figure 3.1.9). DC obtained from FK methods seems to lay just in between two modes, so the picked DC could be a mixture of the two modes and does not simply correspond to DC of the Love fundamental mode.

It was not possible to identify the mode number of the two higher Rayleigh modes (Figure 3.1.5), so these were not considered in the inversion. The higher modes lay very close to each other in this frequency band (10 - 30 Hz) for the ensemble of models retrieved by joint inversion of ELL and DC of Rayleigh fundamental mode.

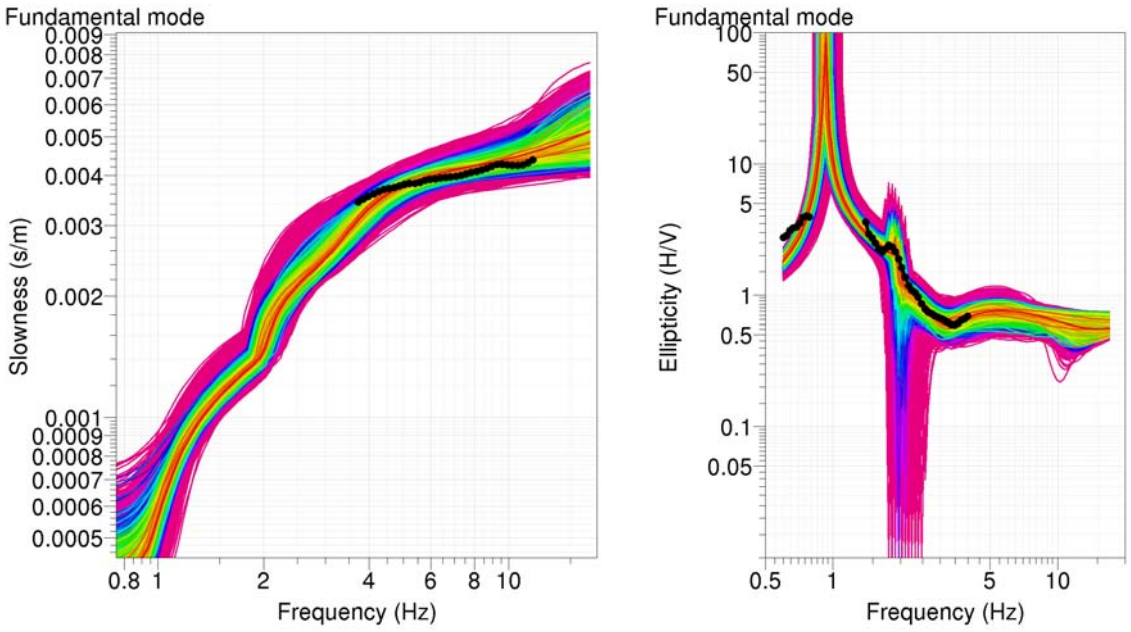

Figure 3.1.7: *An ensemble of dispersion curves (left) and ellipticities (right) of fundamental mode of Rayleigh waves. Observed curves used in the inversion are in black, the color distinguishes the misfit value. Corresponding models are in the Figure 3.1.8.*

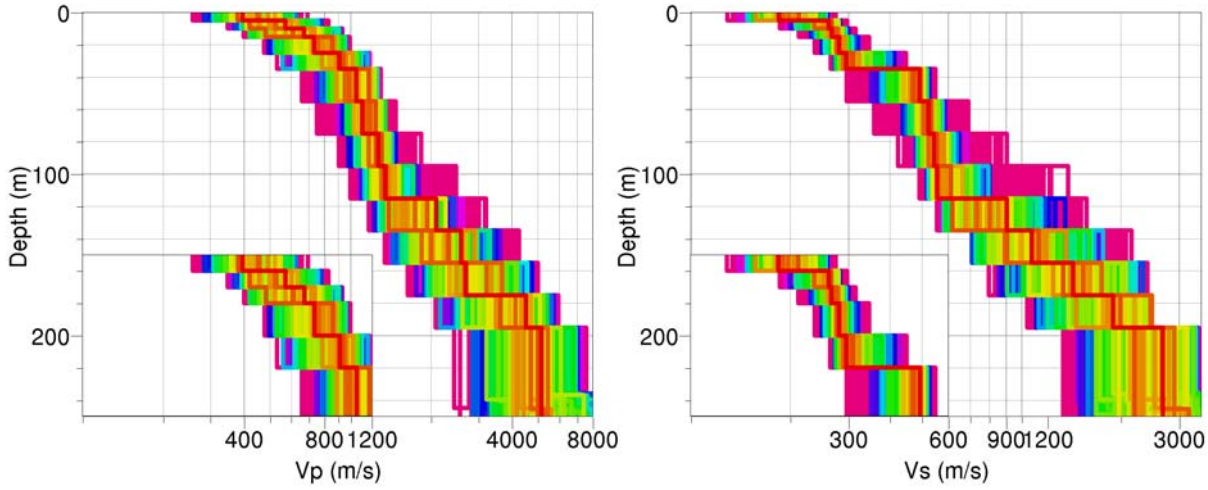

Figure 3.1.8: *An ensemble of inverted velocity profiles. First 50m are enlarged in the inset. Colors distinguish the misfit value in the same way as in the Figure 3.1.7.*

Other issues arise during joint inversion of ELL and DC. It is not straightforward which of the intervals of the picked ellipticity curve correspond to the true ellipticity of Rayleigh waves. In particular, the true ellipticity of Rayleigh waves reaches infinite values at frequency where the particle motion changes from retrograde to prograde. This happens usually in presence of a sharp contrast in the velocity profile. On the other hand, the true ellipticity may also contain a smooth peak in case of gradual

increase of the velocity with the depth. Unfortunately, it is very hard to distinguish the two cases, as all methods for estimation of Rayleigh wave ellipticity provide just smoothed curves.

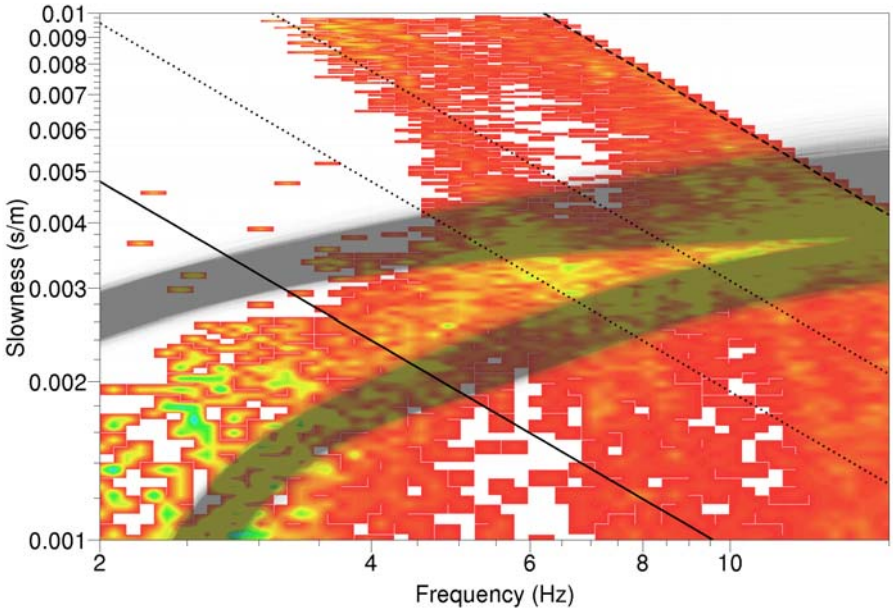

***Figure 3.1.9**: Results of FK processing of transversal component - frequency of occurrence of picked peaks in FK plane (colorful background), resolution limits calculated from array response (kmin/2 – solid, kmin & kmax/2 – dotted, kmax - dashed thin lines). Grey strips are the fundamental and first higher mode of Love waves calculated for the ensemble of models depicted in the Figure 3.1.8.*

Retrieved shear wave velocity profile (Figure 3.1.8) is reliable down to 120 m, as the scatter increases rapidly bellow 120 m. The discontinuity present around 40 m is constrained mainly by the bump in the observed ellipticity curve at 2 Hz (Figure 3.1.6).

3.2 Site AVIS2

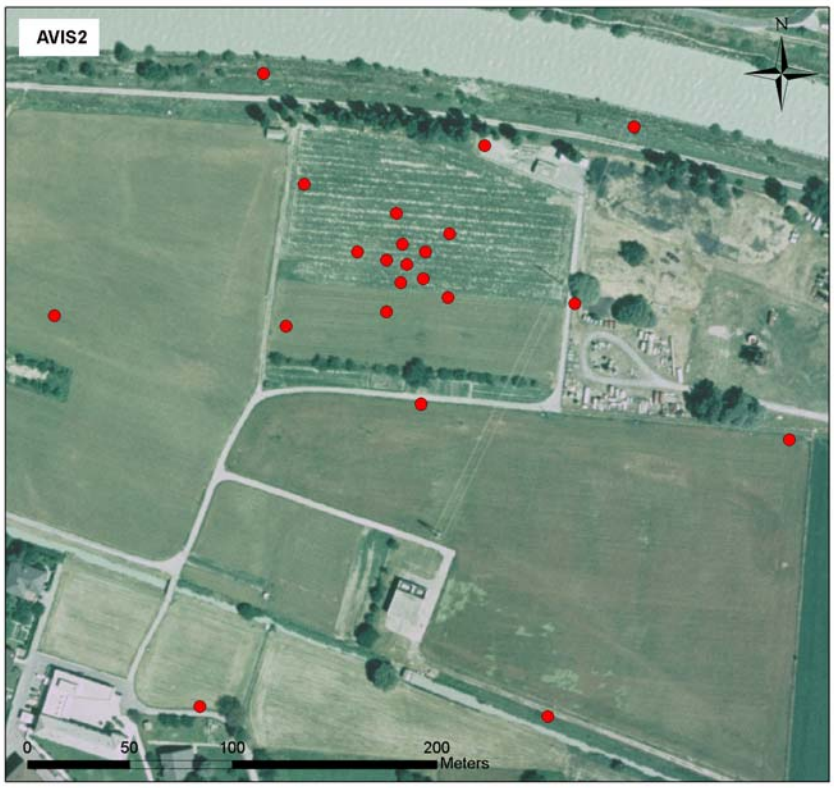

AVIS2 has a maximal diameter of 360 m and consists of 22 stations, set up in three steps. It was mainly located on a field that belongs to the Lonza.

Figure 3.2.1: *Sensor setup for array "AVIS2" in Visp.*

Array processing

Recordings were processed by different high-resolution FK methods. It was possible to follow the dispersion curve of fundamental mode of both Rayleigh and Love wave down to 1.2Hz with FK method. All picked dispersion curves for both Love and Rayleigh waves are plotted in Figure 3.2.2. Note the remarkable agreement between different codes and methods. Ellipticity of Rayleigh waves was estimated using wavelet-based (TFA) method and FK method. All ellipticity curves are depicted in Figure 3.2.3. Ellipticity curves are in good agreement across the array in the frequency range of 2- 15 Hz.

Inversion

Models are parametrized by 18 layers of fixed thickness, and a density of 2100kg/m^3 was used for the final inversion. It was possible to perform joint inversion of the DC (fundamental for both Rayleigh and Love waves) and ellipticity (fundamental Rayleigh mode) with the reasonable result (see Figures: 3.2.4, 3.2.5).
Retrieved shear wave velocity profile (Figure 3.2.6) is reliable down to 70 m, as the scatter increases rapidly below 70 m.

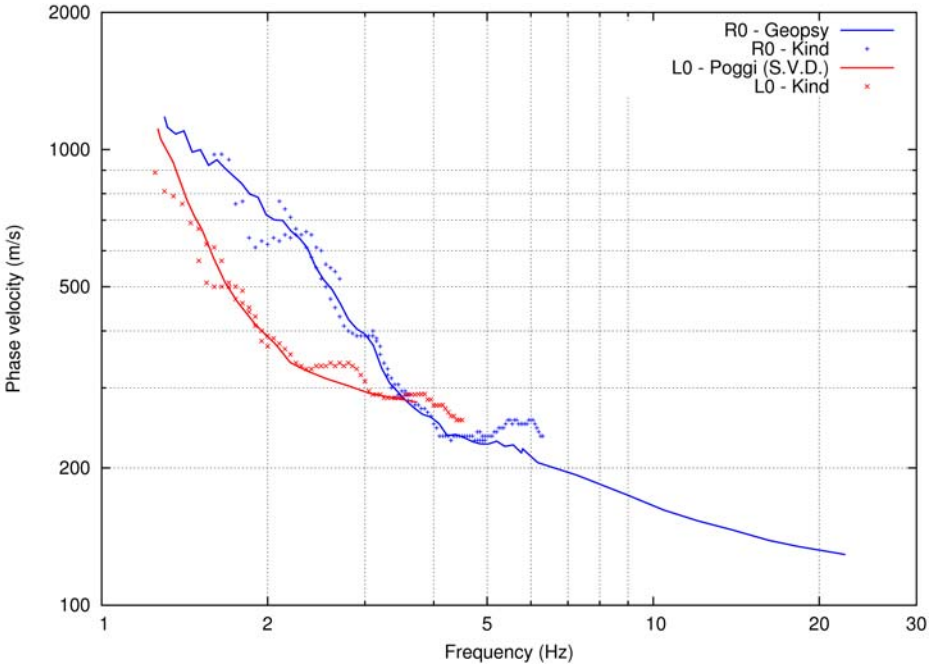

***Figure 3.2.2*: :** *Dispersion curves for AVIS2 array: R0 stands for fundamental mode of Rayleigh waves, L0 stands for fundamental mode of Love waves.*

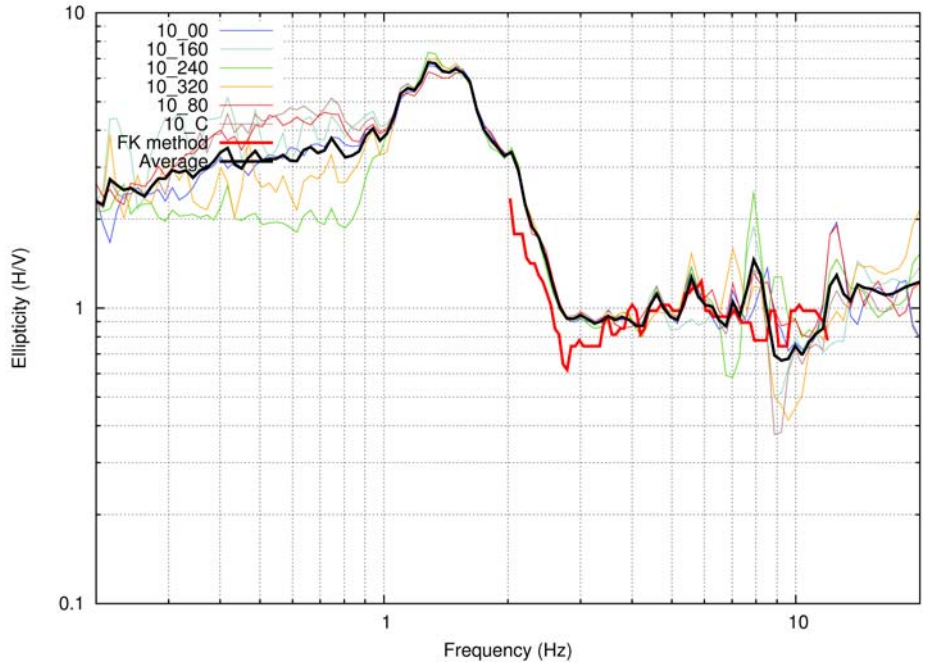

Figure 3.2.3: *Ellipticity curves for AVIS2 array obtained by wavelet and FK method.*

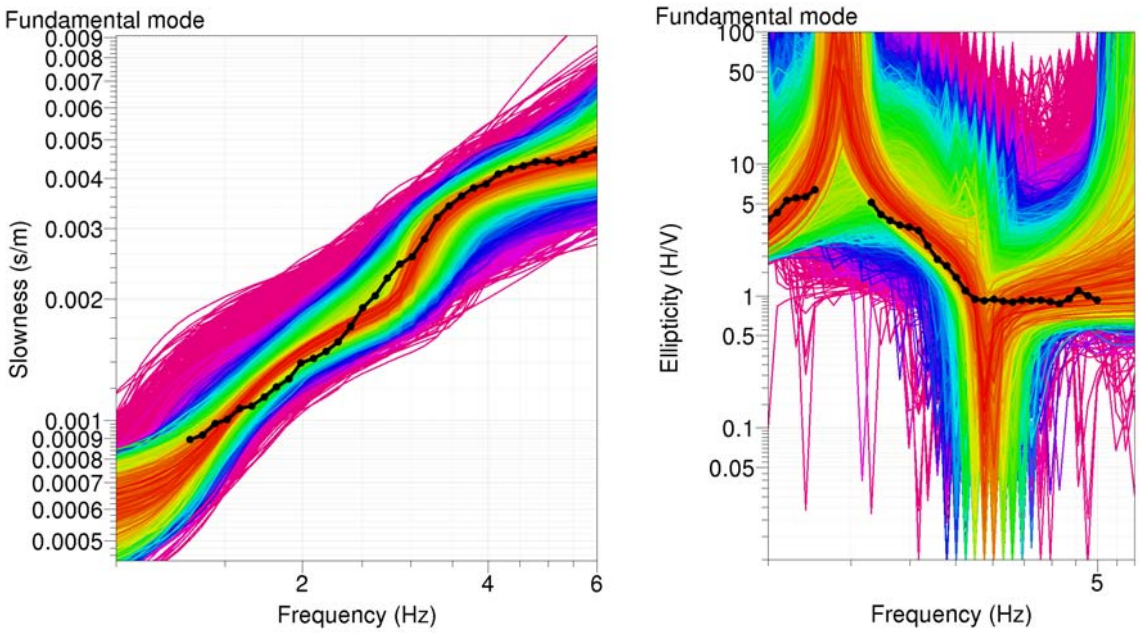

Figure 3.2.4: *An ensemble of dispersion curves (left) and ellipticities (right) of fundamental mode of Rayleigh waves. Observed curves used in the inversion are in black, the color distinguishes the misfit value. Corresponding models are in the Figure 3.2.6.*

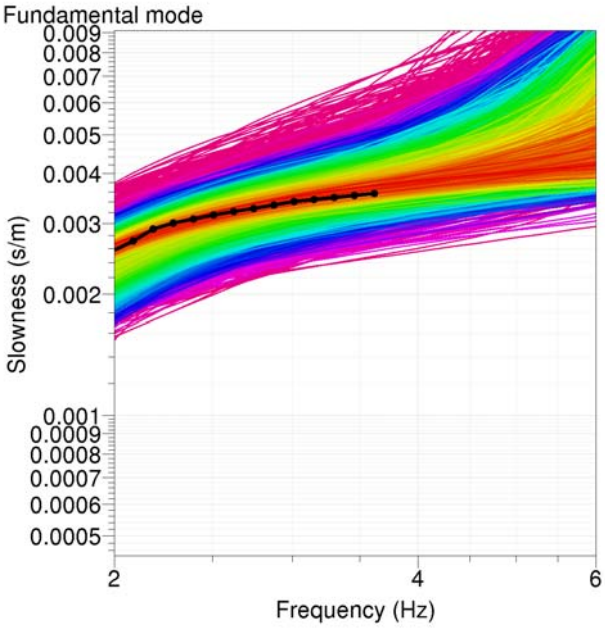

Figure 3.2.5: *An ensemble of dispersion curves of the fundamental mode of Love waves. Observed curves used in the inversion are in black, the color distinguishes the misfit value. Corresponding models are in the Figure 3.2.6.*

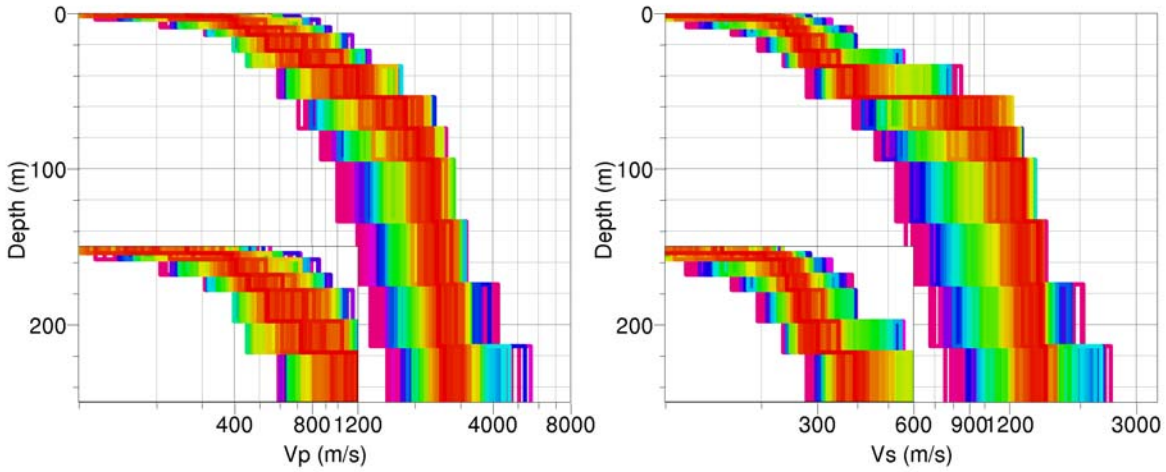

Figure 3.2.6: *An ensemble of inverted velocity profiles. First 50m are enlarged in the inset. Colors distinguish the misfit value in the same way as in the Figures 3.2.4, 3.2.5.*

3.3 Site VIS1

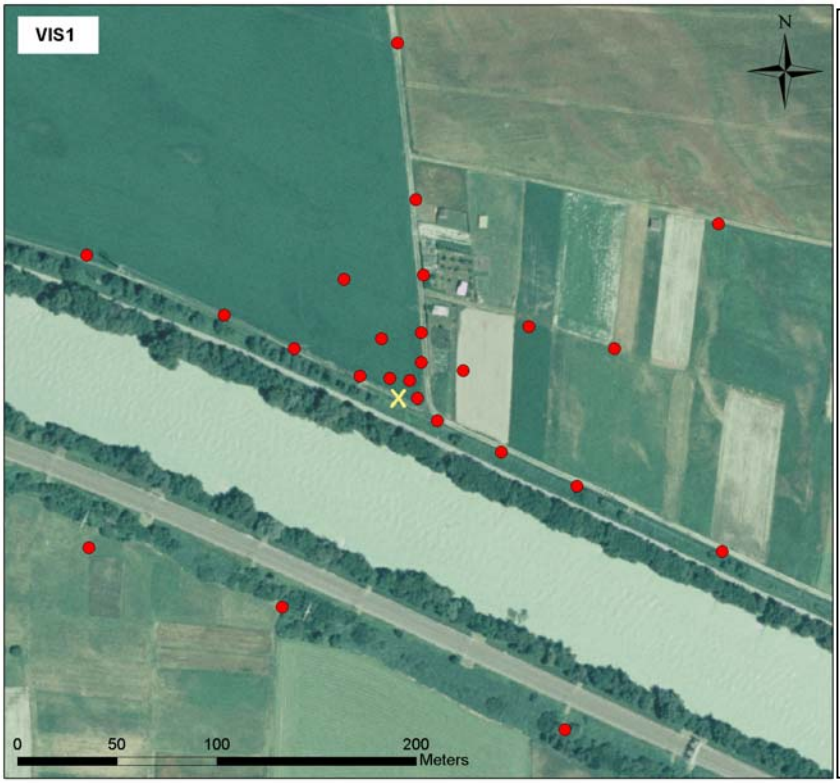

VIS1 has a maximal diameter of 360 m and consists of 25 stations, set up in three steps. It was located on grassland near to the river Rhone in Baltschieder, where a borehole (X) for the third adjustment of the river had been drilled.

Figure 3.3.1: *Sensor setup for array "VIS1" in Visp.*

Array processing

Recordings were processed by different high-resolution FK methods and SPAC method. It was possible to follow the dispersion curve of fundamental mode of both Rayleigh and Love wave down to 1Hz with FK method. It was also possible to pick higher modes. All picked dispersion curves for both Love and Rayleigh waves are plotted in Figure 3.3.2. Note the remarkable agreement between different codes and methods. SPAC did not improve the result in this case and is not presented here.
Ellipticity of Rayleigh waves was estimated for each station of the array using wavelet-based (TFA) method and FK method. All ellipticity curves are depicted in Figure 3.3.3. Ellipticity curves are in good agreement across the array in the frequency range of 0.5 - 15 Hz. The peak close to 2.5 Hz is artificial and probably related to some continuously operating machine in Lonza factory. This disturbance is not present in the data acquired during year 2006 (array AVIS1, AVIS2).

Inversion

Models are parametrized by 18 layers of fixed thickness and a density of 2100 kg/m^3 was used for the final inversion. It was possible to perform joint inversion of the DC (fundamental and 1st higher mode for both Rayleigh and Love waves) and ellipticity (fundamental Rayleigh mode) with a reasonable result (see Figures: 3.3.4, 3.3.5, 3.3.6, 3.3.7).

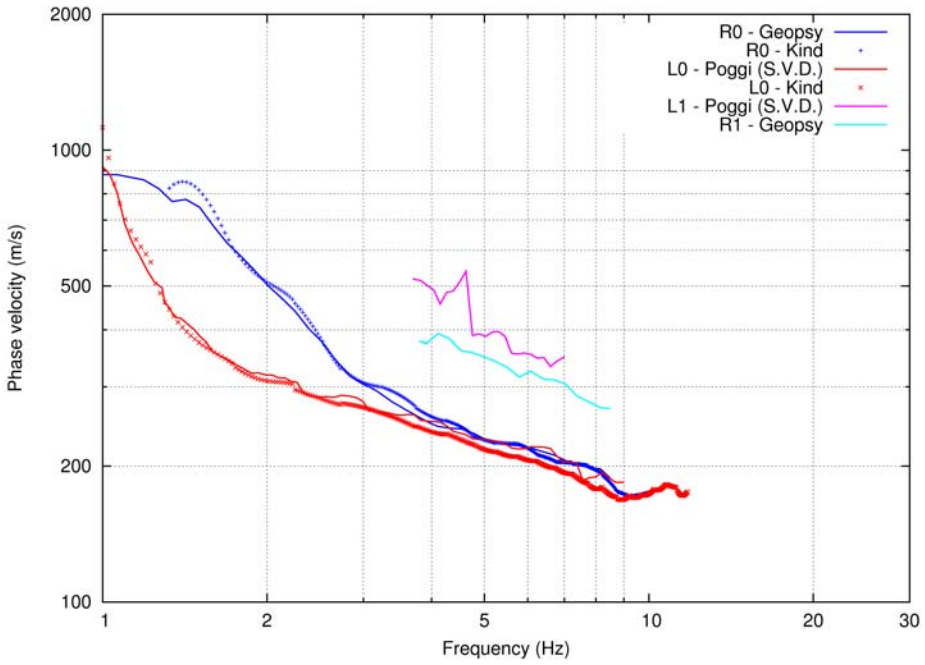

Figure 3.3.2**: :** *Dispersion curves for VIS1 array: R0 stands for fundamental mode of Rayleigh waves, L0 stands for fundamental mode of Love waves, R1 and L1 denote higher modes of Rayleigh waves and Love waves, respectively.*

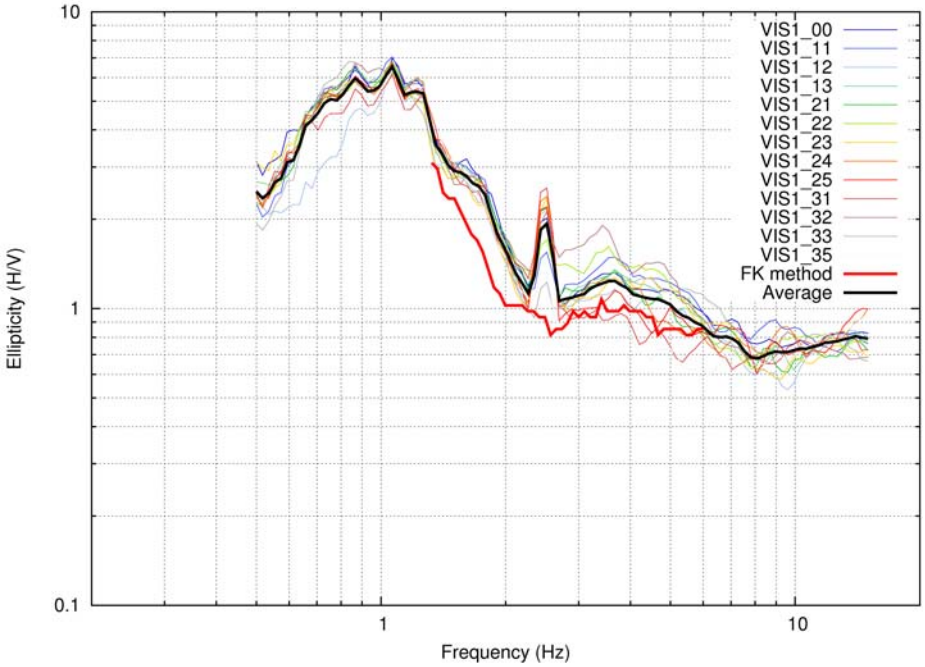

Figure 3.3.3**:** Ellipticity curves for VIS1 array obtained by wavelet and FK method.

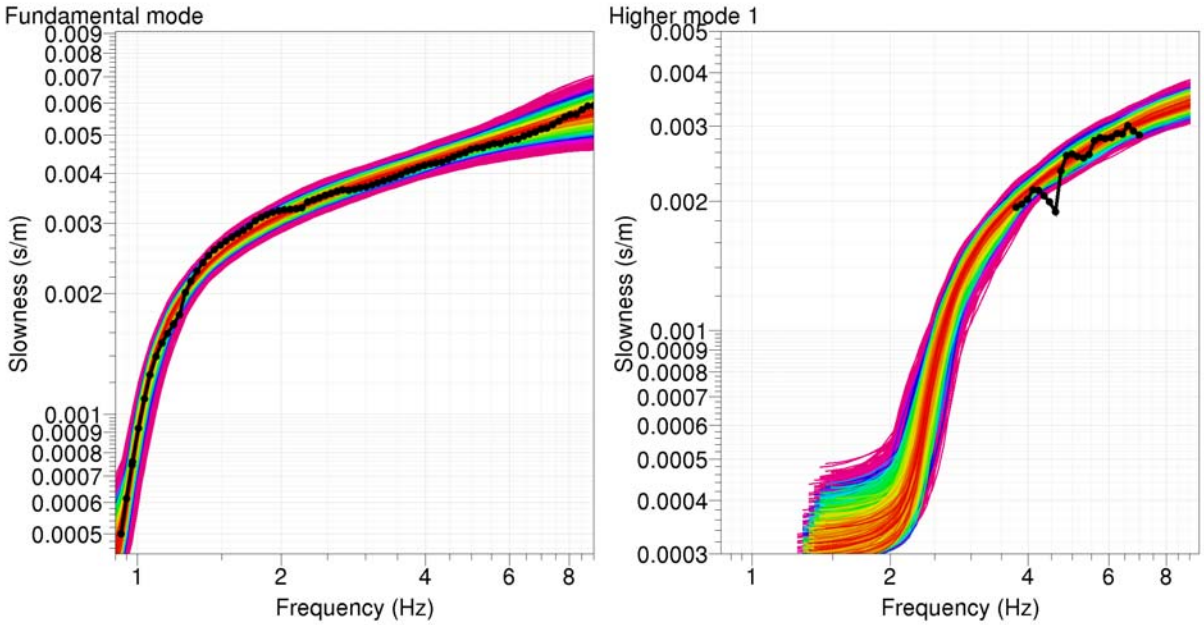

Figure 3.3.4: *An ensemble of dispersion curves of the fundamental (left) and first higher (right) mode of Love waves. Observed curves used in the inversion are in black, the color distinguishes the misfit value. Corresponding models are in the Figure 3.3.7.*

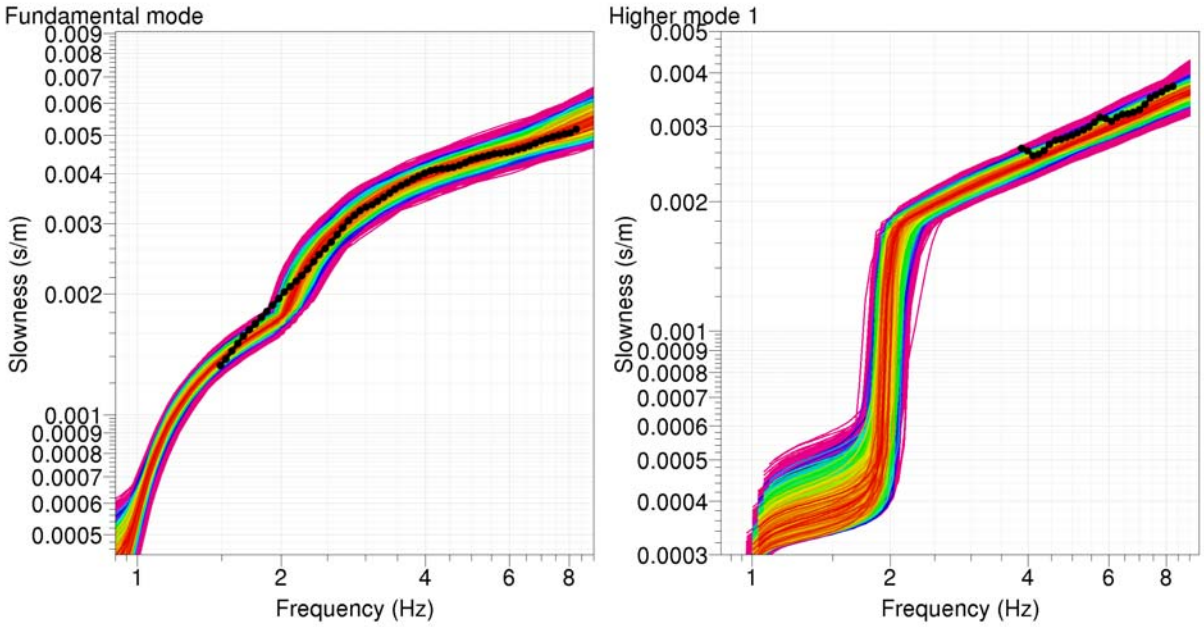

Figure 3.3.5: *An ensemble of dispersion curves of the fundamental (left) and first higher (right) mode Rayleigh waves. Observed curves used in the inversion are in black, the color distinguishes the misfit value. Corresponding models are in the Figure 3.3.7.*

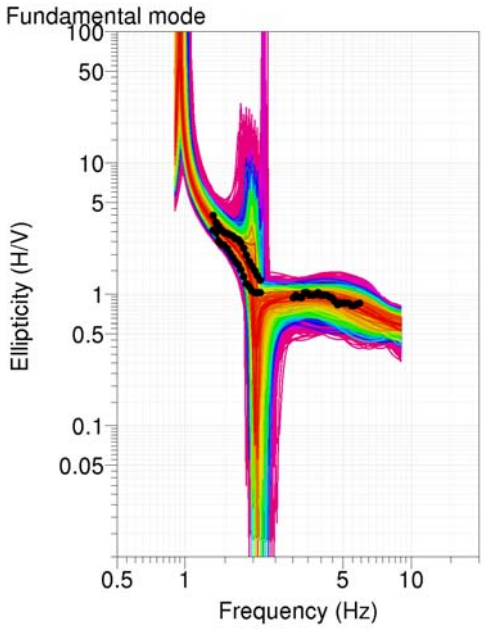

Figure 3.3.6: *An ensemble of ellipticities of fundamental mode of Rayleigh waves. Observed curves used in the inversion are in black, the color distinguishes the misfit value. Corresponding models are in the Figure 3.3.7.*

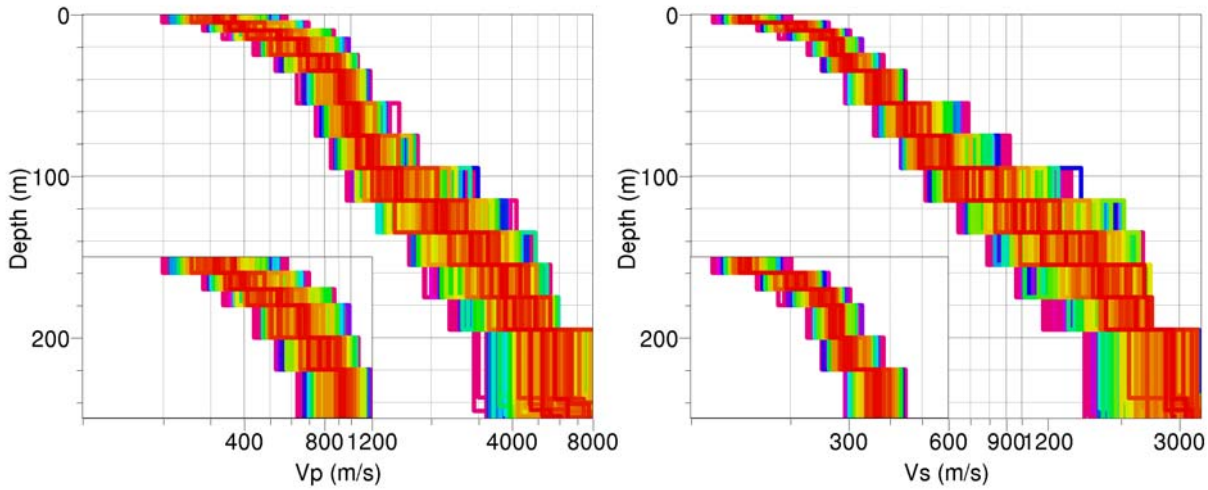

Figure 3.3.7: *An ensemble of inverted velocity profiles. First 50m are enlarged in the inset. Colors distinguish the misfit value in the same way as in the Figures 3.3.4, 3.3.5, 3.3.6.*

Retrieved shear wave velocity profile (Figure 3.3.7) is reliable down to 100 m, as the scatter increases rapidly bellow 100 m.

3.4 VIS2

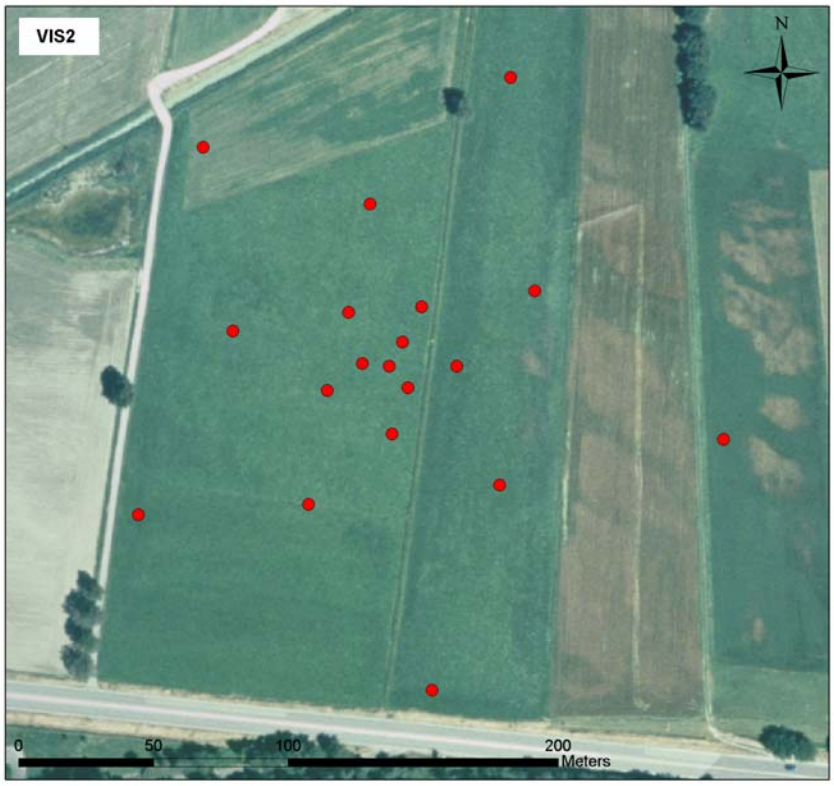

VIS2 has a maximal diameter of 240 m and consists of 19 stations, set up in two steps. It was located on grass-land, approx. 2 km westward outside from Visp.

Figure 3.4.1: *Sensor setup for array "VIS2" in Visp.*

Array processing

Recordings of vertical components were processed by several different high-resolution FK methods and SPAC method. It was possible to follow the dispersion curve of fundamental mode of both Rayleigh and Love wave down to 1.2Hz with FK method. It was also possible to pick higher modes. All picked dispersion curves for both Love and Rayleigh waves are plotted in Figure 3.4.2. Note the remarkable agreement between different codes and methods. The dispersion curves obtained with SPAC and FK are in good agreement.
Ellipticity of Rayleigh waves was estimated using wavelet-based (TFA) method and FK method. All ellipticity curves are depicted in Figure 3.4.3. The scatter between curves retrieved by TFA method is higher from station to station. The peak close to 2.5 Hz is artificial and probably related to some continuously operating machine in Lonza factory. The mean TFA curve is in good agreement with FK curve for frequencies higher than 4Hz. On the other hand, FK curve is bellow TFA curve for lower frequencies. The result of TFA method can be influenced by contribution of SH-waves which are amplified for this frequency band in this area (result of site-to-reference spectral ratios, not presented in this report). A more probable explanation is the poor performance of FK method on the radial component in this case.

Inversion

Model parametrized by 18 layers of fixed thickness and density of 2100kg/m^3 was used for the final inversion. It was possible to perform joint inversion of the DC (fundamental and fisrt higher mode for Rayleigh and fundamental mode for Love waves) and ellipticity (fundamental Rayleigh mode) with the reasonable result (see Figures: 3.4.4, 3.4.5). Mean TFA ellipticity was used in the inversion, as it was systematically

preferred by inversions of standalone DC. In other words, ellipticity curves retrieved by FK method seem to be incompatible with DC estimates.
Retrieved shear wave velocity profile (Figure 3.4.6) is reliable down to 90 m, as the scatter increases rapidly bellow 90 m.

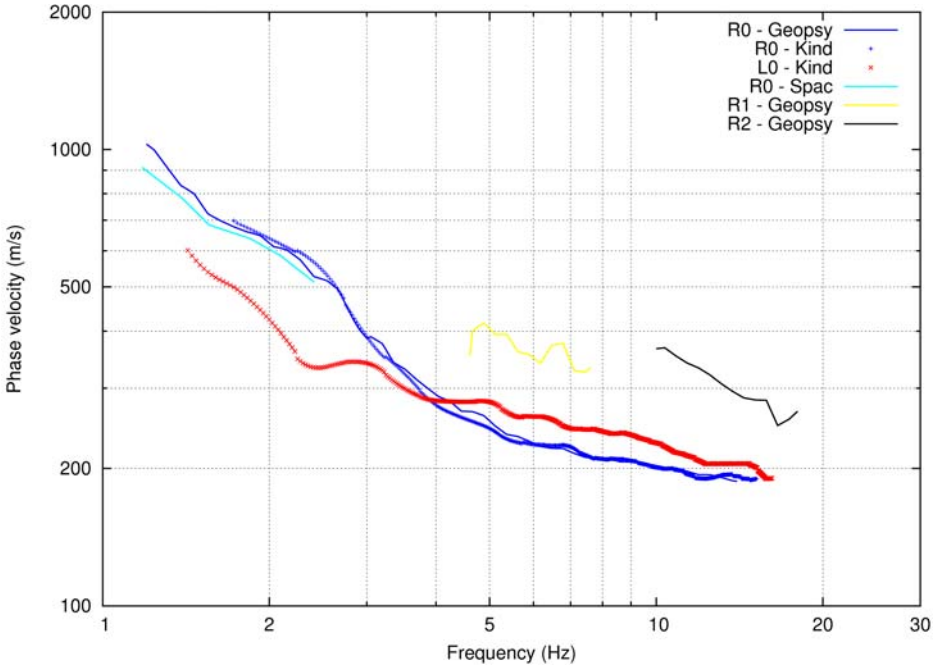

***Figure 3.4.2*: :** *Dispersion curves for VIS2 array: R0 stands for fundamental mode of Rayleigh waves, L0 stands for fundamental mode of Love waves, R1 and R2 denote higher modes of Rayleigh waves.*

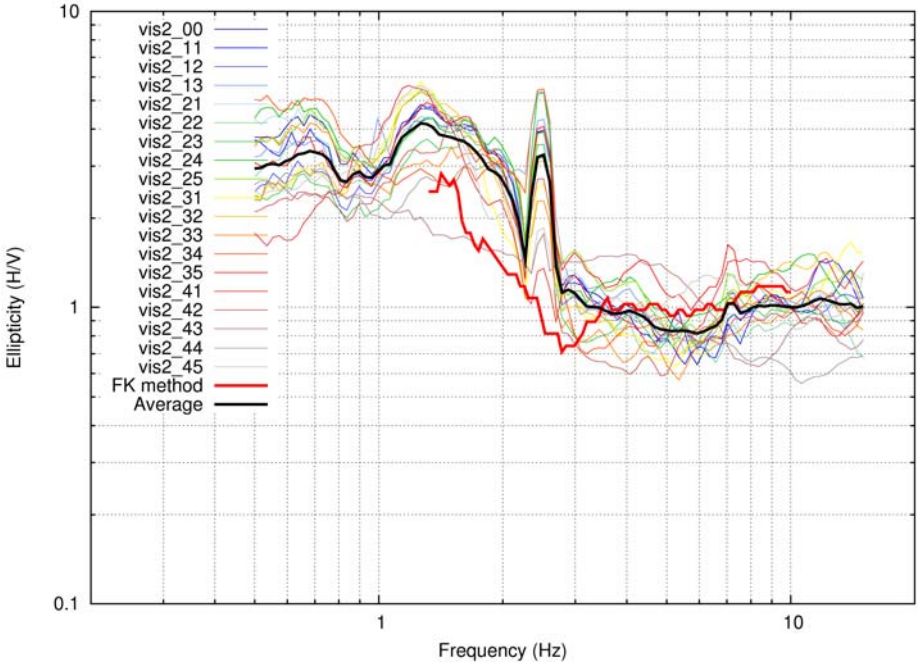

Figure 3.4.3: Ellipticity curves for VIS2 array obtained by wavelet and FK method.

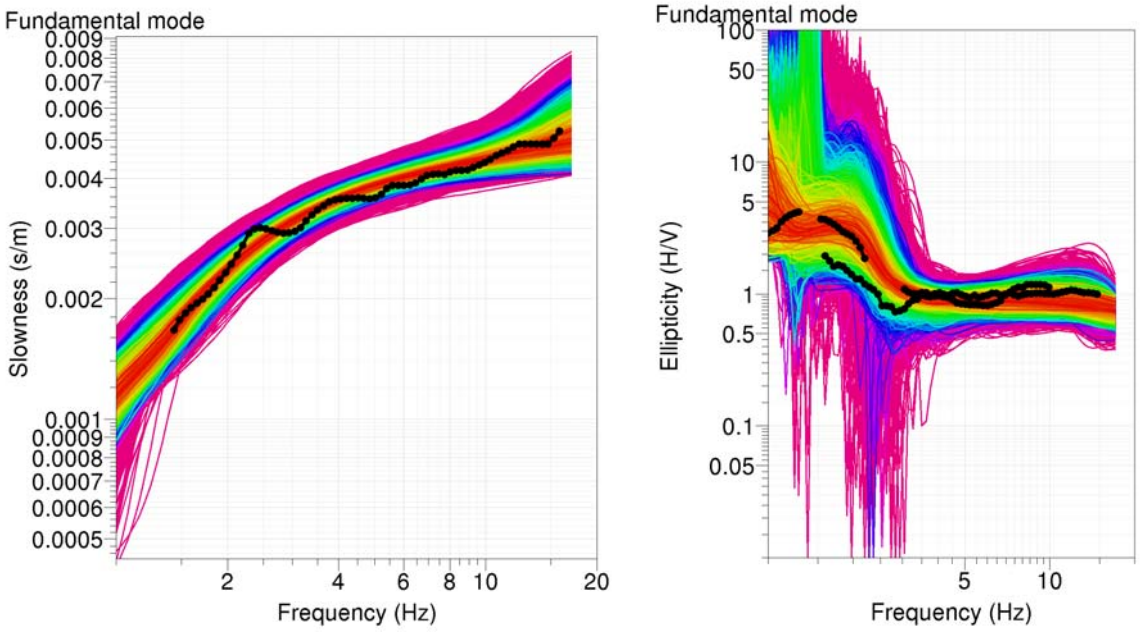

Figure 3.4.4: *An ensemble of dispersion curves (left)) of fundamental mode of Love waves and ellipticities (right) of fundamental mode of Rayleigh waves. Observed curves used in the inversion are in black, the color distinguishes the misfit value. Corresponding models are in the Figure 3.4.7.*

.

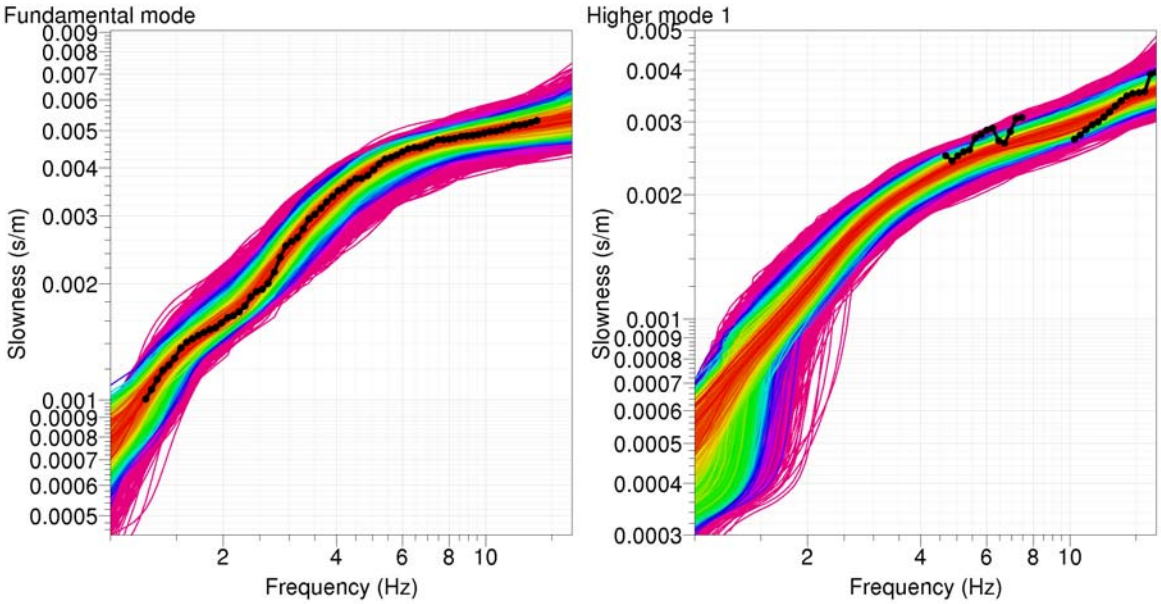

Figure 3.4.5: *An ensemble of dispersion curves of the fundamental (left) and first higher (right) mode of Rayleigh waves. Observed curves used in the inversion are in black, the color distinguishes the misfit value. Corresponding models are in the Figure 3.4.7.*

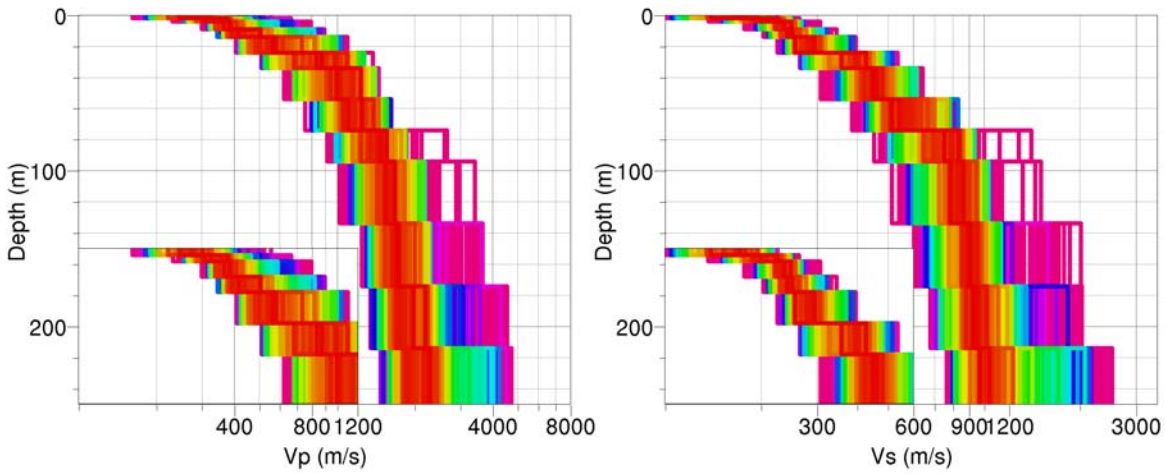

Figure 3.4.6: *An ensemble of inverted velocity profiles. First 50m are enlarged in the inset. Colors distinguish the misfit value in the same way as in the Figures 3.4.4, 3.4.5.*

3.5 Site VIS3

VIS3 has a maximal diameter of 200 m and consists of 17 stations, set up in two steps. It was located halfway on grassland and halfway on a street (without traffic!) in an area a little bit outside Visp, where soon new houses will be built. (Aerial picture on map is not up to date!)

Figure 3.5.1: *Sensor setup for array "VIS3" in Visp.*

Array processing

Recordings of vertical components were processed by several different high-resolution FK methods and SPAC method. It was possible to follow the dispersion curve of fundamental mode of both Rayleigh and Love wave down to 1.5Hz with FK method. It was also possible to pick a higher mode. All picked dispersion curves for both Love and Rayleigh waves are plotted in Figure 3.5.2. Note the remarkable agreement between different codes and methods. The dispersion curves obtained with SPAC and FK are in good agreement. There was a problem matching DC curves obtained for the outer and inner rings for both Love and Rayleigh waves. We did not introduce any smoothing, both overlapping chunks were used in the inversion. Ellipticity of Rayleigh waves was estimated using wavelet-based (TFA) method and FK method. All ellipticity curves are depicted in Figure 3.5.3. Ellipticity curves are in good agreement across the array in the frequency range of 0.5 - 15 Hz. The peak close to 2.5 Hz is artificial and probably related to some continuously operating machine in Lonza factory. FK curve is systematically bellow TFA curve for frequencies lower than 4Hz.

Inversion

Models are parametrized by 18 layers of fixed thickness and a density of 2100kg/m^3 was used for the final inversion. It was possible to perform joint inversion of the DC (fundamental and first higher mode for Rayleigh and fundamental mode for Love waves) and ellipticity (fundamental Rayleigh mode) with the reasonable result (see Figures: 3.5.4, 3.5.5), except first higher mode of Rayleigh waves. The observed phase velocities of the higher mode are too slow, forcing very low velocity of S-waves (100 m/s) in first two meters (see Figure 3.5.6).

Retrieved shear wave velocity profile (Figure 3.5.6) is than reliable down to 100 m, as the scatter increases rapidly below 100 m. Particularly, two branches of models appear, one with and one without a strong interface at 100 m. The trend of DC below 2 Hz seems to prefer the models with the interface.

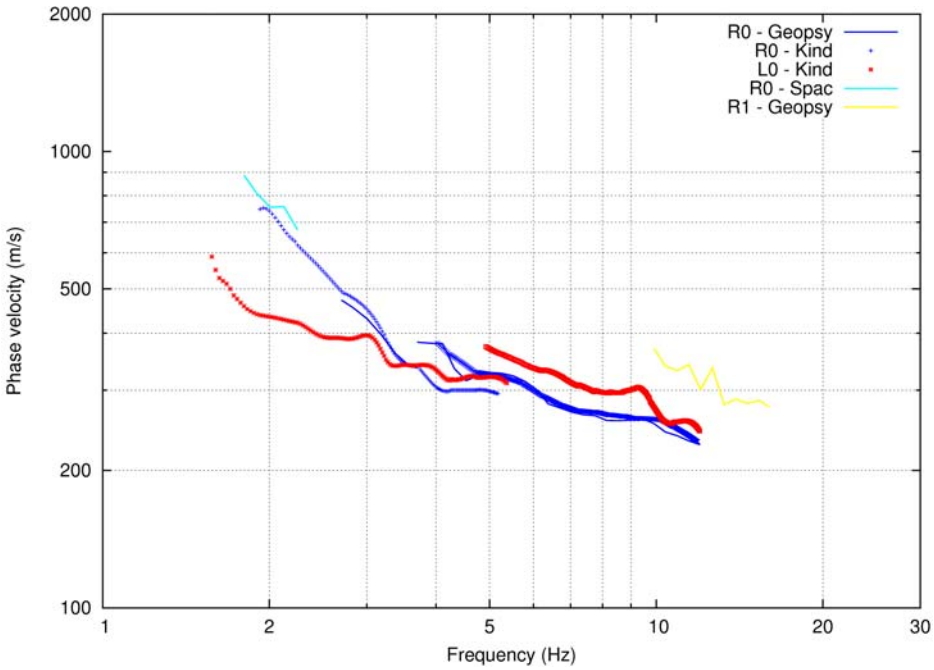

***Figure 3.5.2*: :** *Dispersion curves for VIS3 array: R0 stands for fundamental mode of Rayleigh waves, L0 stands for fundamental mode of Love waves, R1 denotes higher mode of Rayleigh waves.*

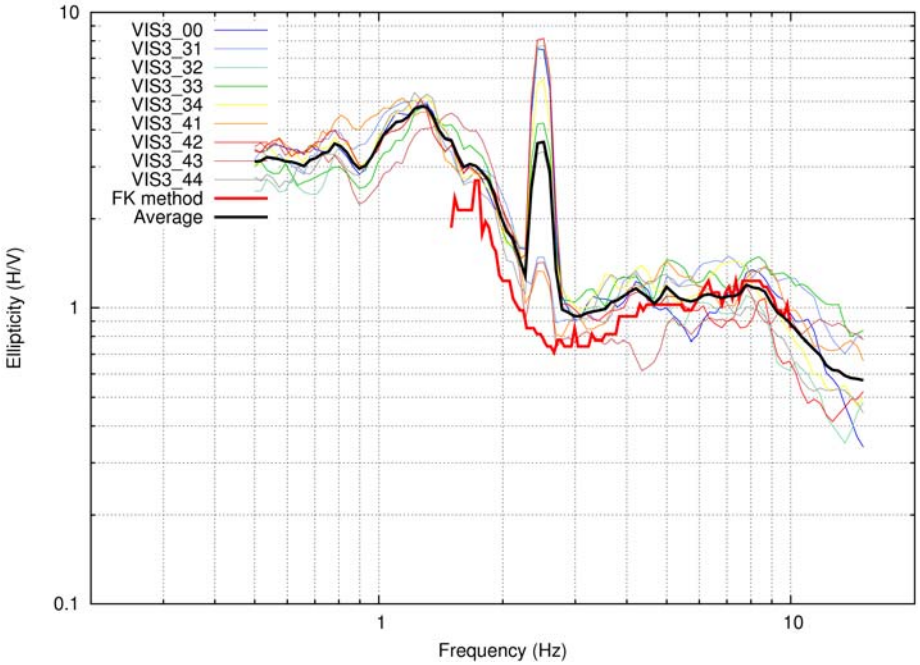

Figure 3.5.3: Ellipticity curves for VIS3 array obtained by wavelet and FK method.

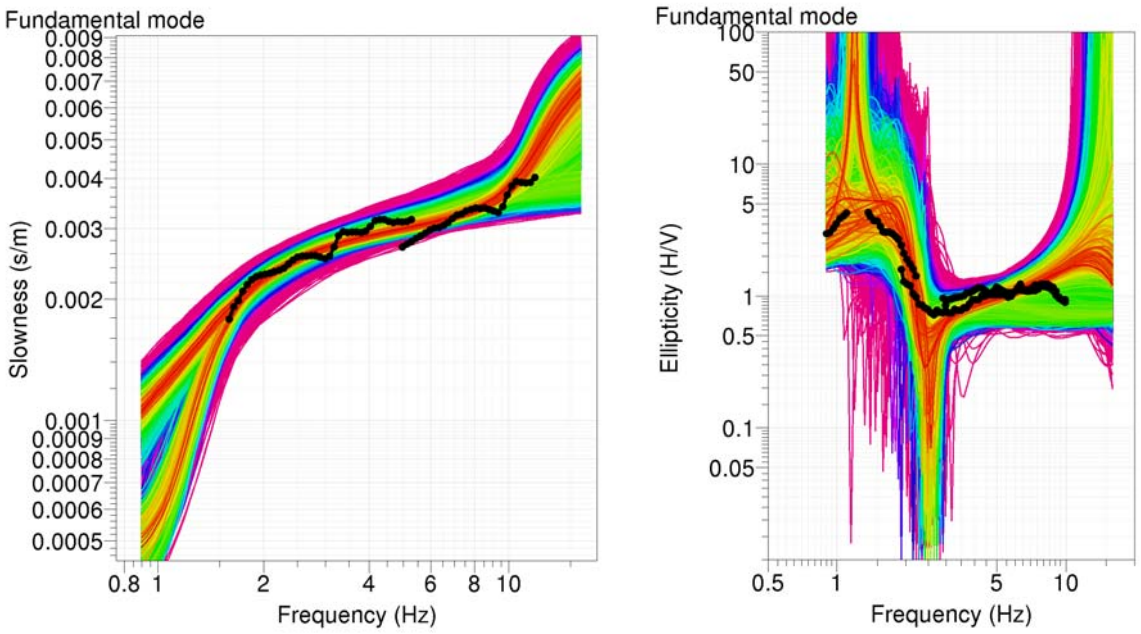

Figure 3.5.4: *An ensemble of dispersion curves (left) of fundamental mode of Love waves and ellipticities (right) of fundamental mode of Rayleigh waves. Observed curves used in the inversion are in black, the color distinguishes the misfit value. Corresponding models are in the Figure 3.5.6.*

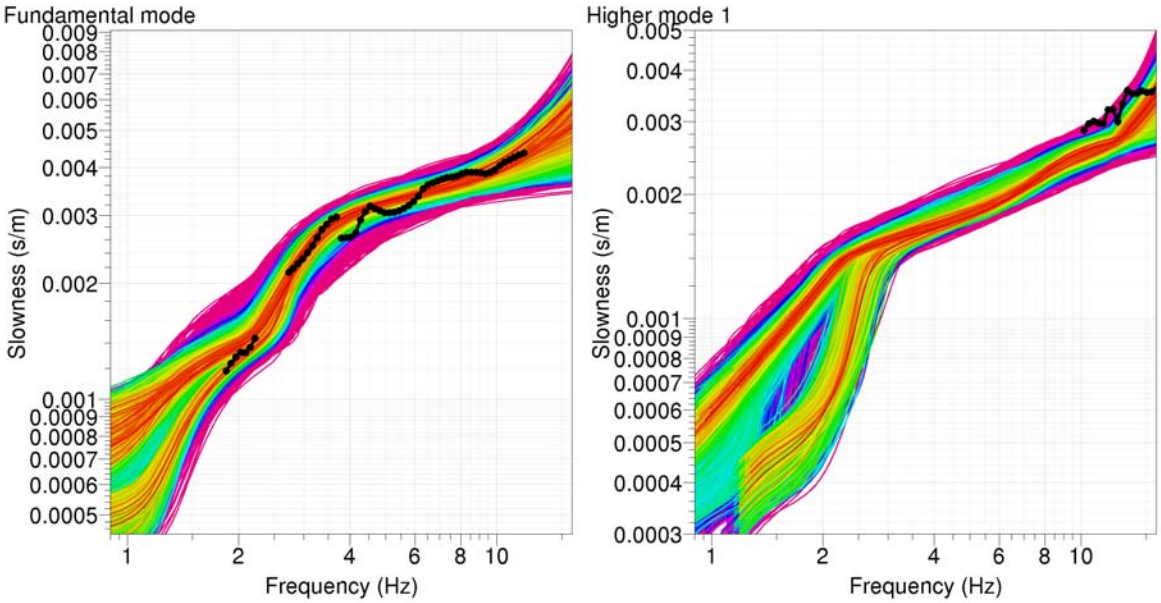

Figure 3.5.5: *An ensemble of dispersion curves of the fundamental (left) and first higher (right) mode of Rayleigh waves. Observed curves used in the inversion are in black, the color distinguishes the misfit value. Corresponding models are in the Figure 3.5.6.*

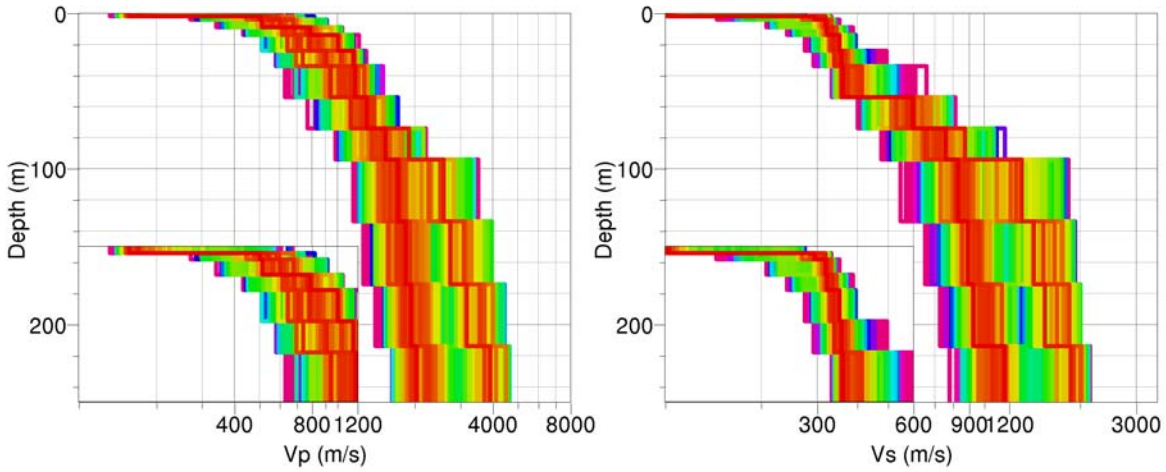

Figure 3.5.6: *An ensemble of inverted velocity profiles. First 50m are enlarged in the inset. Colors distinguish the misfit value in the same way as in the Figures 3.5.4, 3.5.5.*

3.6 Site VIS4

VIS4 has a maximal diameter of 240 m and consists of 20 stations, set up in two steps. It was located mainly on asphalt-streets in a calm quarter of Visp. In winter 07/08 and 08/09 one of the temporary stations (VISP1) was installed in the cellar of a house right in the centre of this array.

Figure 3.6.1: *Sensor setup for array "VIS4" in Visp.*

Array processing

Recordings were processed by different high-resolution FK methods. It was possible to follow the dispersion curve of fundamental mode of both Rayleigh and Love wave down to 1.9Hz with FK method. All picked dispersion curves for both Love and Rayleigh waves are plotted in Figure 3.6.2. Note the remarkable agreement between different codes and methods.

Ellipticity of Rayleigh waves was estimated using wavelet-based (TFA) method and FK method. All ellipticity curves are depicted in Figure 3.6.3. The scatter between curves retrieved by TFA method is higher from station to station. The peaks close to 2.5 Hz and 5 Hz are artificial and probably related to some continuously operating machine in Lonza factory. The mean TFA curve is in good agreement with FK curve for frequencies higher than 4Hz. On the other hand, FK curve is systematically below TFA curve for lower frequencies. The result of TFA method can be influenced by contribution of SH-waves that are amplified in this frequency band in this area (result of site-to-reference spectral ratios, not presented in this report). A more probable explanation is the poor performance of FK method on the radial component in this case.

Inversion

Model are parametrized by 18 layers of fixed thickness and a density of 2100kg/m^3 was used for the final inversion. It was possible to perform joint inversion of the DC (fundamental for both Rayleigh and Love waves) and ellipticity (fundamental Rayleigh mode) with a reasonable result (see Figures: 3.6.4, 3.6.5). Mean TFA ellipticity was used in the inversion, as it was systematically preferred in the inversions. In other words, ellipticity curves below 3Hz retrieved by FK method seem to be incompatible with DC estimates.

Retrieved shear wave velocity profile (Figure 3.6.6) is reliable down to 60 m, as the scatter increases rapidly below 60 m.

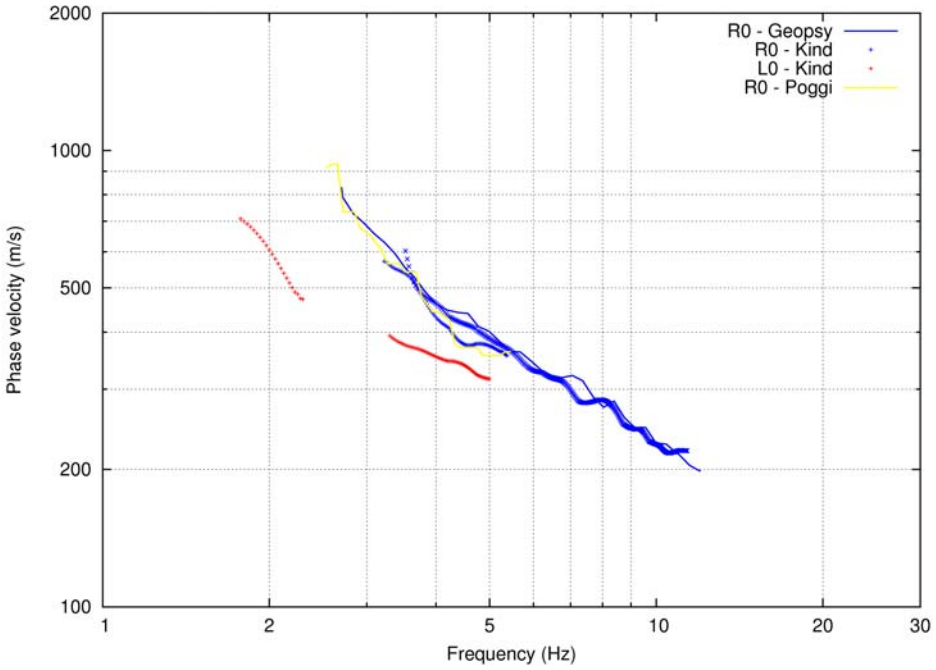

Figure 3.6.2**:** *Dispersion curves for VIS4 array: R0 stands for fundamental mode of Rayleigh waves, L0 stands for fundamental mode of Love waves.*

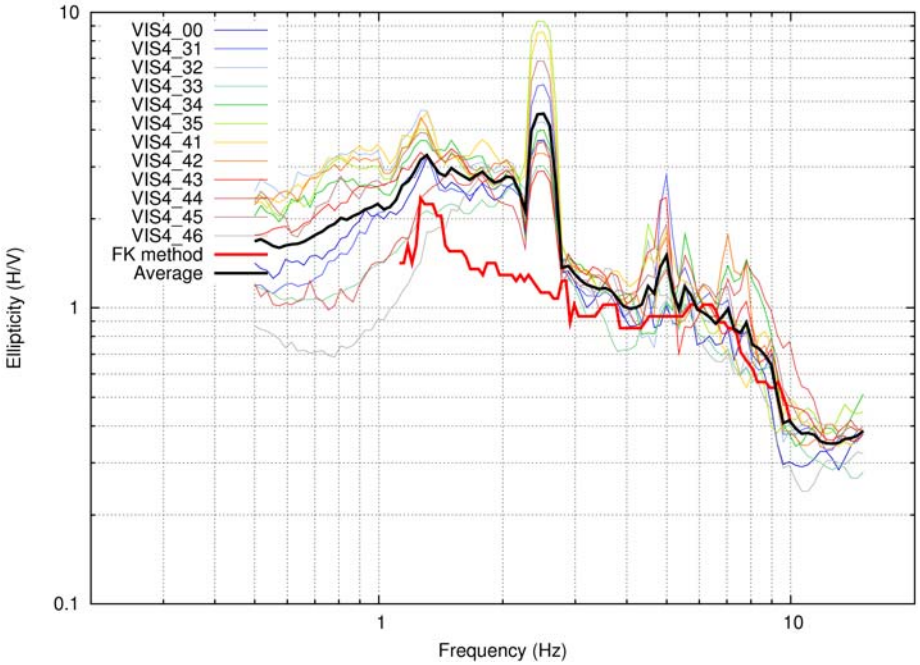

Figure 3.6.3: *Ellipticity curves for VIS4 array obtained by wavelet and FK method.*

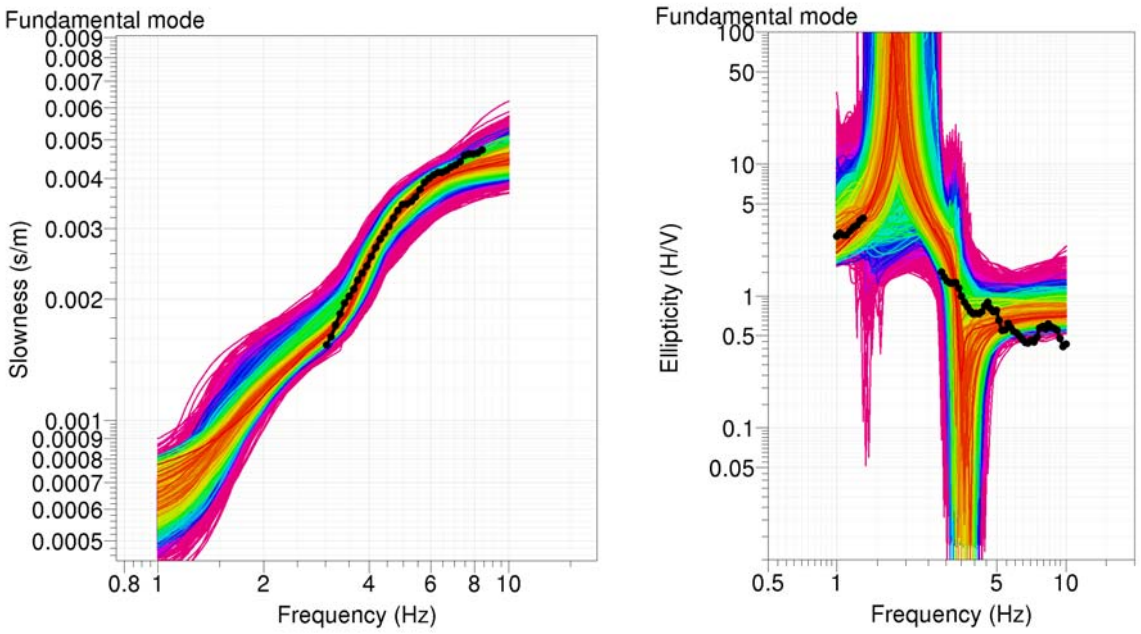

Figure 3.6.4: *An ensemble of dispersion curves (left) and ellipticities (right) of fundamental mode of Rayleigh waves. Observed curves used in the inversion are in black, the color distinguishes the misfit value. Corresponding models are in the Figure 3.6.6.*

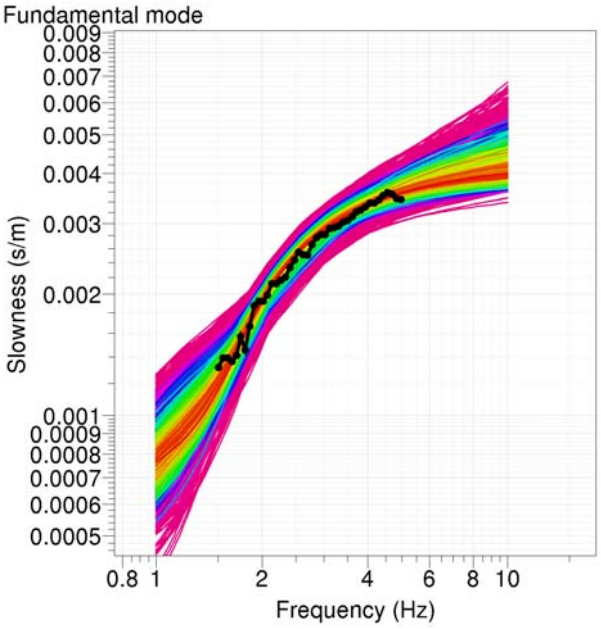

Figure 3.6.5: *An ensemble of dispersion curves of the fundamental mode of Love waves. Observed curves used in the inversion are in black, the color distinguishes the misfit value. Corresponding models are in the Figure 3.6.6.*

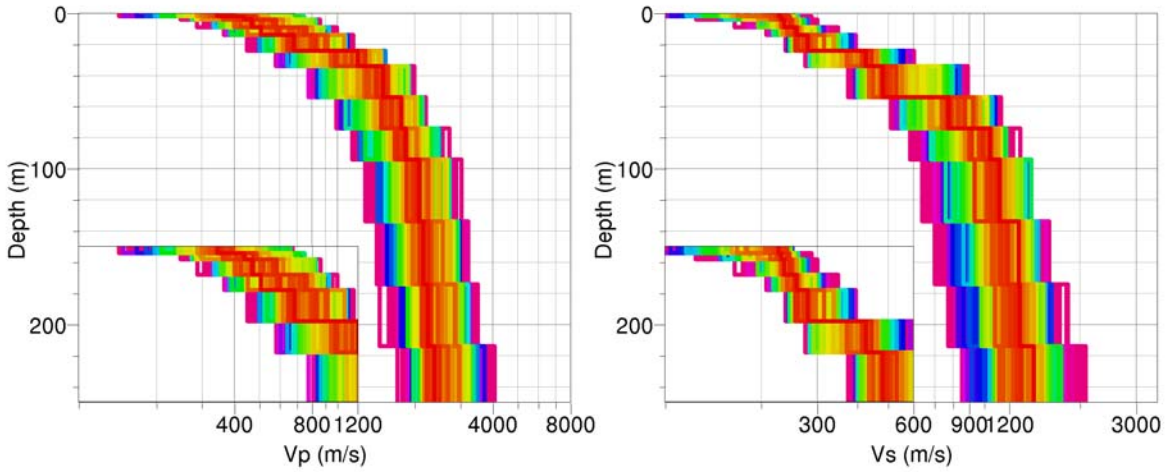

Figure 3.6.6: *An ensemble of inverted velocity profiles. First 50m are enlarged in the inset. Colors distinguish the misfit value in the same way as in the Figures 3.6.4, 3.6.5.*

3.7 Site VIS5

VIS5 has a maximal diameter of 200 m and consists of 14 stations, all set up simultaneously. It was located on a street next to the premises of Lonza, therefore its shape is quite asymmetric.

Figure 3.7.1: *Sensor setup for array "VIS5" in Visp.*

Array processing

Recordings were processed by different high-resolution FK methods. It was possible to follow the dispersion curve of fundamental mode of both Rayleigh and Love wave down to 1.5Hz with FK method. All picked dispersion curves for both Love and Rayleigh waves are plotted in Figure 3.7.2. Note the remarkable agreement between different codes and methods.

Ellipticity of Rayleigh waves was estimated using wavelet-based (TFA) method and FK method. All ellipticity curves are depicted in Figure 3.7.3. The scatter between curves retrieved by TFA method is high from station to station. The peaks close to 2.5 Hz, 5 Hz, 9 Hz are artificial and probably related to some continuously operating machine in Lonza factory. The mean TFA curve is in good agreement with FK curve for frequencies higher than 4Hz. On the other hand, FK curve is systematically below TFA curve for lower frequencies. The result of TFA method can be influenced by contribution of SH-waves that are amplified in this frequency band in this area (result of site-to-reference spectral ratios, not presented in this report). A more probable explanation is the poor performance of FK method on the radial component in this case.

Inversion

Models are parametrized by 18 layers of fixed thickness and a density of 2100kg/m^3 was used for the final inversion. It was possible to perform joint inversion of the DC (fundamental for both Rayleigh and Love waves) and ellipticity (fundamental Rayleigh mode) with a reasonable result (see Figures: 3.7.4, 3.7.5). Mean TFA ellipticity was used in the inversion, as it was systematically preferred in the inversions. In other words, ellipticity curves below 3Hz retrieved by FK method seem to be incompatible with DC estimates.

Retrieved shear wave velocity profile (Figure 3.7.6) is reliable down to 60 m, as the scatter increases rapidly below 60 m.

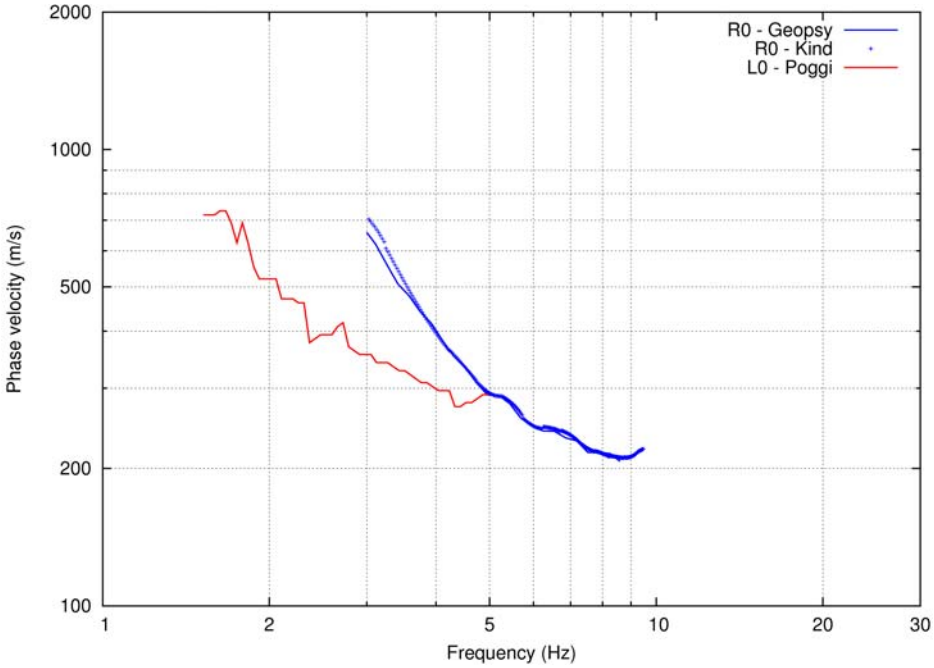

Figure 3.7.2**:** *Dispersion curves for VIS5 array: R0 stands for fundamental mode of Rayleigh waves, L0 stands for fundamental mode of Love waves.*

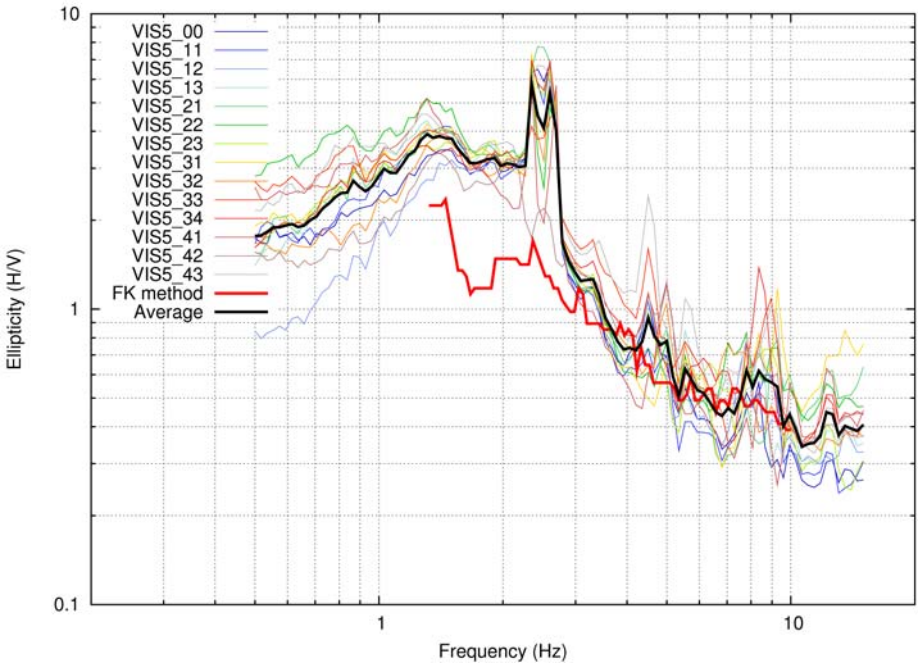

Figure 3.7.3: *Ellipticity curves for VIS5 array obtained by wavelet and FK method.*

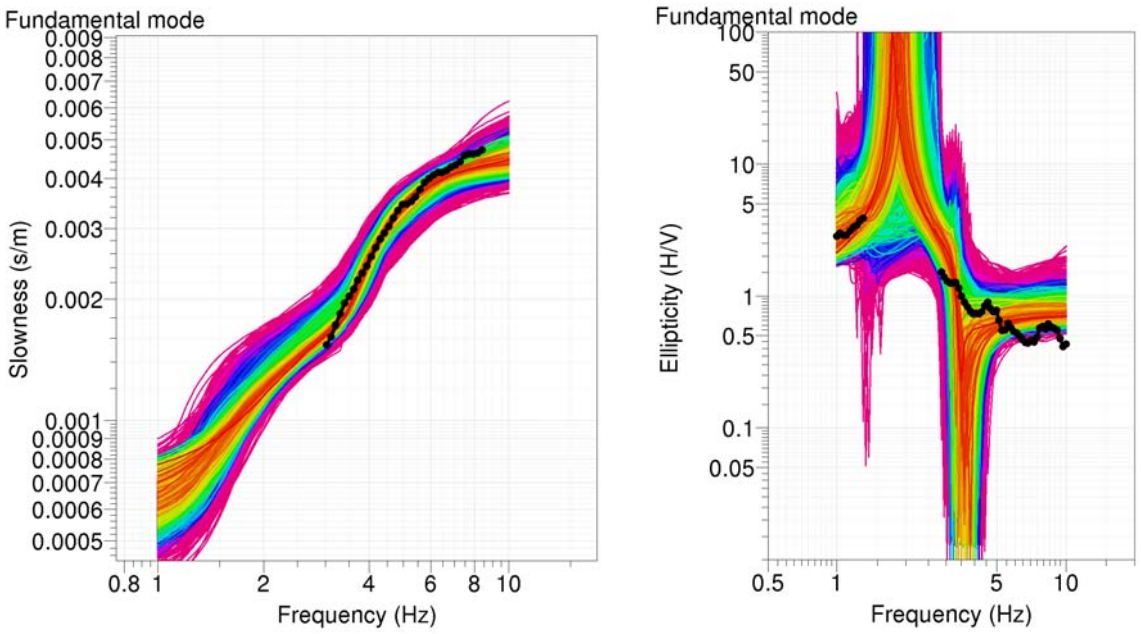

Figure 3.7.4: *An ensemble of dispersion curves (left) and ellipticities (right) of fundamental mode of Rayleigh waves. Observed curves used in the inversion are in black, the color distinguishes the misfit value. Corresponding models are in the Figure 3.7.6.*

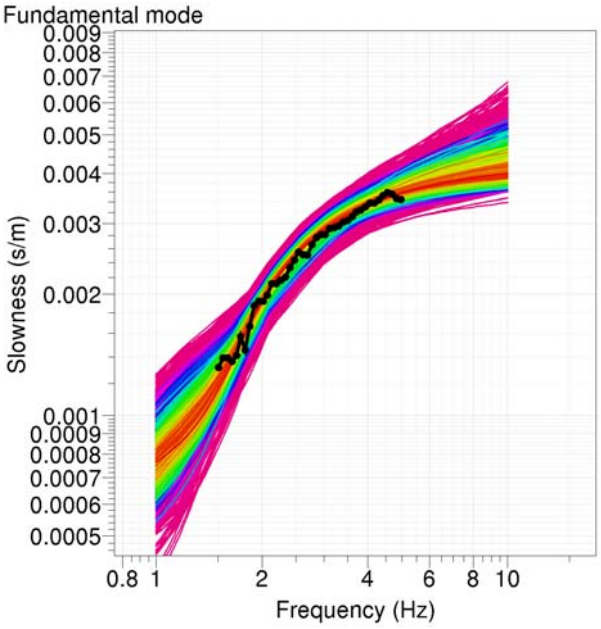

Figure 3.7.5: *An ensemble of dispersion curves of the fundamental mode of Love waves. Observed curves used in the inversion are in black, the color distinguishes the misfit value. Corresponding models are in the Figure 3.7.6.*

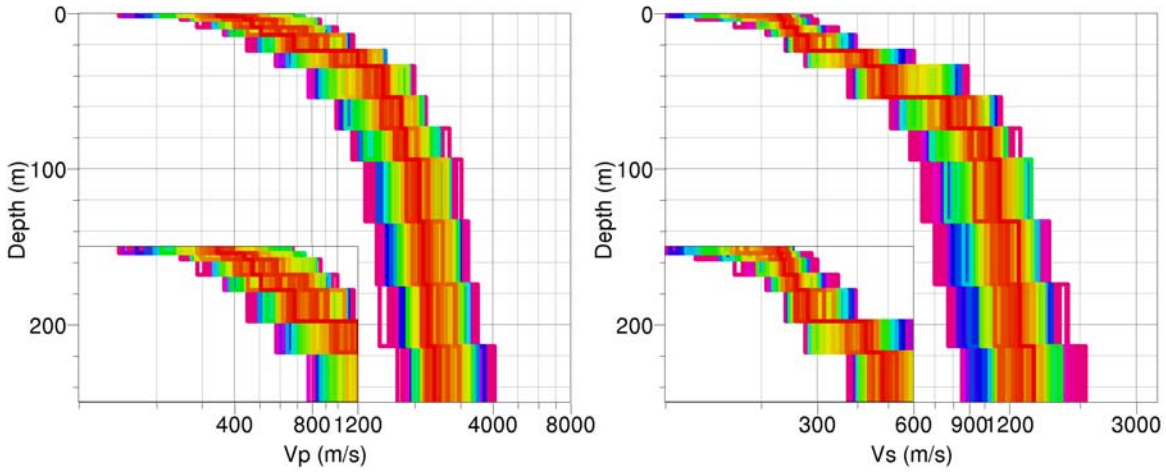

Figure 3.7.6: *An ensemble of inverted velocity profiles. First 50m are enlarged in the inset. Colors distinguish the misfit value in the same way as in the Figures 3.7.4, 3.7.5.*

3.8 Site VIS6

VIS6 has a maximal diameter of 180 m and consists of 18 stations, set up in two steps. It was located on the pavement of a cross-road with modest traffic in Visp.

Figure 3.8.1: *Sensor setup for array "VIS6" in Visp.*

Array processing

Recordings were processed by different high-resolution FK methods. It was possible to follow the dispersion curve of fundamental mode of Rayleigh wave down to 2Hz with FK method. All picked dispersion curves for Rayleigh waves are plotted in Figure 3.8.2. Note the agreement between different codes and methods. There was a problem matching DC curves obtained for the outer and inner rings. The overall quality of estimated DC is low, so the inversion has not been performed for this array. Array VIS6 is located close to the border of the sedimentary basin, so 2D/3D wave propagation effects could be responsible for the scatter in DC. Moreover, the measurement was strongly affected by anthropic noise, as it was located directly in the city.

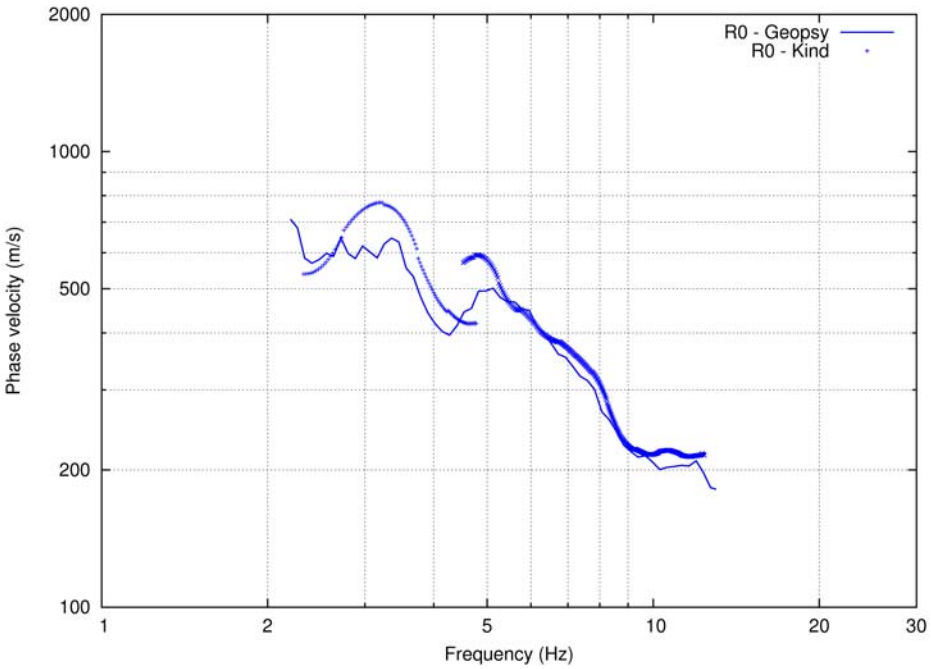

Figure 3.8.1**:** *Dispersion curves for VIS6 array: R0 stands for fundamental mode of Rayleigh waves.*

3.9 Site VIS7

VIS7 has a maximal diameter of 120 m and consists of 12 stations, all set up simultaneously. It was located on a crossroad in an area with very few traffic inside Visp.

Figure 3.9.1: *Sensor setup for array "VIS7" in Visp.*

Array processing

Recordings were processed by different high-resolution FK methods. It was possible to follow the dispersion curve of fundamental mode of Rayleigh wave down to 2Hz with FK method. All picked dispersion curves for Rayleigh waves are plotted in Figure 3.9.2. Note the agreement between different codes and methods. It was not possible to pick any Love dispersion curve with any method.

Ellipticity of Rayleigh waves was estimated using wavelet-based (TFA) method and FK method. All ellipticity curves are depicted in Figure 3.9.3. The peaks close to 2.5 Hz, 5 Hz, 9 Hz are artificial and probably related to some continuously operating machine in Lonza factory. FK curve is systematically bellow mean TFA curve for the whole frequency band.

Inversion

Models are parametrized by 18 layers of fixed thickness and a density of 2100kg/m^3 was used for the final inversion. It was possible to perform joint inversion of the DC (fundamental mode of Rayleigh waves) and ellipticity (fundamental Rayleigh mode) with a reasonable result (see Figure: 3.9.4). Mean TFA ellipticity was used in the inversion, as it was systematically preferred in the inversions.

Retrieved shear wave velocity profile (Figure 3.9.5) is reliable down to 50 m, as the scatter increases rapidly below 50 m.

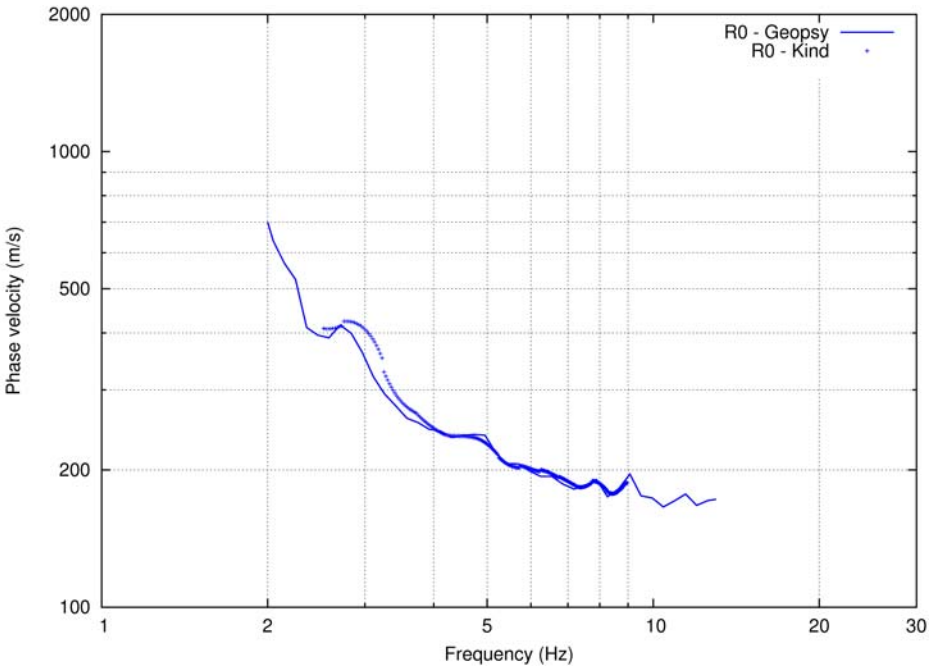

Figure 3.9.2**:** *Dispersion curves for VIS7 array: R0 stands for fundamental mode of Rayleigh waves*

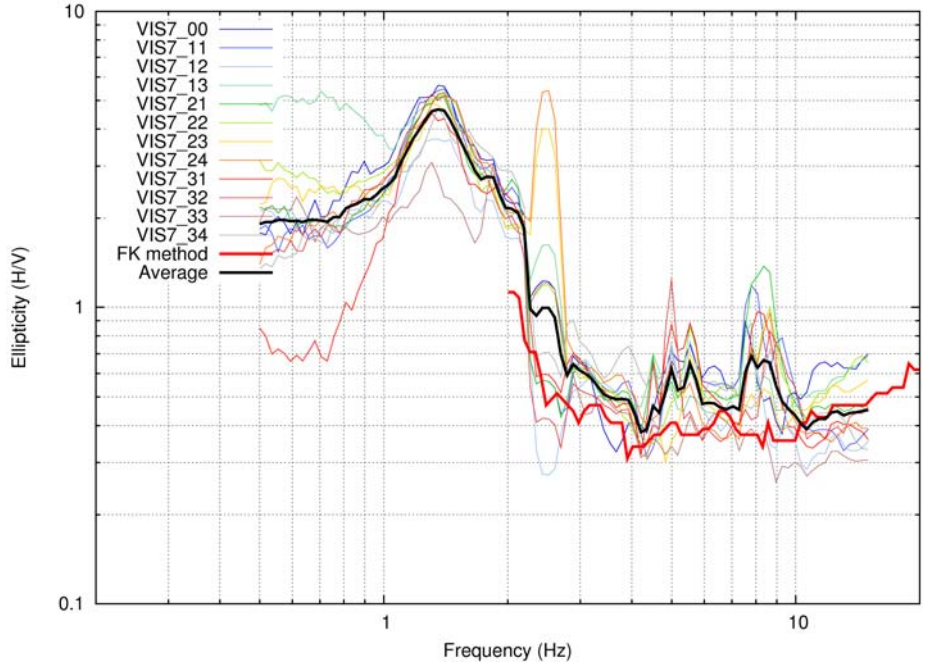

Figure 3.9.3**:** *Ellipticity curves for VIS7 array obtained by wavelet and FK method.*

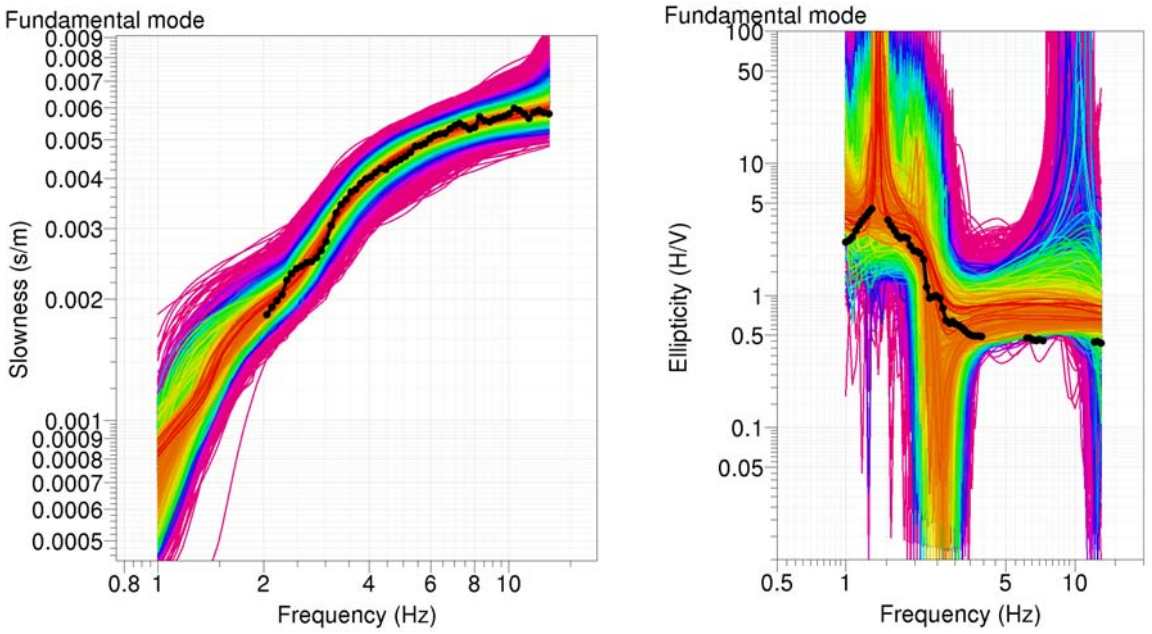

Figure 3.9.4: *An ensemble of dispersion curves (left) and ellipticities (right) of fundamental mode of Rayleigh waves. Observed curves used in the inversion are in black, the color distinguishes the misfit value. Corresponding models are in the Figure 3.9.5*

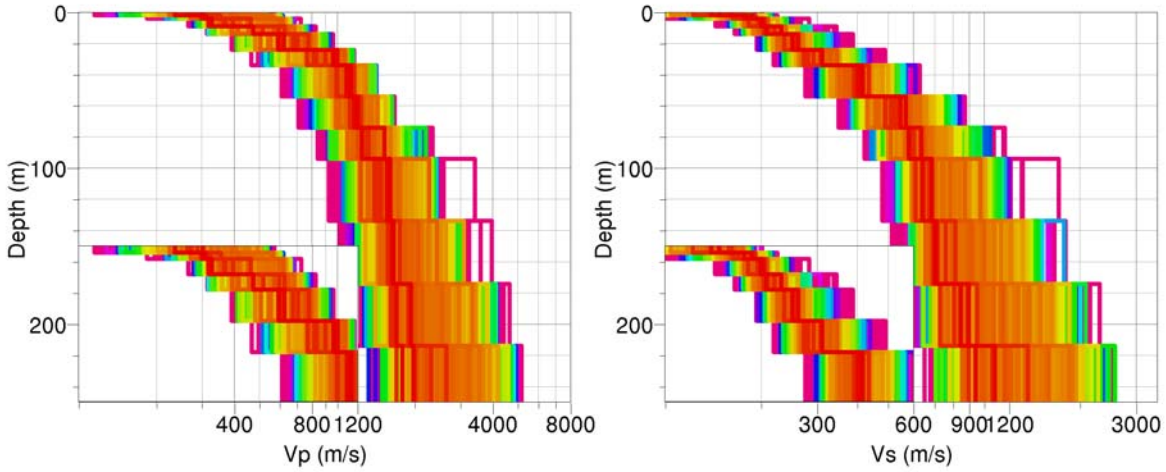

Figure 3.9.5: *An ensemble of inverted velocity profiles. First 50m are enlarged in the inset. Colors distinguish the misfit value in the same way as in the Figure 3.9.4.*

3.10 Site VIS8

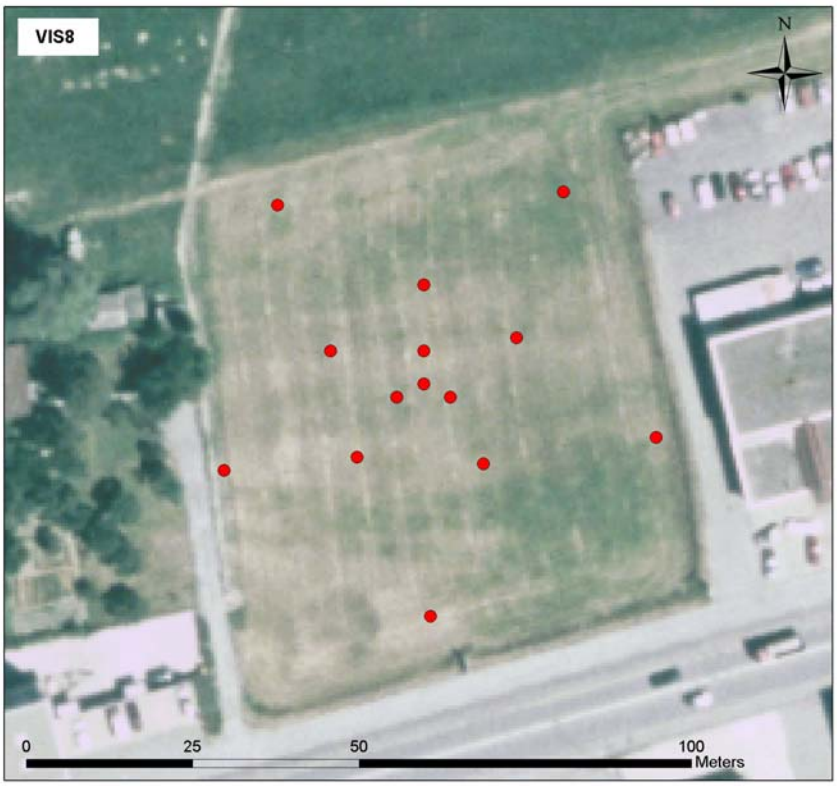

VIS8 has a maximal diameter of 70 m and consists of 14 stations, all set up simultaneously. It was located a little bit outside the centre of Visp, on a free piece of land between two industrial buildings.

Figure 3.10.1: *Sensor setup for array "VIS8" in Visp.*

Array processing

Recordings were processed by different high-resolution FK methods. It was possible to follow the dispersion curve of fundamental mode of both Rayleigh and Love wave down to 3Hz with FK method. It was also possible to pick a higher mode. All picked dispersion curves for both Love and Rayleigh waves are plotted in Figure 3.10.2. Note the remarkable agreement between different codes and methods.

Ellipticity of Rayleigh waves was estimated using wavelet-based (TFA) method and FK method. All ellipticity curves are depicted in Figure 3.10.3. The peaks close to 2.5 Hz, 5 Hz, 9 Hz are artificial and probably related to some continuously operating machine in Lonza factory. The mean TFA curve is in good agreement with FK curve, however the scatter between curves retrieved by TFA method is high from station to station.

Inversion

Models are parametrized by 18 layers of fixed thickness and a density of 2100kg/m^3 was used for the final inversion. It was possible to perform joint inversion of the DC (fundamental and first higher mode for Rayleigh and fundamental mode for Love waves) and ellipticity (fundamental Rayleigh mode) with a reasonable result (see Figures: 3.10.4, 3.10.5), except for the ellipticity.

Retrieved shear wave velocity profile (Figure 3.10.6) is reliable down to 50 m, as the scatter increases rapidly below 50 m.

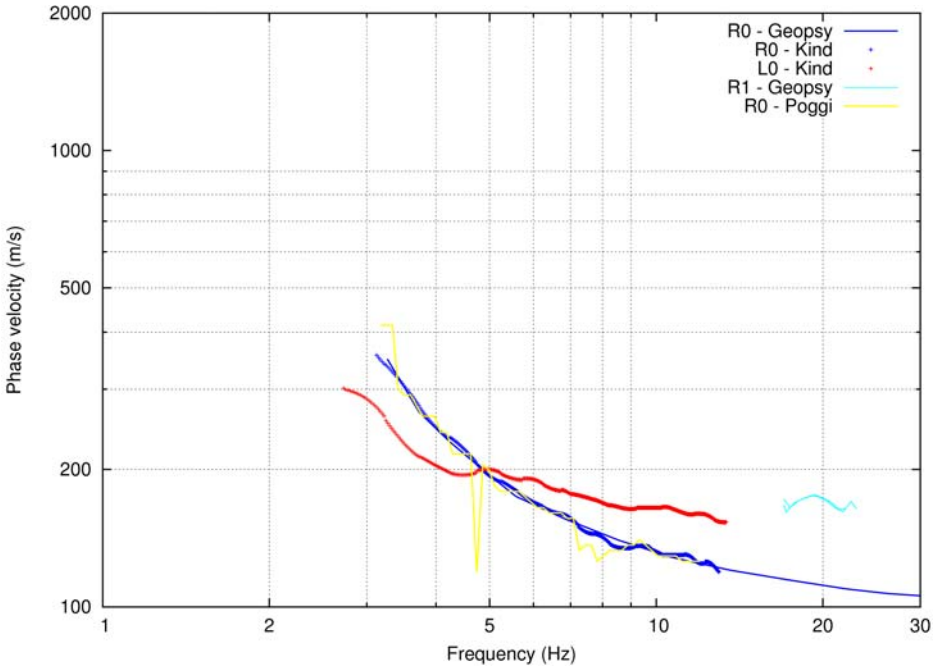

Figure 3.10.2**:** *Dispersion curves for VIS8 array: R0 stands for fundamental mode of Rayleigh waves, L0 stands for fundamental mode of Love waves, R1 denotes higher mode of Rayleigh waves.*

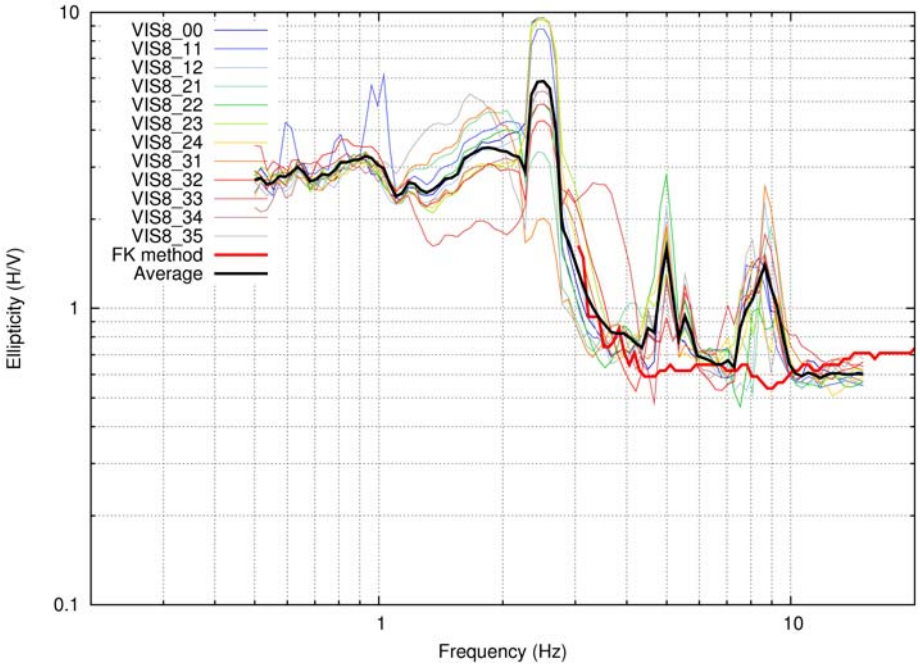

Figure 3.10.3**:** *Ellipticity curves for VIS8 array obtained by wavelet and FK method.*

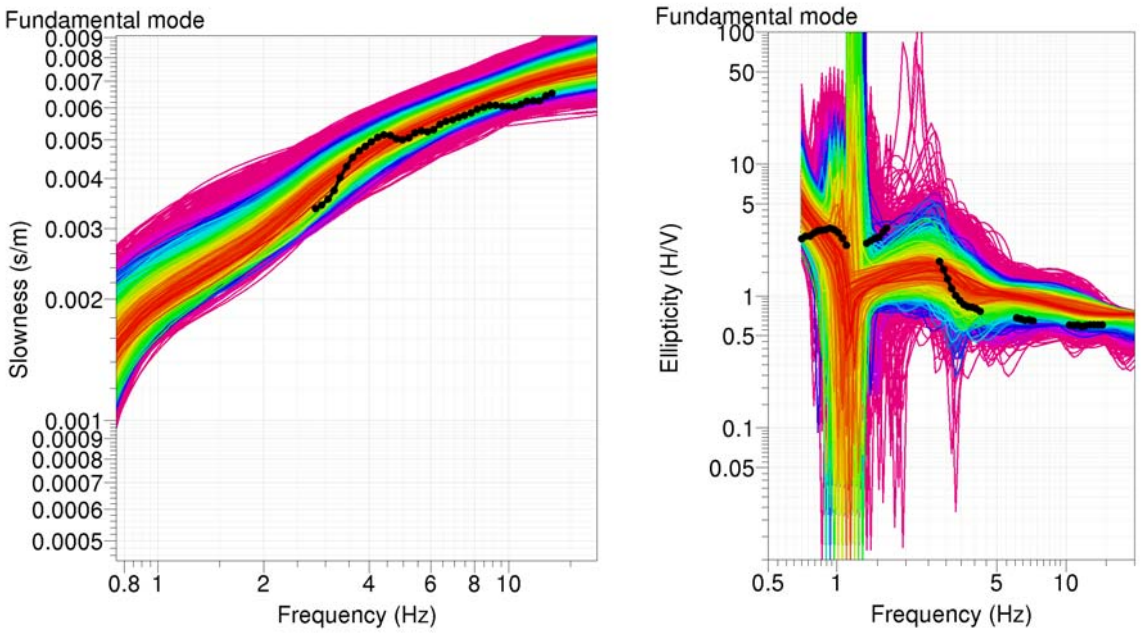

Figure 3.10.4: *An ensemble of dispersion curves (left) of fundamental mode of Love waves and ellipticities (right) of fundamental mode of Rayleigh waves. Observed curves used in the inversion are in black, the color distinguishes the misfit value. Corresponding models are in the Figure 3.10.6.*

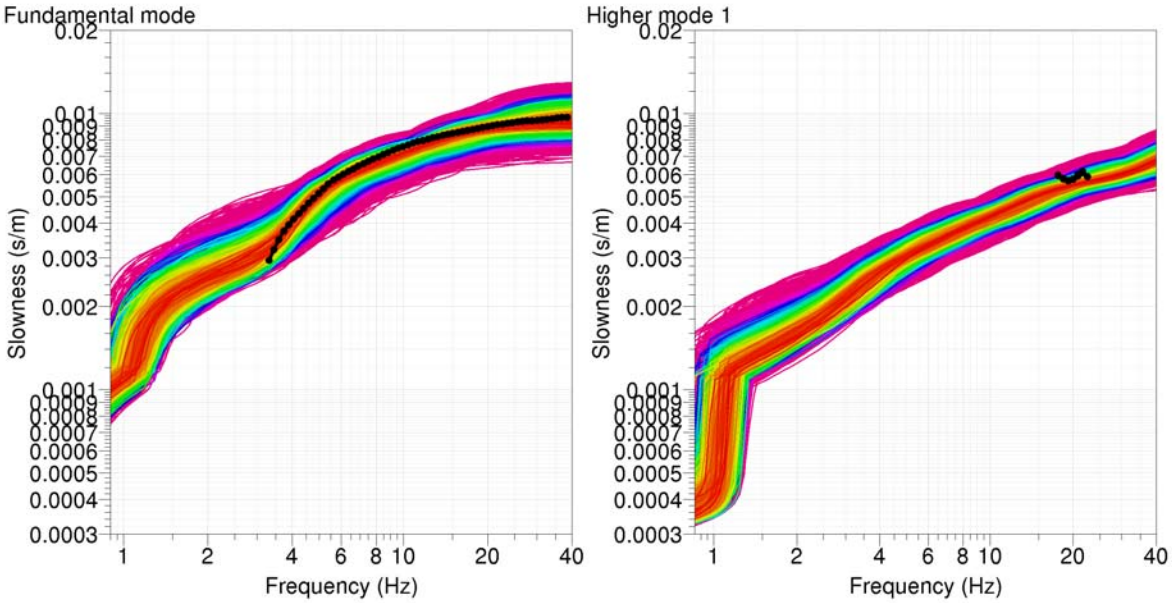

Figure 3.10.5: *An ensemble of dispersion curves of the fundamental (left) and first higher (right) mode Rayleigh waves. Observed curves used in the inversion are in black, the color distinguishes the misfit value. Corresponding models are in the Figure 3.10.6.*

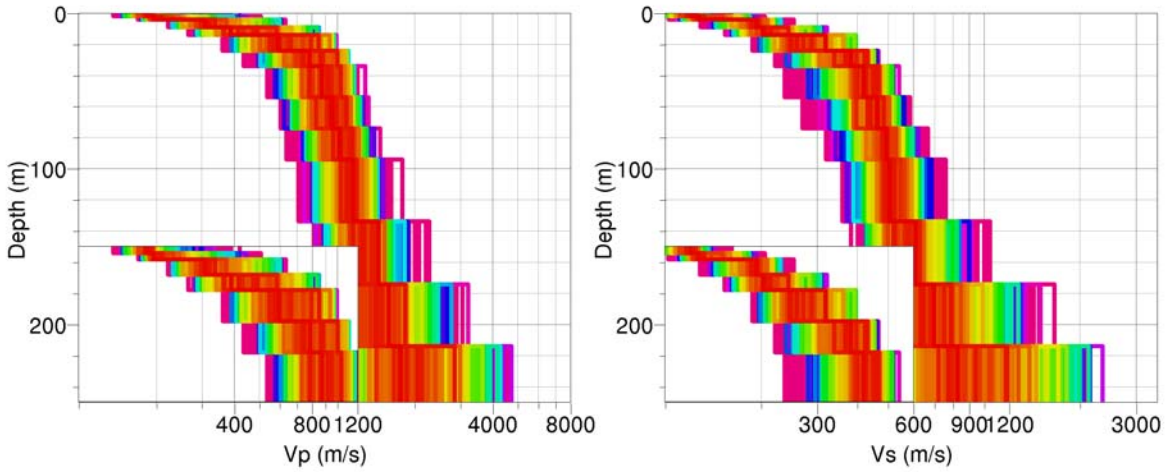

Figure 3.10.6: *An ensemble of inverted velocity profiles. First 50m are enlarged in the inset. Colors distinguish the misfit value in the same way as in the Figures 3.10.4, 3.10.5.*

3.11 Site StN_Array1

StN_Array1 has a maximal diameter of 240 m and consists of 25 stations, set up in three steps. It was located in the old part of St. Niklaus, mainly on asphalt. In winter 07/08 and 08/09 one of the temporary stations (STNI1) was installed in the cellar of the manse right in the centre of this array.

Figure 3.11.1: *Sensor setup for array "StN_Array1" in St. Niklaus.*

Array processing

Recordings were processed by different high-resolution FK methods. It was possible to follow the dispersion curve of fundamental mode of both Rayleigh and Love wave down to 2Hz with FK method. All picked dispersion curves for both Love and Rayleigh waves are plotted in Figure 3.11.2. Note the remarkable agreement between different codes and methods.

Ellipticity of Rayleigh waves was estimated using wavelet-based (TFA) method and FK method. All ellipticity curves are depicted in Figure 3.11.3. The scatter between curves retrieved by TFA method is high from station to station. The mean TFA curve is in good agreement with FK curve.

Inversion

Models are parametrized by 15 layers of fixed thickness and a density of 2100kg/m^3 was used for the final inversion. It was possible to perform joint inversion of the DC (fundamental for both Rayleigh and Love waves) and ellipticity (fundamental Rayleigh mode) with a reasonable result (see Figures: 3.11.4, 3.11.5), except for the ellipticity, which is not fitted well. Mean TFA ellipticity was used in the inversion.

Retrieved shear wave velocity profile (Figure 3.11.6) is reliable down to 80 m, as the scatter increases rapidly below 80 m.

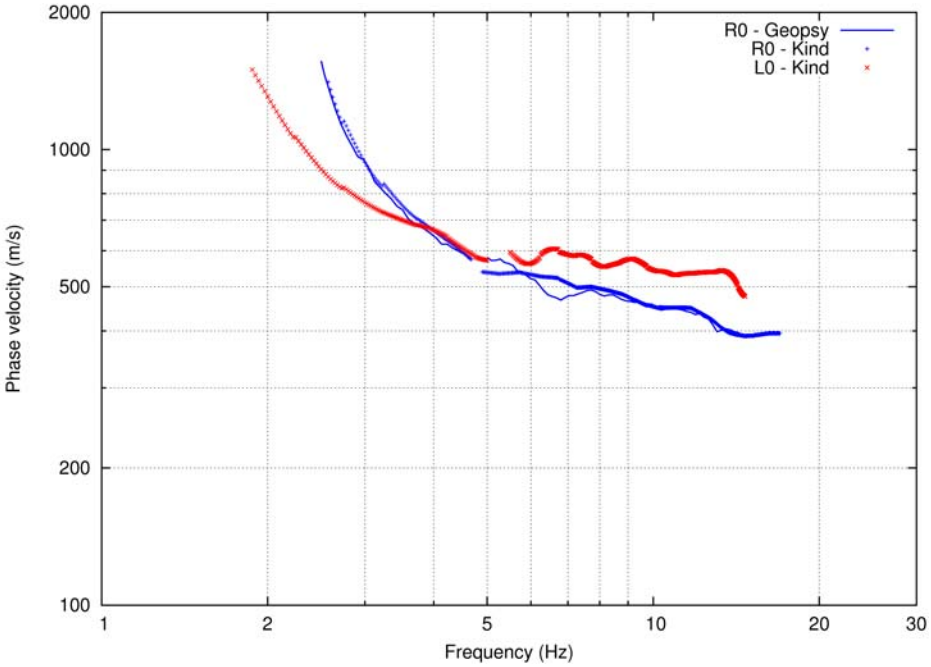

Figure 3.11.2**:** *Dispersion curves for StN_Array1 array: R0 stands for fundamental mode of Rayleigh waves, L0 stands for fundamental mode of Love waves.*

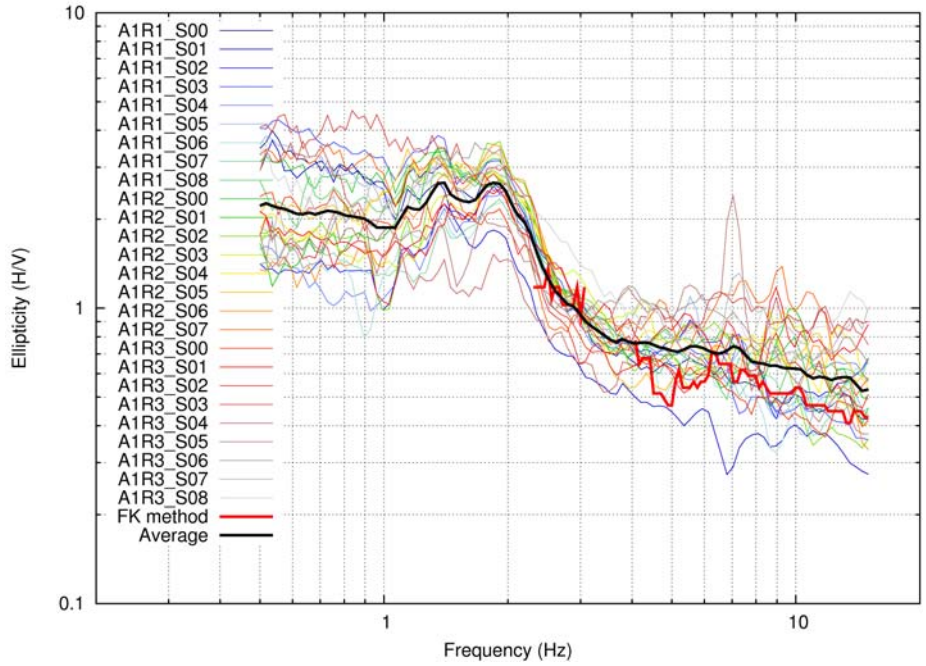

Figure 3.11.3: *Ellipticity curves for StN_Array1 array obtained by wavelet and FK method.*

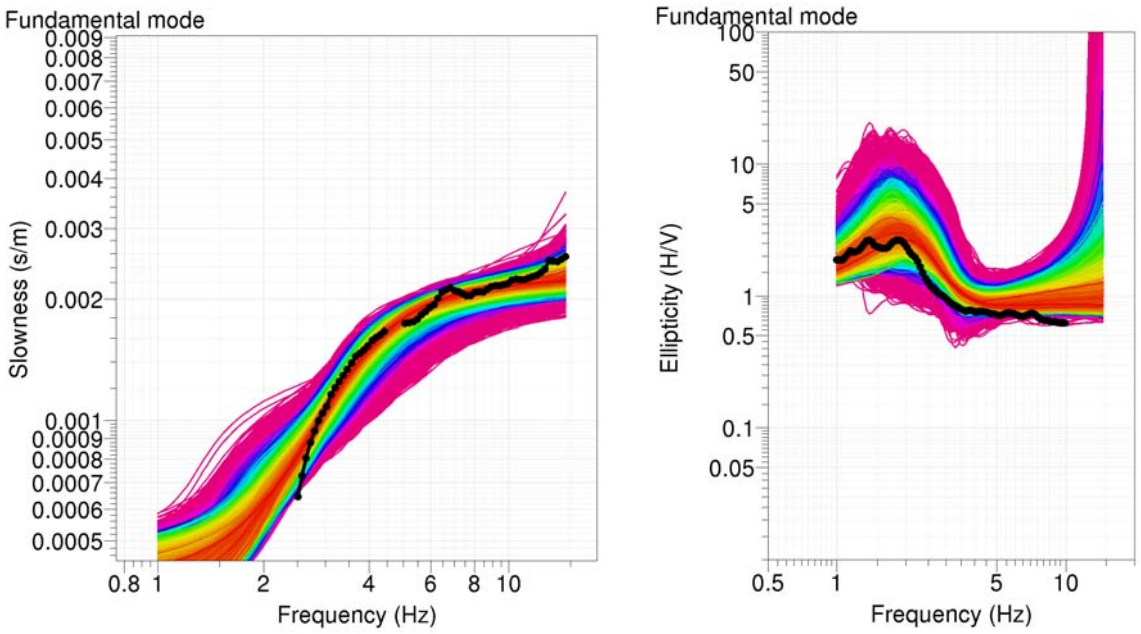

Figure 3.11.4: *An ensemble of dispersion curves (left) and ellipticities (right) of fundamental mode of Rayleigh waves. Observed curves used in the inversion are in black, the color distinguishes the misfit value. Corresponding models are in the Figure 3.11.6.*

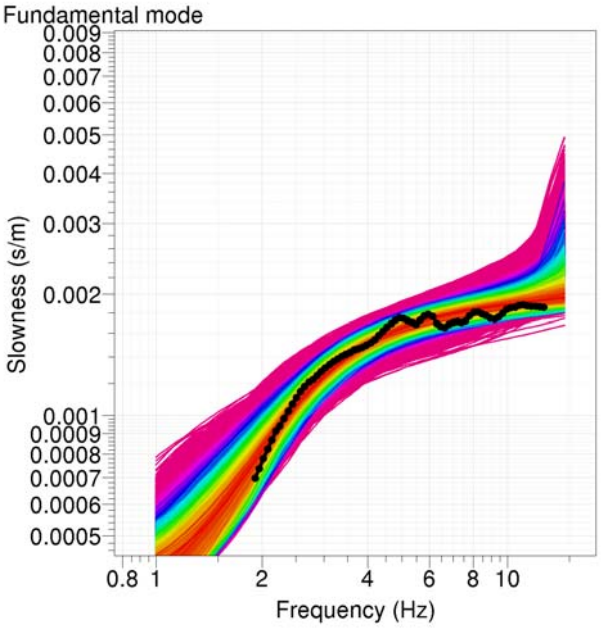

Figure 3.11.5: *An ensemble of dispersion curves of the fundamental mode of Love waves. Observed curves used in the inversion are in black, the color distinguishes the misfit value. Corresponding models are in the Figure 3.11.6.*

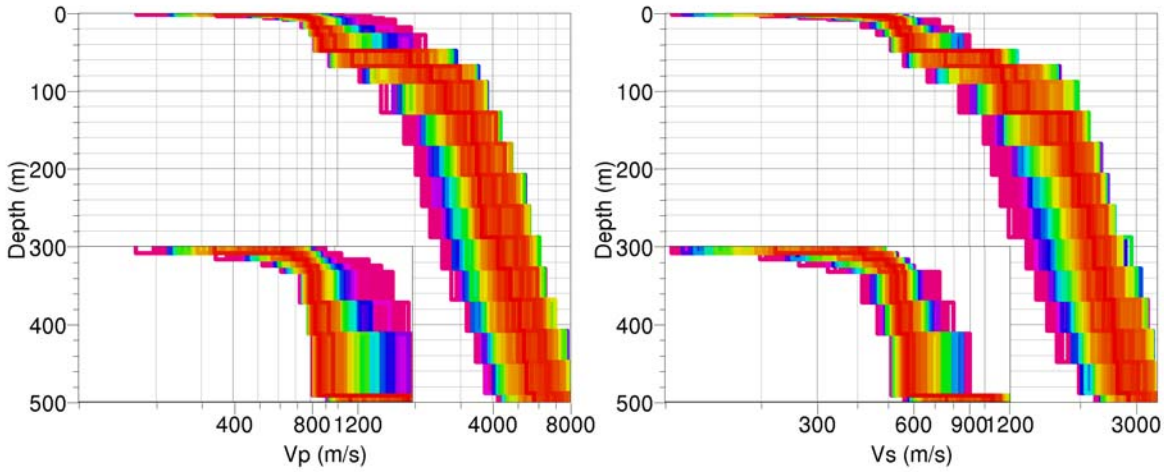

Figure 3.11.6: *An ensemble of inverted velocity profiles. First 50m are enlarged in the inset. Colors distinguish the misfit value in the same way as in the Figures 3.11.4, 3.11.5.*

3.12 Site StN_Array2

StN_Array2 has a maximal diameter of 200 m and consists of 17 stations, set up in two steps. It was located partly on grassland and partly on streets a little bit outside the centre of St. Niklaus.

Figure 3.12.1: *Sensor setup for array "StN_Array2" in St. Niklaus.*

Array processing

Recordings were processed by different high-resolution FK methods. It was possible to follow the dispersion curve of fundamental mode of both Rayleigh and Love wave down to 2.1Hz with FK method. It was also possible to pick a higher mode. All picked dispersion curves for both Love and Rayleigh waves are plotted in Figure 3.12.2. Note the remarkable agreement between different codes and methods.

Ellipticity of Rayleigh waves was estimated using wavelet-based (TFA) method and FK method. All ellipticity curves are depicted in Figure 3.12.3. The scatter between curves retrieved by TFA method is high from station to station. The mean TFA curve is in good agreement with FK curve.

Inversion

Models are parametrized by 15 layers of fixed thickness and a density of 2100kg/m^3 was used for the final inversion. It was possible to perform joint inversion of the DC (fundamental for both Rayleigh and Love waves) and ellipticity (fundamental Rayleigh mode) with a reasonable result (see Figures: 3.12.4, 3.12.5), except for the ellipticity, which is not fitted so well. Mean TFA ellipticity was used in the inversion. It was not possible to address the mode number of the observed higher mode DC (Figure 3.12.2).

Retrieved shear wave velocity profile (Figure 3.12.6) is reliable down to 100 m, as the scatter increases rapidly below 100 m.

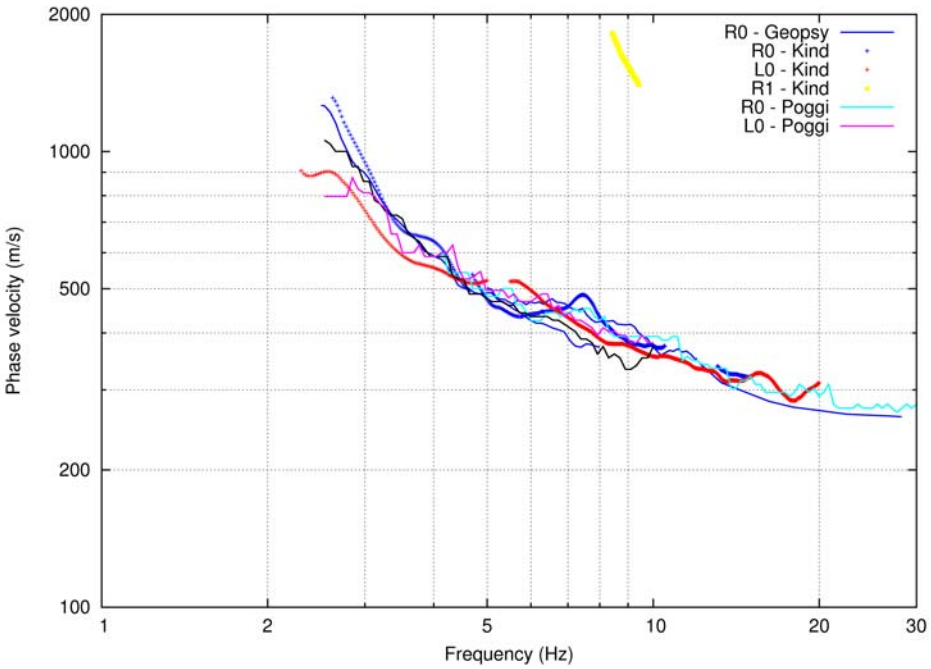

Figure 3.12.2**:** *Dispersion curves for StN_Array2 array: R0 stands for fundamental mode of Rayleigh waves, L0 stands for fundamental mode of Love waves, R1 denotes higher mode of Rayleigh waves.*

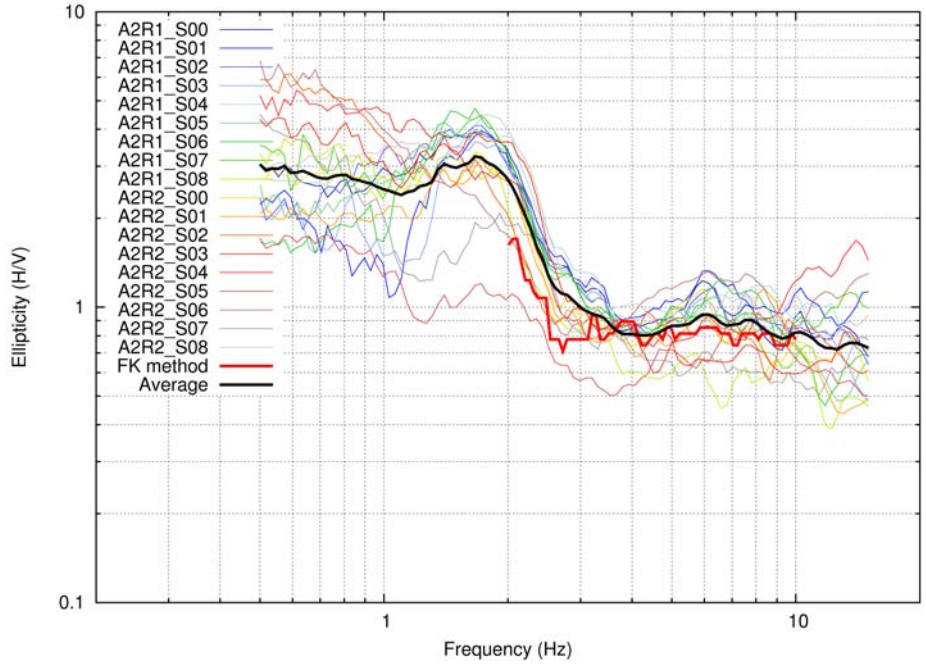

Figure 3.12.3: *Ellipticity curves for StN_Array2 array obtained by wavelet and FK method.*

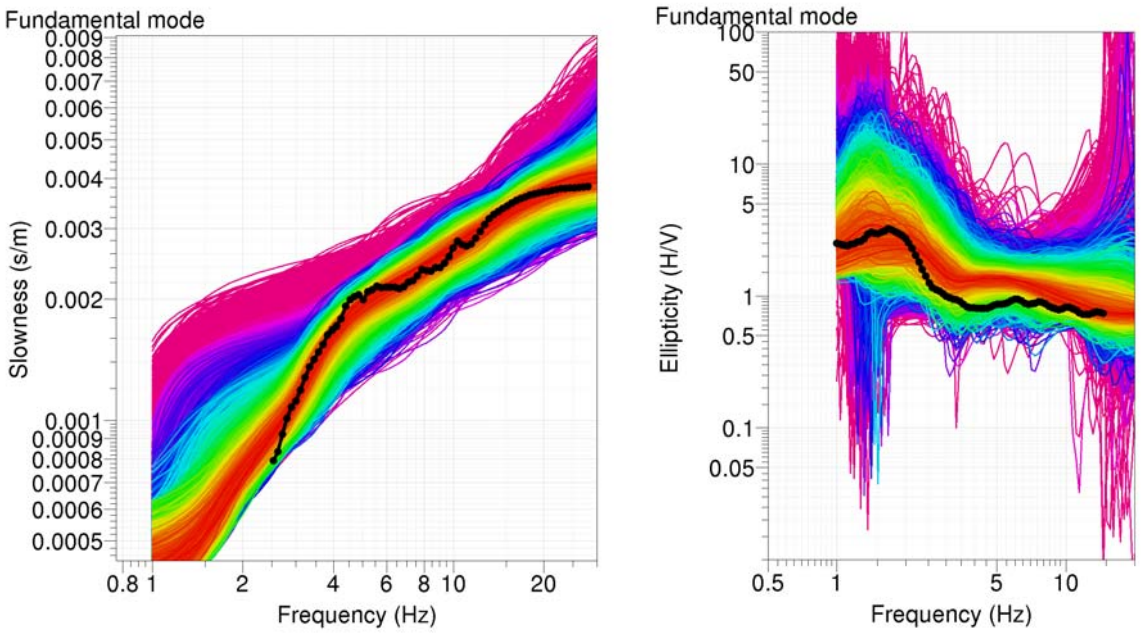

Figure 3.12.4: *An ensemble of dispersion curves (left) and ellipticities (right) of fundamental mode of Rayleigh waves. Observed curves used in the inversion are in black, the color distinguishes the misfit value. Corresponding models are in the Figure 3.12.6.*

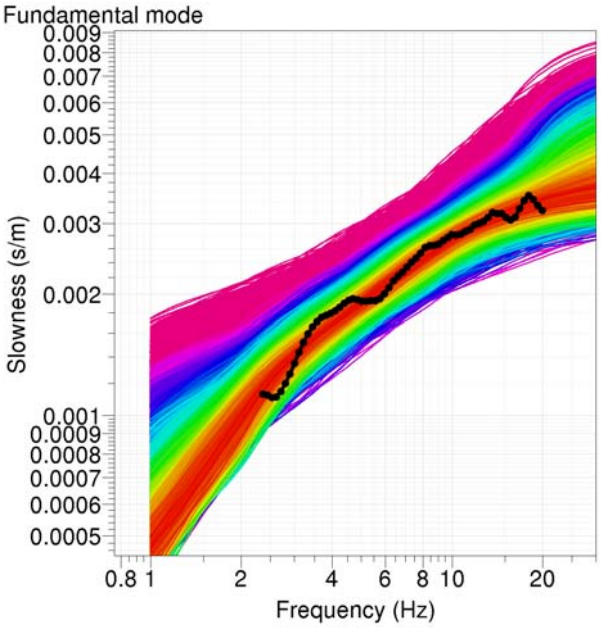

Figure 3.12.5: *An ensemble of dispersion curves of the fundamental mode of Love waves. Observed curves used in the inversion are in black, the color distinguishes the misfit value. Corresponding models are in the Figure 3.12.6.*

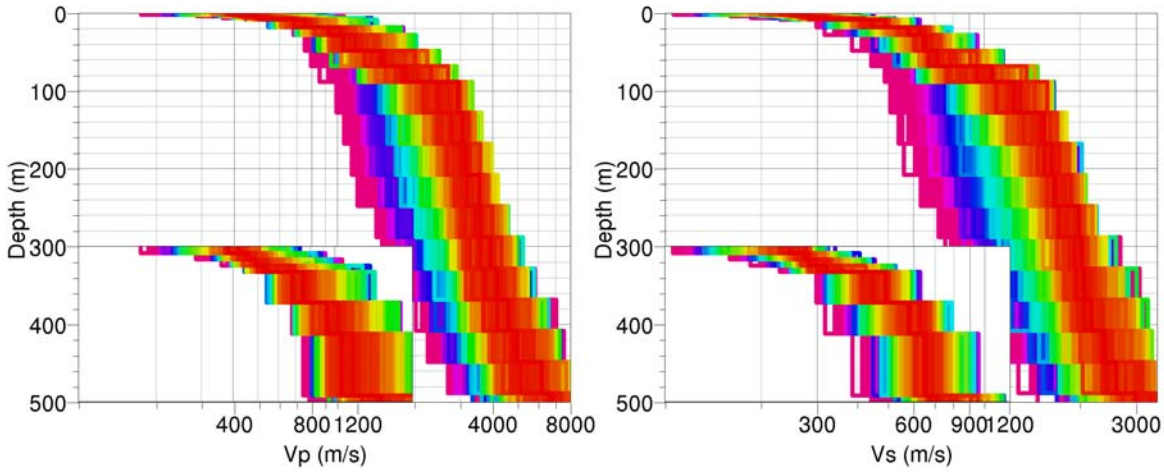

Figure 3.12.6: *An ensemble of inverted velocity profiles. First 50m are enlarged in the inset. Colors distinguish the misfit value in the same way as in the Figures 3.12.4, 3.12.5.*

3.13 Site StN_Array3

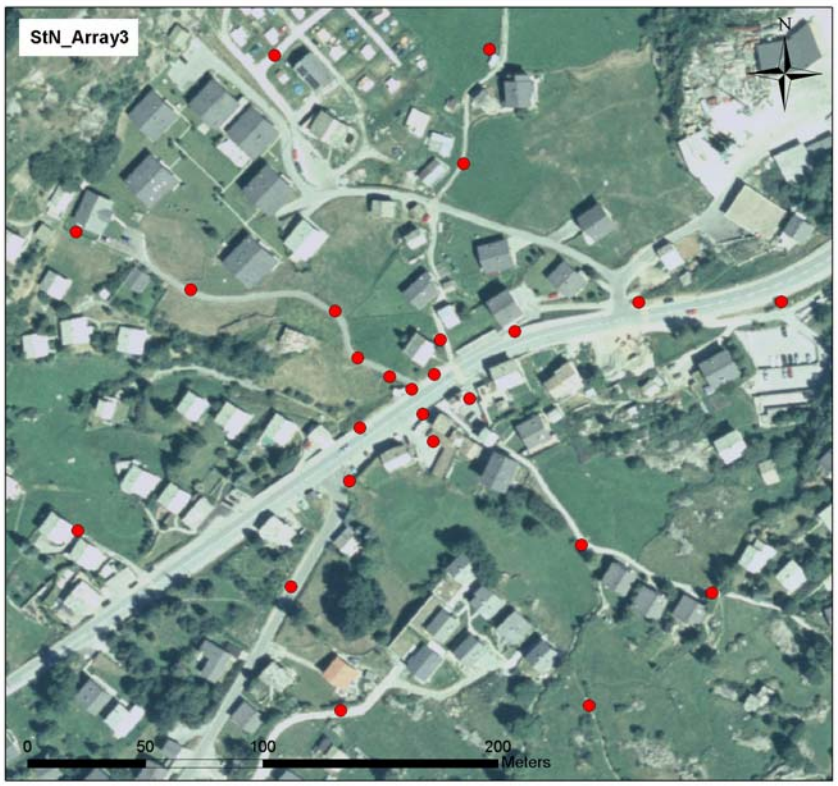

StN_Array3 has a maximal diameter of 300 m and consists of 25 stations, set up in three steps. It was located on an asphalt-street and a net of small paths in Niedergrächen.

Figure 3.13.1: *Sensor setup for array "StN_Array3" in Niedergrächen.*

Array processing

Recordings were processed by different high-resolution FK methods. It was possible to follow the dispersion curve of fundamental mode of both Rayleigh and Love wave down to 2Hz with FK method. All picked dispersion curves for both Love and Rayleigh waves are plotted in Figure 3.13.2. Note the difference between DC of Rayleigh fundamental mode estimated with different methods. In particular, DC estimated by method of Kind et al (2005) deviates from others in this case. The DC estimated by *Geopsy* was used further in the inversion as it agrees with independent estimate made with method of Poggi and Fäh (2010). Moreover, there was a problem matching Love DC curves obtained for the different rings. We did not introduce any smoothing, all three chunks were used in the inversion.

Ellipticity of Rayleigh waves was estimated using wavelet-based (TFA) method and FK method. All ellipticity curves are depicted in Figure 3.13.3. The scatter between curves retrieved by TFA method is high from station to station. The mean TFA curve is in good agreement with FK curve.

Inversion

Models are parametrized by 20 layers of fixed thickness and a density of 2100kg/m^3 was used for the final inversion. It was possible to perform joint inversion of the DC (fundamental for both Rayleigh and Love waves) and ellipticity (fundamental Rayleigh mode) with a reasonable result (see Figures: 3.13.4, 3.13.5). Mean TFA ellipticity was used in the inversion.

Retrieved shear wave velocity profile (Figure 3.13.6) is reliable down to 100 m, as the scatter increases rapidly below 100 m.

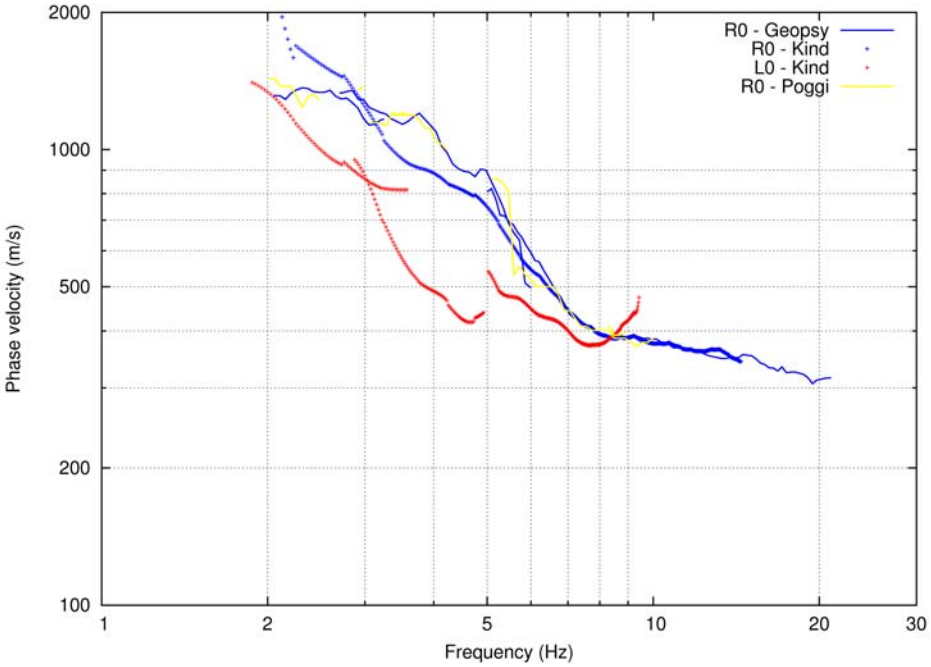

Figure 3.13.2**:** *Dispersion curves for StN_Array3 array: R0 stands for fundamental mode of Rayleigh waves, L0 stands for fundamental mode of Love waves.*

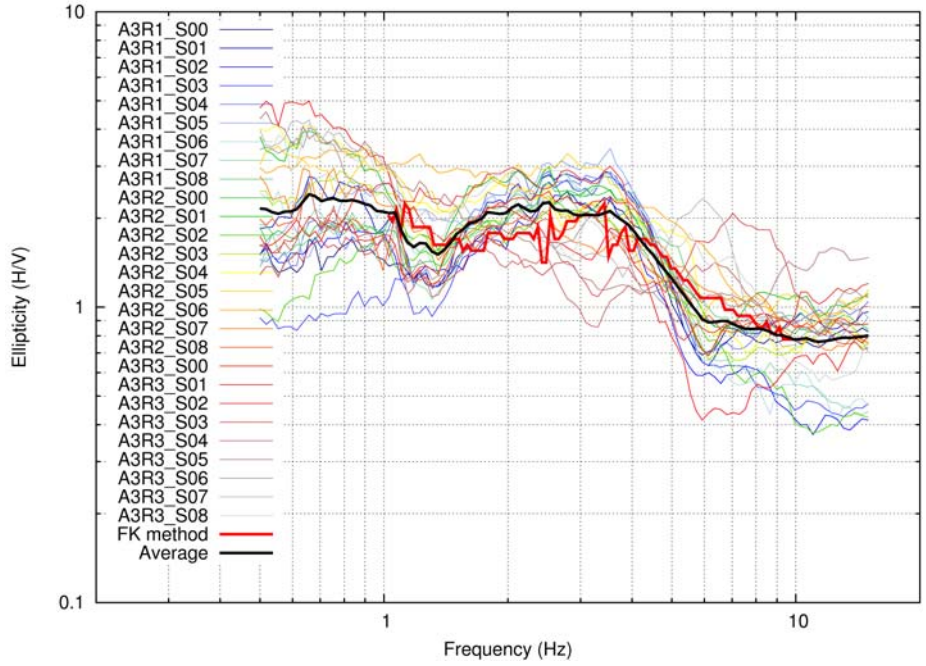

Figure 3.13.3: *Ellipticity curves for StN_Array3 array obtained by wavelet and FK method.*

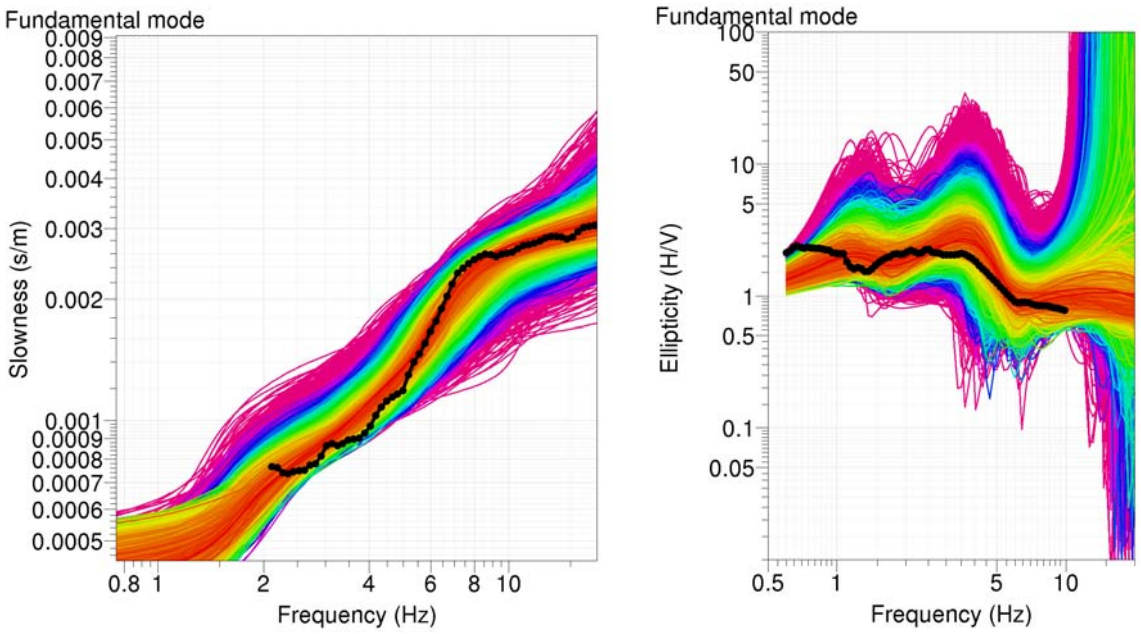

Figure 3.13.4: *An ensemble of dispersion curves (left) and ellipticities (right) of fundamental mode of Rayleigh waves. Observed curves used in the inversion are in black, the color distinguishes the misfit value. Corresponding models are in the Figure 3.13.6.*

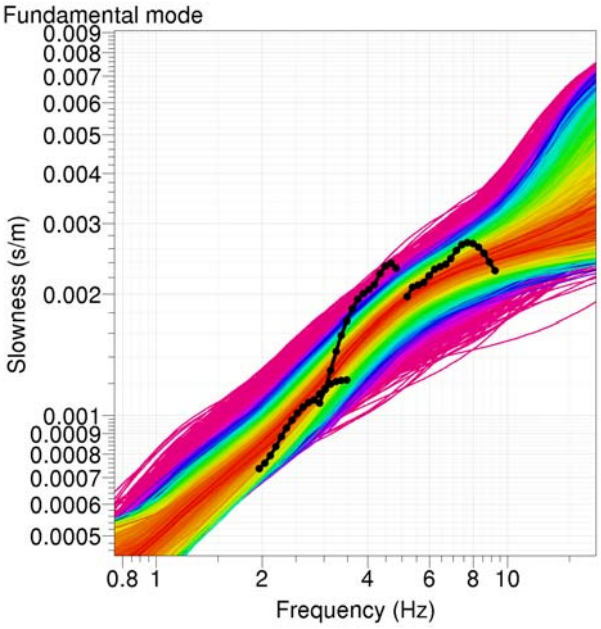

Figure 3.13.5: *An ensemble of dispersion curves of the fundamental mode of Love waves. Observed curves used in the inversion are in black, the color distinguishes the misfit value. Corresponding models are in the Figure 3.13.6.*

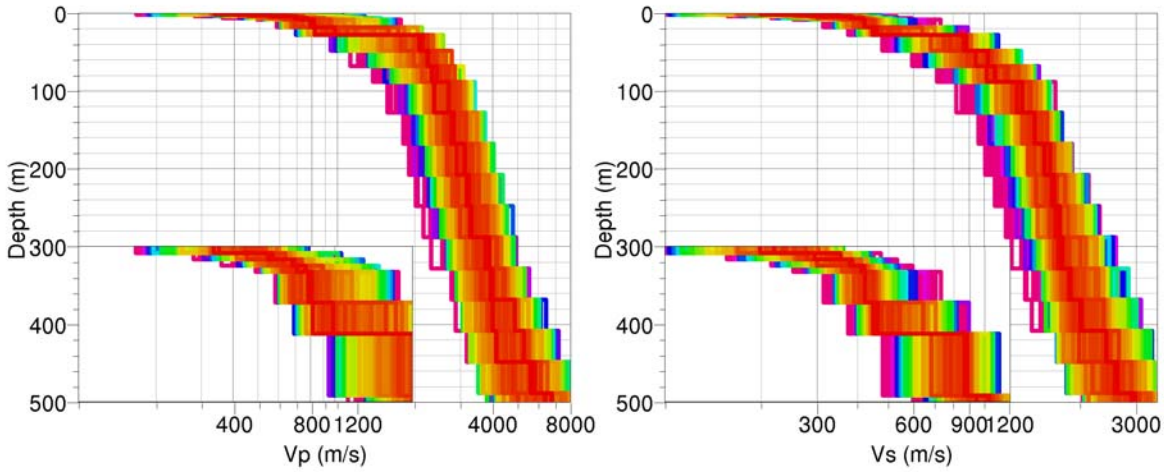

Figure 3.13.6: *An ensemble of inverted velocity profiles. First 50m are enlarged in the inset. Colors distinguish the misfit value in the same way as in the Figures 3.13.4, 3.13.5.*

3.14 Site STN1

STN1 has a maximal diameter of 200 m and consists of 21 stations, set up in two steps. It was located partly on grassland and partly on asphalt-streets, on a slope northward above St. Niklaus.

Figure 3.14.1: *Sensor setup for array "STN1" in St. Niklaus.*

Array processing

Recordings were processed by different high-resolution FK methods. It was possible to follow the dispersion curve of fundamental mode of both Rayleigh and Love wave down to 2.5 Hz with FK method. It was also possible to pick a higher mode of Love waves. All picked dispersion curves for both Love and Rayleigh waves are plotted in Figure 3.14.2. The agreement between different codes and methods is not so good as in other cases. Distribution of points picked in wavenumber domain were broad, so the uncertainty of DC is higher in this case.

Ellipticity of Rayleigh waves was estimated using wavelet-based (TFA) method and FK method. All ellipticity curves are depicted in Figure 3.14.3. The mean TFA curve is in good agreement with FK curve.

Inversion

Models are parametrized by 15 layers of fixed thickness and a density of 2100kg/m^3 was used for the final inversion. It was possible to perform joint inversion of the DC (fundamental and first higher mode for Love and fundamental mode for Rayleigh waves) and ellipticity (fundamental Rayleigh mode) with a reasonable result (see Figures: 3.14.4, 3.14.5), except for the Love wave fundamental mode, which was not fitted at all. It was not possible to pick Love fundamental neither with method of Poggi and Fäh (2010) nor with *Geopsy*, so the reliability of this DC is low.

Retrieved shear wave velocity profile (Figure 3.14.6) is reliable down to 120 m, as the scatter increases rapidly below 120 m.

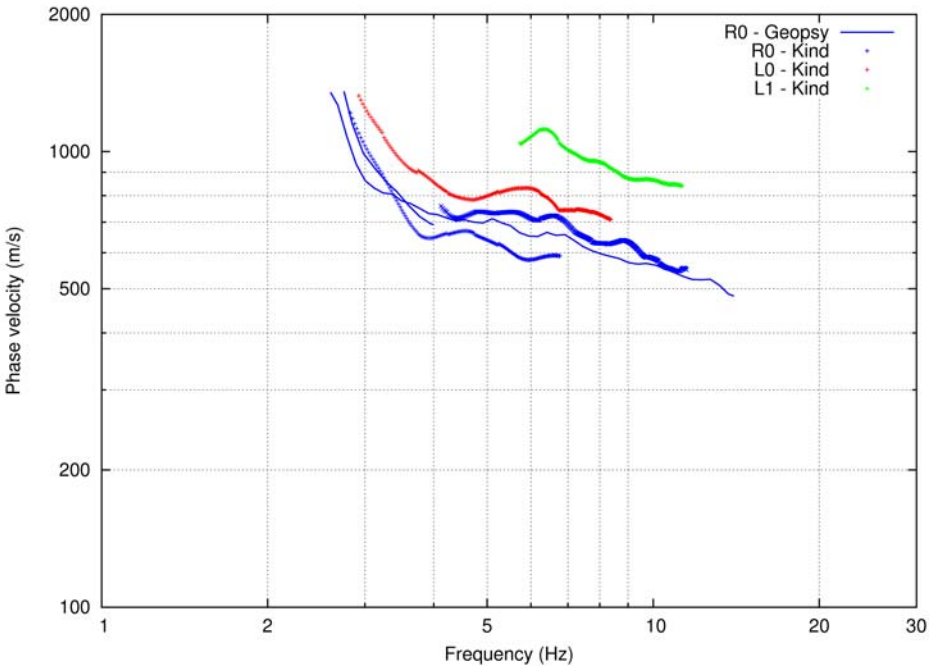

Figure 3.14.2**:** *Dispersion curves for STN1 array: R0 stands for fundamental mode of Rayleigh waves, L0 stands for fundamental mode of Love waves, L1 denotes higher mode of Love waves.*

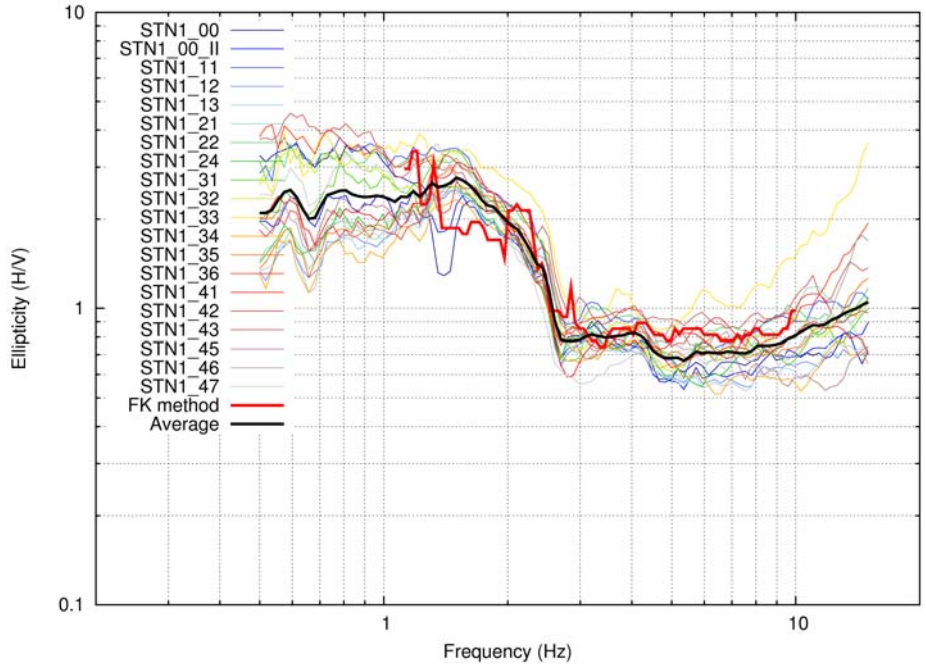

Figure 3.14.3: *Ellipticity curves for STN1 array obtained by wavelet and FK method.*

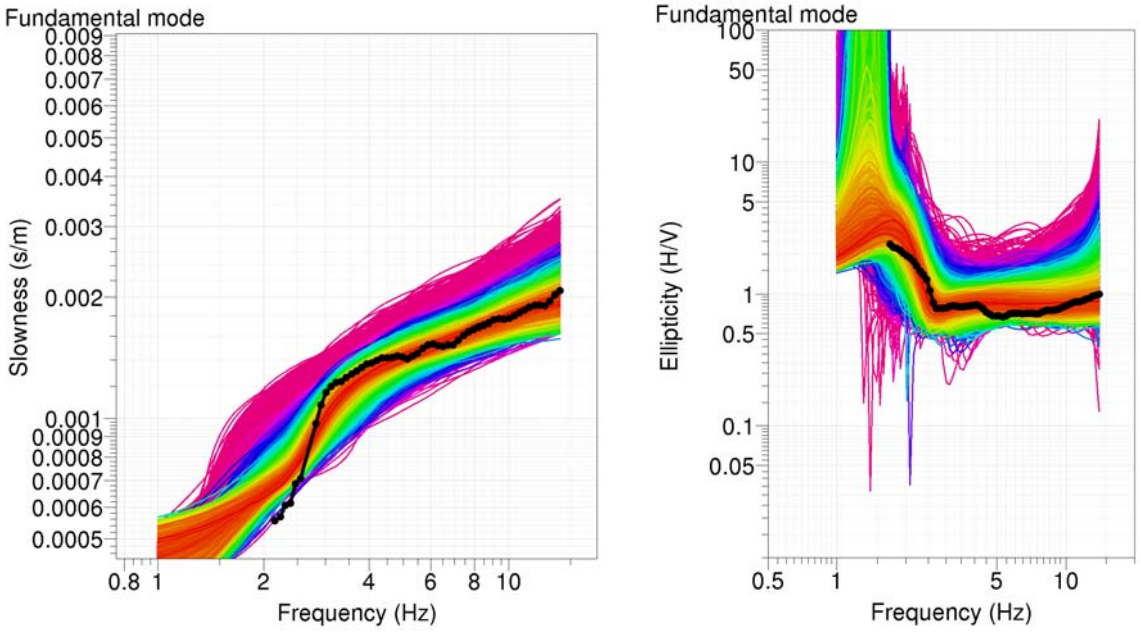

Figure 3.14.4: *An ensemble of dispersion curves (left) and ellipticities (right) of fundamental mode of Rayleigh waves. Observed curves used in the inversion are in black, the color distinguishes the misfit value. Corresponding models are in the Figure 3.14.6.*

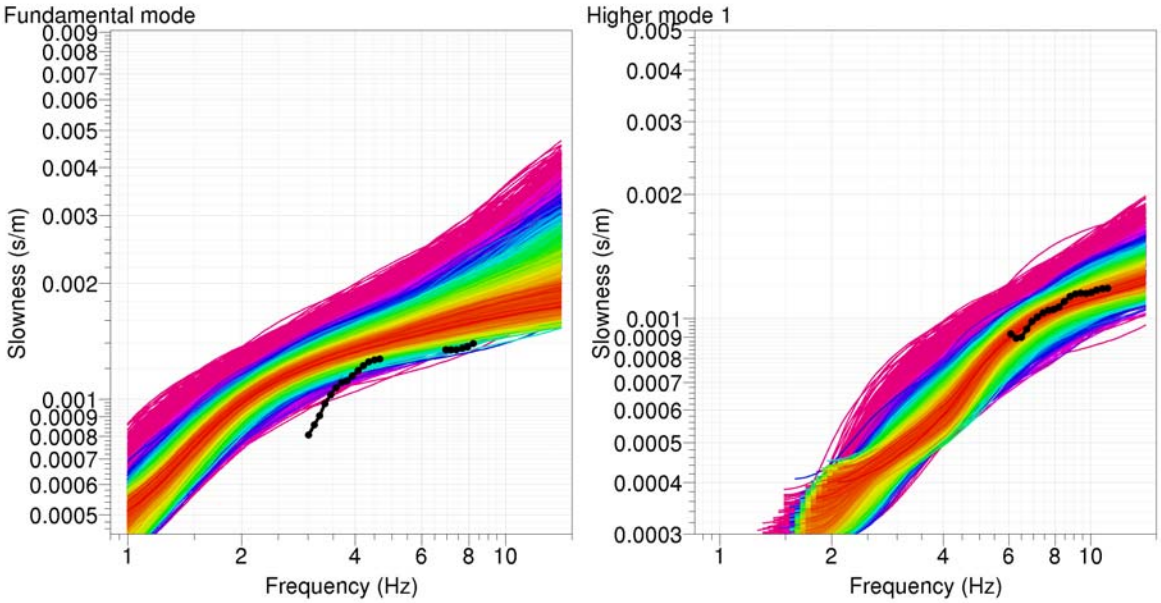

Figure 3.14.5: *An ensemble of dispersion curves of the fundamental (left) and first higher (right) mode of Love waves. Observed curves used in the inversion are in black, the color distinguishes the misfit value. Corresponding models are in the Figure 3.14.6.*

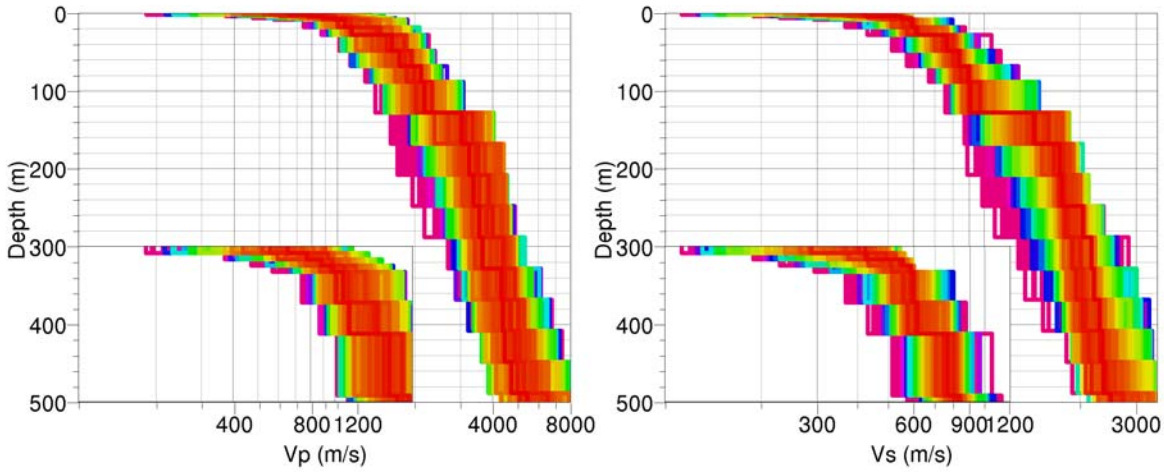

Figure 3.14.6: *An ensemble of inverted velocity profiles. First 50m are enlarged in the inset. Colors distinguish the misfit value in the same way as in the Figures 3.14.4, 3.14.5.*

3.15 Site STN2

STN2 has a maximal diameter of 120 m and consists of 14 stations, all set up simultaneously. It was located on grassland and small paths in the small village Bodme on the slope between St. Niklaus and Grächen.

Figure 3.15.1: *Sensor setup for array "STN2" in St. Niklaus/Bodme.*

Array processing

Recordings were processed by different high-resolution FK methods. It was possible to follow the dispersion curve of fundamental mode of both Rayleigh and Love wave down to 4 Hz with FK method. It was also possible to pick a higher mode of Love waves. All picked dispersion curves for both Love and Rayleigh waves are plotted in Figure 3.15.2. Distributions of points picked in wavenumber domain were broad, so the uncertainty of DC is higher in this case. Especially, in case of Love fundamental mode DC, it was very difficult to pick a single curve.

Ellipticity of Rayleigh waves was estimated using wavelet-based (TFA) method and FK method. All ellipticity curves are depicted in Figure 3.15.3. The mean TFA curve is in good agreement with FK curve (for the frequency band of FK curve available).

Inversion

Models are parametrized by 20 layers of fixed thickness and a density of 2100kg/m^3 was used for the final inversion. It was possible to perform joint inversion of the DC (fundamental mode for Rayleigh waves) and ellipticity (fundamental Rayleigh mode) with a reasonable result (see Figure: 3.15.4). It was not possible to fit the Love wave fundamental mode (not presented here). The pick of Love DC was however very uncertain in this case (see above).

Retrieved shear wave velocity profile (Figure 3.15.5) is reliable down to 100 m, as the scatter increases rapidly below 100 m.

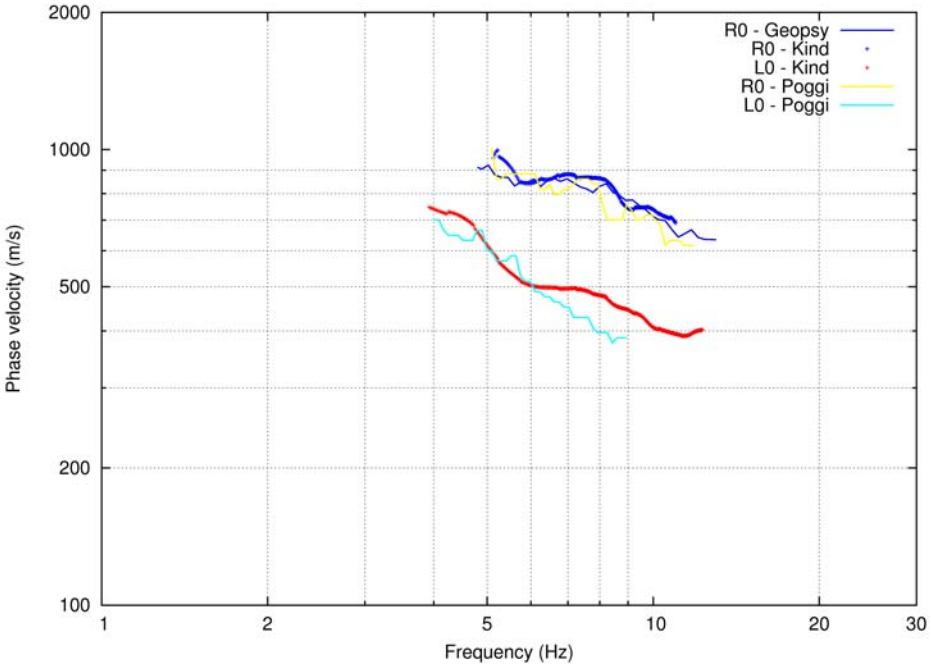

Figure 3.15.2**:** *Dispersion curves for STN2 array: R0 stands for fundamental mode of Rayleigh waves, L0 stands for fundamental mode of Love waves.*

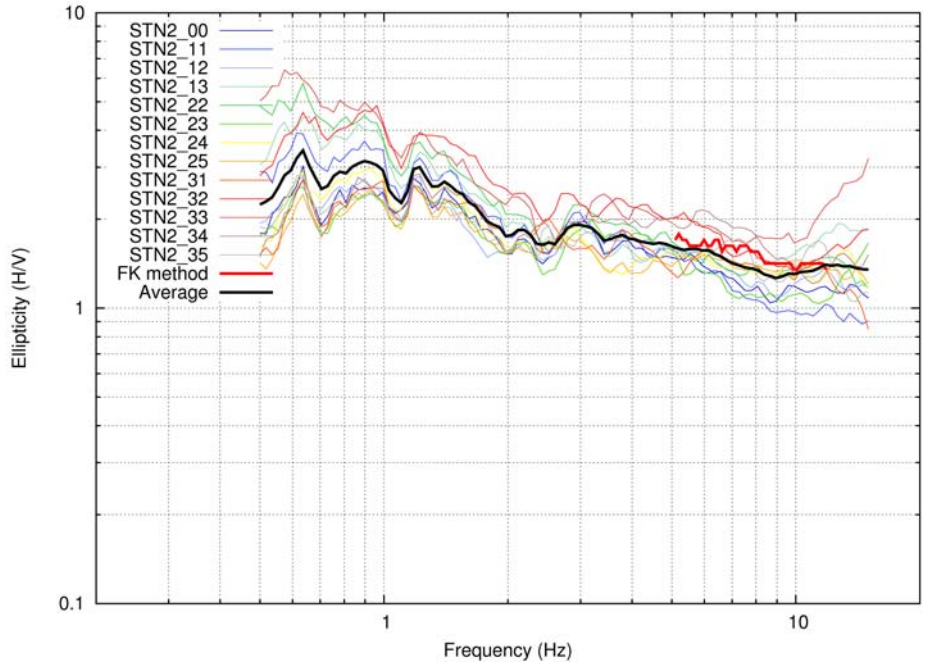

Figure 3.15.3: *Ellipticity curves for STN2 array obtained by wavelet and FK method.*

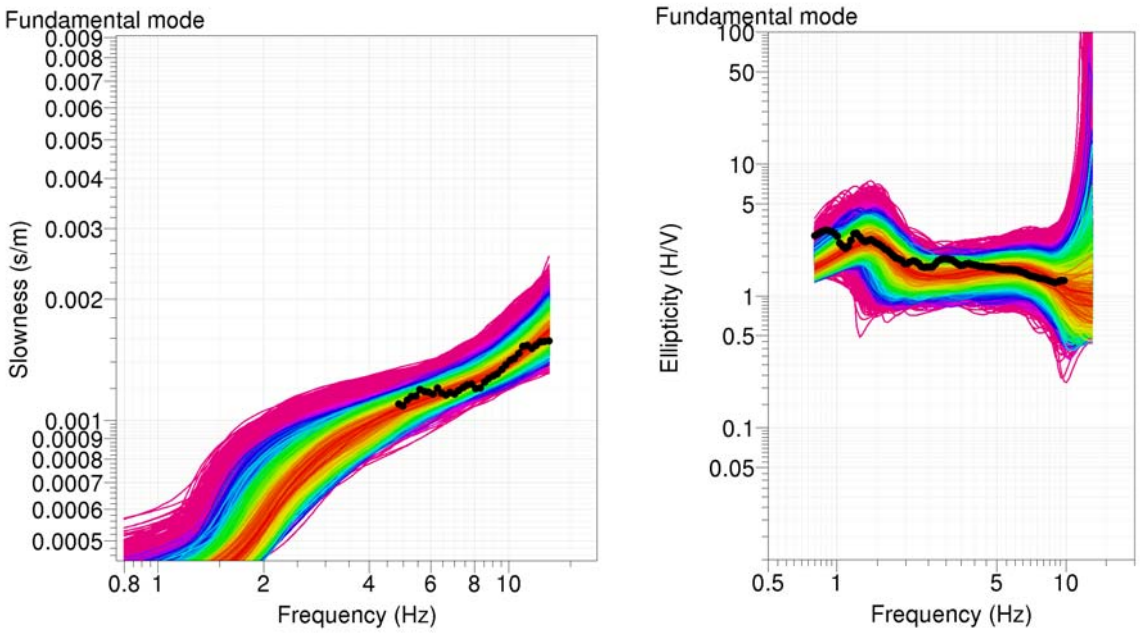

Figure 3.15.4: *An ensemble of dispersion curves (left) and ellipticities (right) of fundamental mode of Rayleigh waves. Observed curves used in the inversion are in black, the color distinguishes the misfit value. Corresponding models are in the Figure 3.15.5.*

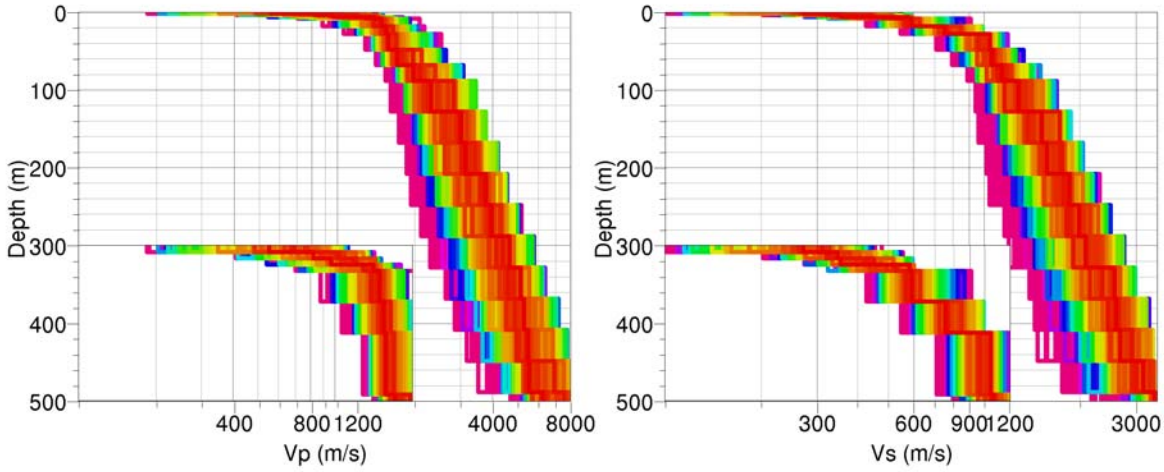

Figure 3.15.5: *An ensemble of inverted velocity profiles. First 50m are enlarged in the inset. Colors distinguish the misfit value in the same way as in the Figures 3.11.4.*

3.16 Site GRA2

GRA2 has a maximal diameter of 110 m and consists of 14 stations, all set up simultaneously. It was located mainly on asphalt, a little bit northward outside Grächen.

Figure 3.16.1: *Sensor setup for array "GRA2" in Grächen.*

Array processing

Recordings were processed by different high-resolution FK methods. It was possible to follow the dispersion curve of fundamental mode of both Rayleigh and Love wave down to 4 Hz with FK method. All picked dispersion curves for both Love and Rayleigh waves are plotted in Figure 3.16.2. The agreement between different codes and methods is not so good as in other cases. Distributions of points picked in wavenumber domain were broad, so the uncertainty of DC is higher in this case. Rayleigh fundamental mode DC obtained with *Geopsy* were more consistent, so these were used further in the inversion.

Ellipticity of Rayleigh waves was estimated using wavelet-based (TFA) method and FK method. All ellipticity curves are depicted in Figure 3.16.3. The mean TFA curve is in good agreement with FK curve in the frequency band 1.2-10 Hz.

Inversion

Models are parametrized by 20 layers of fixed thickness and a density of 2100kg/m^3 was used for the final inversion. It was possible to perform joint inversion of the DC (fundamental mode for Love and fundamental mode for Rayleigh waves) and ellipticity (fundamental Rayleigh mode) with a reasonable result (see Figures: 3.16.4, 3.16.5).

Retrieved shear wave velocity profile (Figure 3.16.6) is reliable down to 120 m, as the scatter increases rapidly below 120 m.

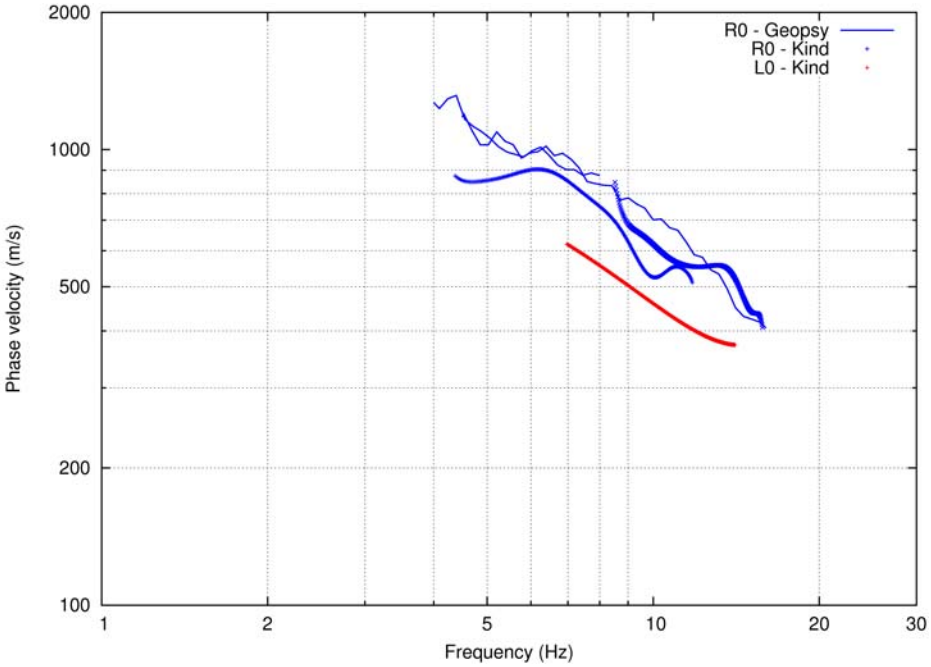

Figure 3.16.2**:** *Dispersion curves for GRA2 array: R0 stands for fundamental mode of Rayleigh waves, L0 stands for fundamental mode of Love waves.*

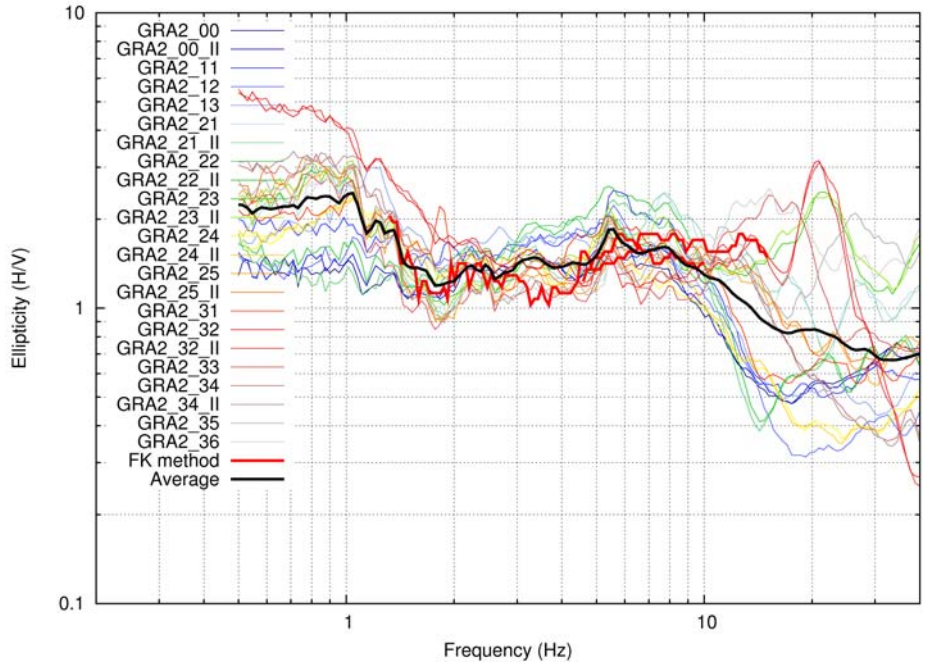

Figure 3.16.3: *Ellipticity curves for GRA2 array obtained by wavelet and FK method.*

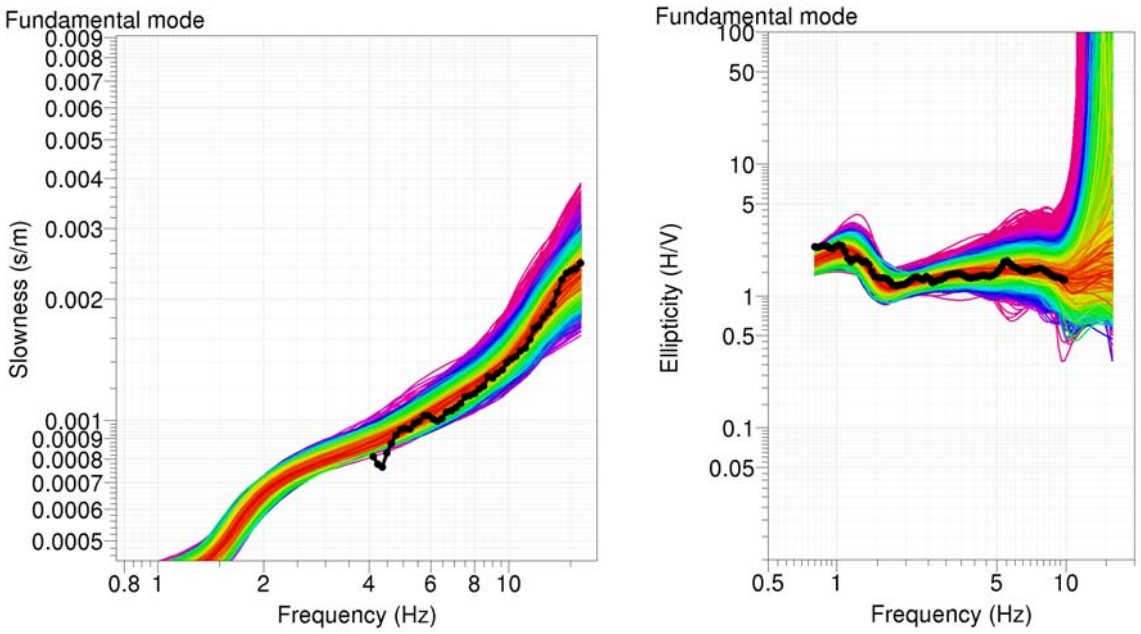

Figure 3.16.4: *An ensemble of dispersion curves (left) and ellipticities (right) of fundamental mode of Rayleigh waves. Observed curves used in the inversion are in black, the color distinguishes the misfit value. Corresponding models are in the Figure 3.16.6.*

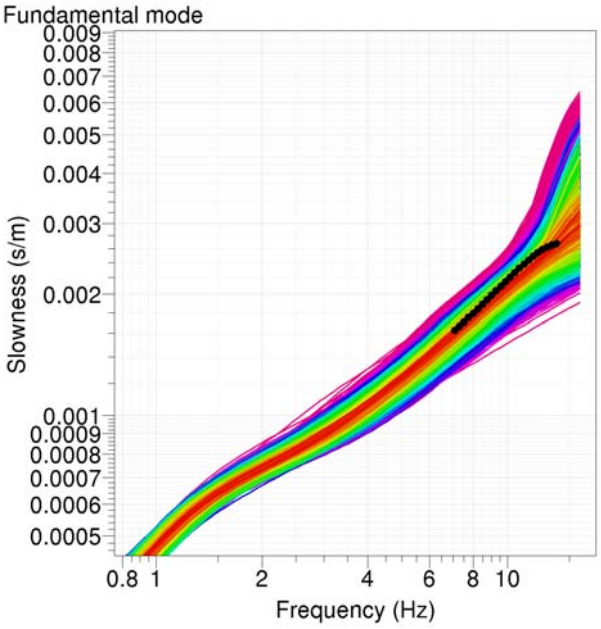

Figure 3.16.5: *An ensemble of dispersion curves of the fundamental mode of Love waves. Observed curves used in the inversion are in black, the color distinguishes the misfit value. Corresponding models are in the Figure 3.16.6.*

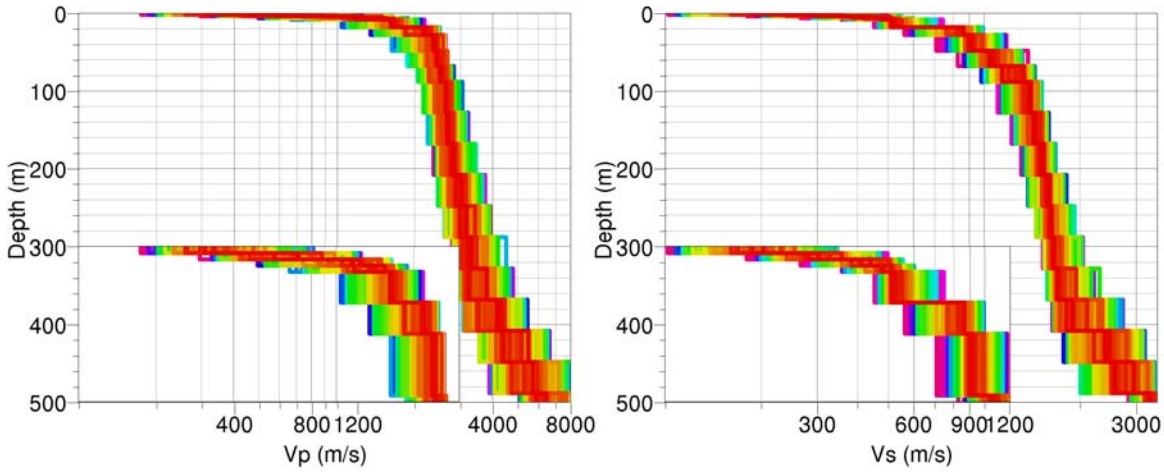

Figure 3.16.6: *An ensemble of inverted velocity profiles. First 50m are enlarged in the inset. Colors distinguish the misfit value in the same way as in the Figures 3.16.4, 3.16.5.*

3.17 Site STNP2

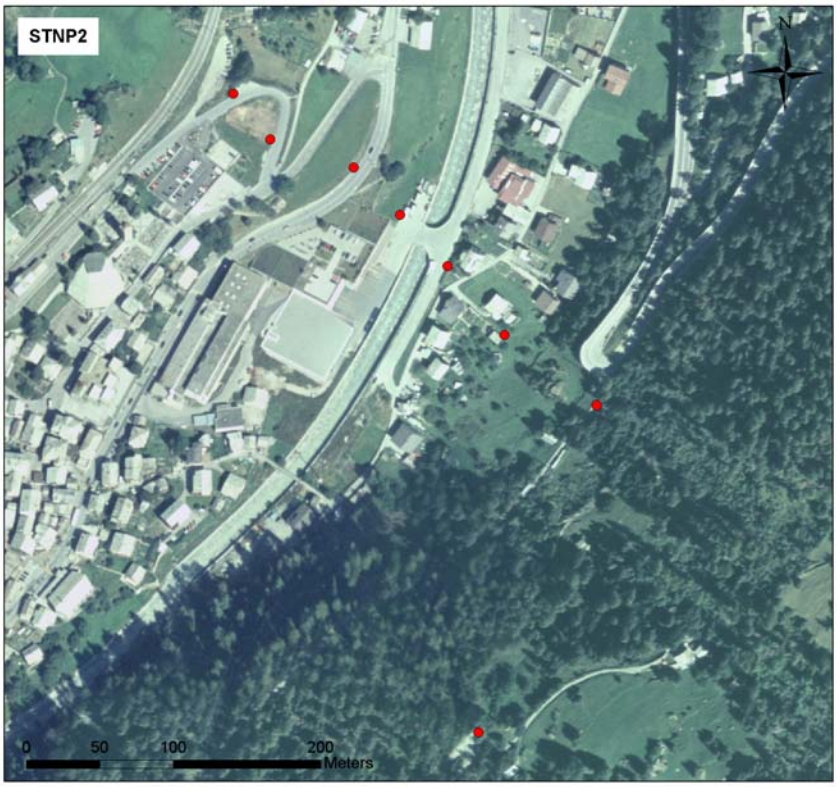

STNP2 is a linear array across the valley in St. Niklaus with a reference-station on rock. It consists of 8 stations, all set up simultaneously.

Figure 3.17.1: *Sensor setup for linear array "STNP2" in St. Niklaus.*

Polarization analysis of ambient noise

This array was setup to detect possible 2D resonance of the sedimentary valley in St. Niklaus as proposed by Fritsche et al. (2005). The reference station method as applied by Roten et al. (2006) and Roten and Fäh (2007) in the Rhone valley between Martigny and Sion was not successful in our case. Therefore a time-frequency polarization analysis of ambient vibrations was performed. The method is described in the paper by Burjanek et al. (2010). The results of the analysis are depicted in Figure 3.17.2. Note the spot localized near frequency of 1.3 Hz and direction 25 degrees from the North. This direction is roughly parallel to the axis of the valley. The polarization is strongest for the station number 3 (from North-West). This may indicate an SH fundamental mode of the 2D resonance. Compared to similar analysis performed in the Martigny area in the Rhone valley (not shown here), the 2D effect in St. Niklaus would be much weaker.

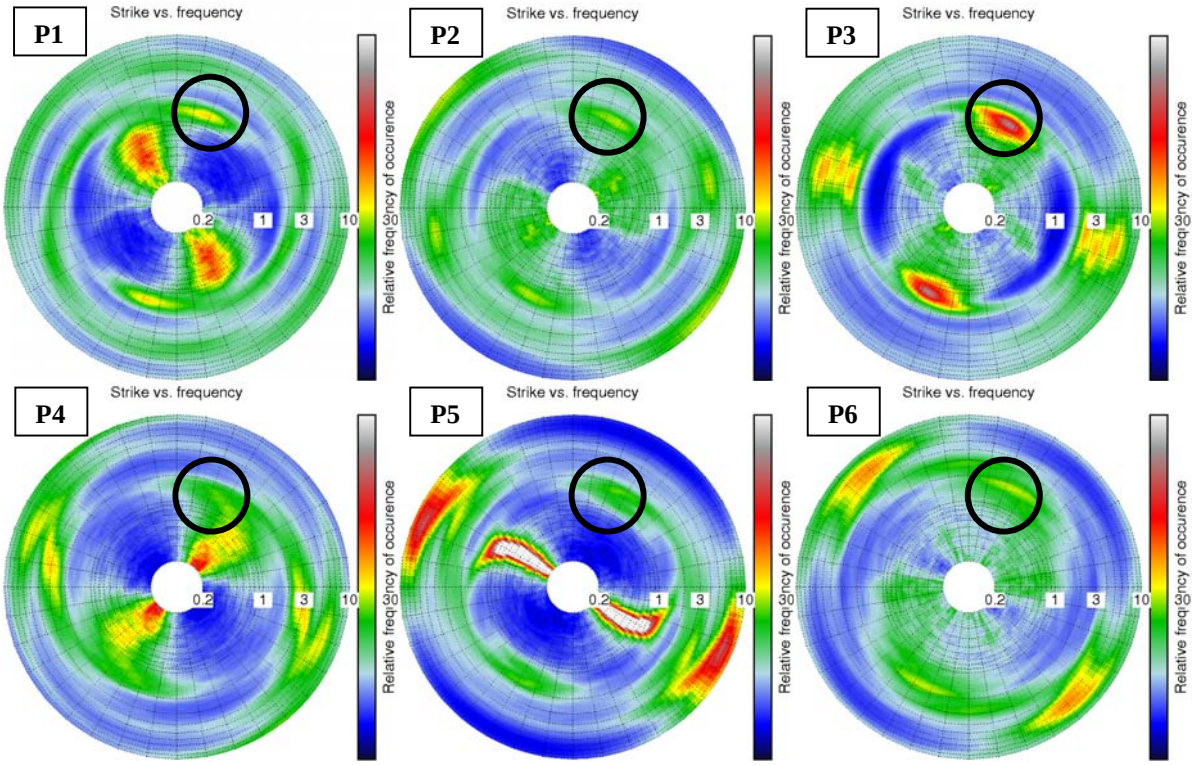

Figure 3.17.2: *Results of polarization analysis for six stations of the profile in the valley (from North-West to South-East). Relative occurrence of azimuth of polarization (in horizontal plane) of the ambient noise wave-field, dependent on frequency (seen on the radius). An area of higher rate of occurrence is denoted by the black circle (the same for all stations).*

4. Discussion and Conclusions

Recordings were processed using different high-resolution FK methods. In most cases it was possible to follow the dispersion curve of fundamental mode of both Rayleigh and Love wave. In some cases it was also possible to pick a higher mode. The agreement between different codes and methods is acceptable to good, depending on the relative amplitude of the mode and the velocity of the surface wave at a given frequency in relation to the array dimension. Regarding the array processing, SPAC method did perform well only in the fields outside Visp. In these cases, both f-k and SPAC methods give consistent results. SPAC did not perform well in St. Niklaus and Grächen areas.
Ellipticity is difficult to interpret. The choice of the frequency range where the ellipticity is considered for the inversion (i.e., where the estimated ellipticity is close to the unknown true ellipticity) is non-unique. In particular, the true ellipticity of Rayleigh waves reaches infinite values at frequency where the particle motion changes from retrograde to prograde. This happens usually for sites with a sharp contrast in the S-wave velocity profile. On the other hand, the true ellipticity may also contain a smooth peak in case of gradual increase of the velocity with depth. Unfortunately, it is not possible to distinguish the two cases, as all methods for estimation of Rayleigh wave ellipticity provide just smoothed curves.
We made a systematic comparison of ellipticities retrieved from f-k and wavelet-based method. Ellipticity obtained from the f-k method is systematically lower with respect to the wavelet method (in the vicinity of fundamental frequency, i.e., for the right flank). We cannot decide which of the two methods provides values closer to the real ones. This represents an important issue to be resolved in the future.
The relative weight of DC and ellipticity during the inversion is non-unique. More weight is put on DC in the inversions presented here. The inversion is driven by DC and the ellipticity is used mainly for rejecting models with incompatible ellipticities (e.g., fundamental peak at different frequency). The ellipticity presents a strong constraint in the inversion. However, the topic needs more research.
Finally we resume the results for the three areas of investigation:

Visp area

The best models for all arrays in Visp area are presented in Figure 4.1. Shear wave velocities reach 150-200 m/s in the uppermost layers. This layer is variable in thickness and velocity throughout the city, and we measured the variability in composition of these surface sediments. A configuration of alternating silty, sandy and gravelly layers can be found in most places in the river plain of the Rhone at Visp. A stronger velocity contrast is present for most of the models at depths of 30 - 50 m. The next discontinuity is found around a depth of 120 m. Deeper parts cannot be reliably resolved.

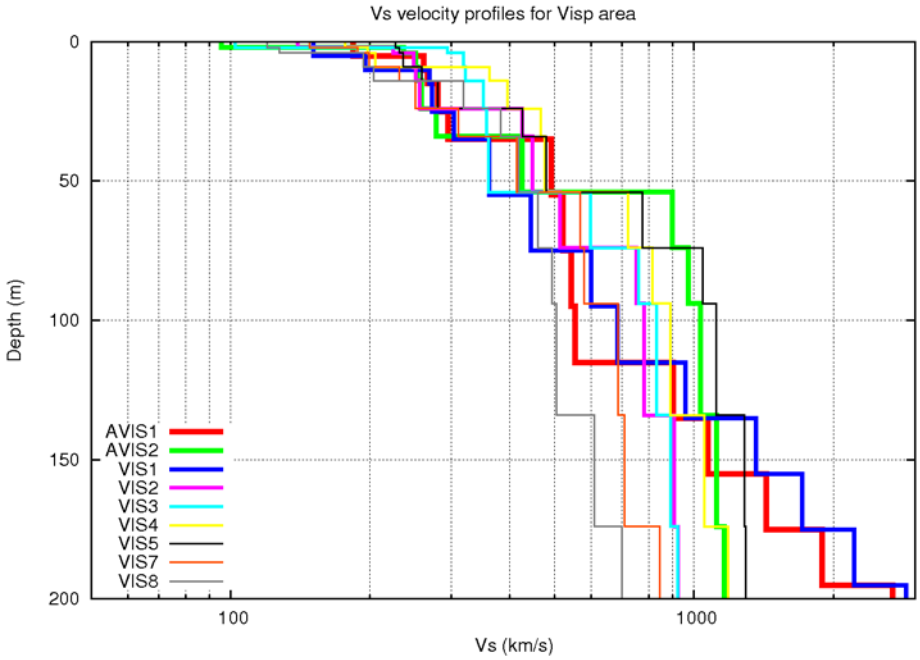

Figure 4.1**:** *Best models for all arrays in Visp area.*

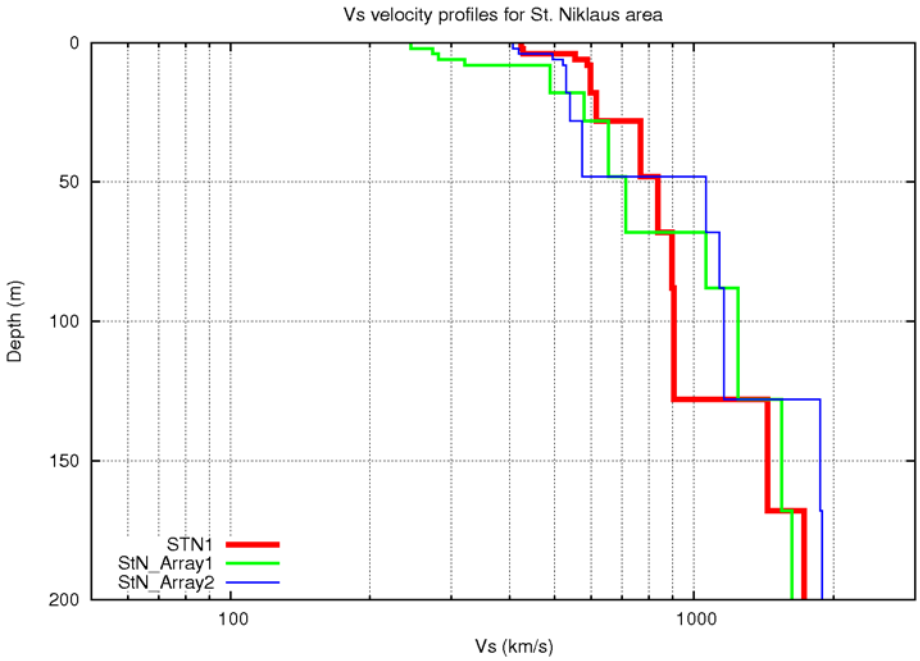

Figure 4.2**:** *Best models for all arrays in St. Niklaus area.*

St. Niklaus area

The best models for all arrays in St. Niklaus area are presented in Figure 4.2. Shear wave velocities reach 250-400 m/s in the uppermost layers. This first layer is rather different at the site StN_Array1, and indicates the presence of a shallow sand or lacustrine layer. A stronger velocity contrast is present at the depths of 40 - 70 m. The next discontinuity is around a depth of 120 m. This discontinuity is probably not real, due to the 2D structure of the U-shaped valley fill. The infill is consisting mainly of alternating layers of gravel, moraine and fluviatil deposits.

A potential 2D SH resonance was identified at frequency of 1.3 Hz. Nevertheless, the phenomenon is quite weak in this case. The results are consistent with the findings by Fritsche et al. (2005). They found at most of the locations in St.Niklaus a clear polarisation in the direction approximately rectangular to the valley axis (from east to southeast). The concerning frequencies are around 1.9 Hz. This part of the wave field was interpreted as the fundamental mode of SV (SV0). On the other hand almost all locations showed a polarisation along the valley axis (north-northeast). The frequencies varied in the range of 1.3 to 1.4 Hz. Accordingly to the direction of the polarisation this part of the wave field was identified as the fundamental mode of SH (SH0). These values of (SV0) ≈ 1.9 Hz and of (SH0) ≈ 1.4 Hz can be explained by theory. Thus the assumption that the Valley of Visp is characterized by a 2-D resonance in the region of St. Niklaus is probably correct.

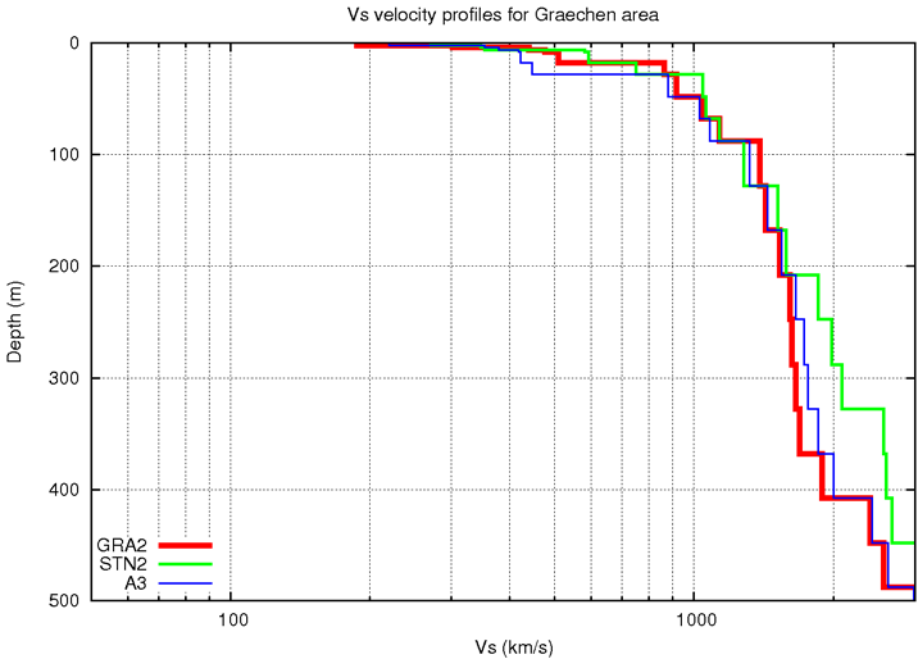

Figure 4.3**:** *Best models for all arrays in Grächen area.*

Grächen area

The best models for all arrays in Grächen area are presented in Figure 4.3. Shear wave velocities reach 200-350 m/s in the uppermost thin layers. A stronger velocity contrast is present at the depth of 20 m. S-wave velocities reach high values in the range 800-1000m/s. All three profiles are consistent. The next discontinuity is around a depth of 300 - 400 m.

5. References

Aki K. (1957). Space and time spectra of stationary stochastic waves, with special reference to microtremors. Bull. Earthq. Res. Inst. 35, 415–456.

Asten, M.W. (2006). On bias and noise in passive seismic data from finite circular array data processed using SPAC methods, Geophysics, 71, 153-162.

Babuska, V., Cara, M. (1991). Seismic Anisotropy in the Earth. Kluwer Academic, Dordrecht, Netherlands.

Bettig, B., Bard, P. Y., Scherbaum, F., Riepl, J., Cotton, F., Cornou, C., and Hatzfeld, D., 2001, Analysis of dense array noise measurements using the modified spatial auto-correlation method (SPAC). Application to the Grenoble area: Bollettino di GeofisicaTeorica d'Applicata, 42, 281–304.

Burjánek, J., Gassner-Stamm, G., Poggi, V., Moore, J. R., and Fäh,D. (2010). Ambient vibration analysis of an unstable mountain slope, Geophys. J. int. 180, 820-828. doi:10.1111/j.1365-246X.2009.04451.x

Capon, J., (1969). High-resolution frequency-wave number spectrum analysis, Proc. IEEE, 57(8), 1408-1418.

Fäh, D., Kind, F. and Giardini, D. (2001). A theoretical investigation of average H/V ratios. Geophys. J. Int., 145, 535-549.

Fäh, D., Kind, F. and Giardini, D., (2003). Inversion of local S-wave velocity structures from average H/V ratios, and their use for the estimation of site-effects, J. Seismol., 7, 449-467.

Fäh, D., Stamm, G. and Havenith, H.-B., (2008). Analysis of three-component ambient vibration array measurements, Geophys. J. Int., 172, 199-213.

Fritsche, S., Fäh, D. and D. Giardini, 2005. Damage Fields and Site-Effects. Investigations on the 1855 Earthquake in Switzerland. Proceedings: 250TH ANNIVERSARY OF THE 1755 LISBON EARTHQUAKE, Lisbon 2005.

Kind, F., Fäh, D. and Giardini, D., (2005). Array measurements of S-wave velocities from ambient vibrations, Geophys. J. Int., 160, 114-126.

Poggi, V. and Fäh,D. (2010). Estimating Rayleigh wave particle motion from three-component array analysis of ambient vibrations, Geophys. J. int. 180, 251-267. doi:10.1111/j.1365-246X.2009.04422.x

Roten, D., Fäh, D., Cornou, C. and Giardini, D. (2006). 2D resonances in Alpine valleys identified from ambient vibration wavefields. Geophys. J. Int., 165, 889-905.

Roten, D. and D. Fäh (2007). A combined inversion of Rayleigh wave dispersion and 2D resonance frequencies. Geophysical J. Int.. 168, 1261–1275.

Wathelet, M. (2008). An improved neighborhood algorithm: parameter conditions and dynamic scaling. Geophysical Research Letters, 35, L09301, doi:10.1029/2008GL033256.

Wathelet M., Jongmans D., Ohrnberger M. (2005). Direct inversion of spatial auto correlation curves with the neighborhood algorithm. Bull. Seismol. Soc. Am. 95,1787–1800.

5. Appendix

AVIS1	Station	X-coord	Y-coord	ring
ring1: 57min	0_C	632796.6	127604.9	1
	0_00	632795.0	127614.8	1
	10_120	632806.2	127602.0	1
	10_240	632789.5	127598.0	1
	25_0	632792.9	127629.6	1
	25_72	632817.2	127618.8	1
	25_144	632815.3	127588.5	1
	25_216	632782.6	127583.7	1
	25_288	632772.4	127611.4	1
AVIS2	**Station**	**X-coord**	**Y-coord**	**ring**
	10_C	633923.4	127855.9	1+2+3
ring1: 67min	10_00	633921.2	127865.8	1
ring2: 49min	10_80	633932	127861.9	1
ring3: 108min	10_160	633930.9	127849.4	1
ring4: 66min	10_240	633919.8	127846.8	1
	10_320	633913.4	127857.6	1
	25_000	633917.7	127880.7	2
	25_080	633943.9	127870.5	2
	25_160	633942.7	127839.5	2
	25_240	633912.8	127833.1	2
	25_320	633898.9	127861.7	2
	70_00	633960.5	127914.1	3
	70_80	634004.8	127836.9	3
	70_160	633930.1	127787.6	3+4
	70_240	633864	127825.9	3
	70_320	633872.8	127894.9	3
	180_60	634110	127771.2	4
	180_120	633991.8	127635.8	4
	180_300	633853.2	127949.1	4
	180_00	634034.3	127923.3	4
	180_240	633751.2	127830.6	4
	180_180	633821.8	127641.4	4
VIS1	**Station**	**X-coord**	**Y-coord**	**ring**
	'0 '	631860.1	128354.4	1+2
ring1: 73min	'11'	631865.6	128362.6	1
ring2: 77min	'12'	631863.6	128344.6	1
	'13'	631850.2	128355	1
	'21'	631866	128378.4	1
	'22'	631886.8	128358.9	1
	'23'	631874.1	128333.6	1
	'24'	631835.3	128355.7	1
	'25'	631846.3	128375	1
	'31'	631867	128406.8	1
	'32'	631920.1	128381.3	1
	'33'	631906.3	128318.3	1
	'34'	631802.1	128369.9	1
	'35'	631827	128404.8	1
	'41'	631862.9	128445.3	2
	'42'	631963.2	128369.7	2
	'43'	631944.3	128301.3	2
	'44'	631796	128240	2
	'45'	631767.1	128386.6	2
	'51'	631853.9	128524.1	2
	'52'	632015.4	128433.1	2
	'53'	632017	128268	2
	'54'	631938	128178	2
	'55'	631699	128270	2
	'56'	631698.4	128416.7	2
VIS2	**Station**	**X-coord**	**Y-coord**	**ring**
	'0 '	632175.5	127582.1	1+2
ring1: 70min	'11'	632180.4	127591	1
ring2: 106min	'12'	632181.9	127573.9	1
	'13'	632165.5	127582.7	1
	'21'	632186.8	127604.4	1

	'22'	632200.4	127581.8	1
	'23'	632175.9	127556.9	1
	'24'	632152.1	127572.9	1
	'25'	632160.3	127602.2	1
	'31'	632167.7	127641.5	1+2
	'32'	632228.9	127609.7	1+2
	'33'	632216.2	127537.8	1+2
	'34'	632144.5	127530.9	1+2
	'35'	632116.5	127594.7	1+2
	'41'	632220.4	127688.8	2
	'42'	632298.6	127554.8	2
	'43'	632190.8	127462.1	2
	'44'	632081.8	127527.1	2
	'45'	632105.6	127663.2	2
VIS3	**Station**	**X-coord**	**Y-coord**	**ring**
	'0 '	633293.4	127436.4	1+2
ring1: 31min	'11'	633293.5	127446.5	1
ring2: 64min	'12'	633303.5	127436.7	1
	'13'	633294.2	127426.5	1
	'14'	633283.3	127435.9	1
	'21'	633294	127461.4	1
	'22'	633318.3	127437.8	1
	'23'	633293.8	127411.5	1
	'24'	633268.3	127434.8	1
	'31'	633294.4	127486.4	2
	'32'	633343.3	127438.5	2
	'33'	633293.4	127386.3	2
	'34'	633243.5	127433.4	2
	'41'	633295.9	127538.2	2
	'42'	633392.4	127440.5	2
	'43'	633298	127336.3	2
	'44'	633195.5	127428.6	2
VIS4	**Station**	**X-coord**	**Y-coord**	**ring**
	'0 '	633899.7	127391.8	1+2
ring1: 61min	'11'	633895.4	127401.1	1
ring2: 72min	'12'	633907.8	127381.5	1
	'13'	633889.5	127387.5	1
	'21'	633887.3	127413.8	1
	'22'	633918.6	127406.2	1
	'23'	633919.7	127381.3	1
	'24'	633898	127366.1	1
	'25'	633872	127383.7	1
	'31'	633866.3	127449.3	1+2
	'32'	633950.4	127414.5	1+2
	'33'	633942.4	127358.7	1+2
	'34'	633896.3	127329.1	1+2
	'35'	633843.4	127377.2	1+2
	'41'	633886.3	127514.5	2
	'42'	634021.8	127411.2	2
	'43'	633992.7	127322.8	2
	'44'	633900.4	127295.4	2
	'45'	633810.2	127364.2	2
	'46'	633818.6	127482.6	2
VIS5	**Station**	**X-coord**	**Y-coord**	**ring**
	'0 '	634270.6	127332.6	1
ring1: 67min	'11'	634281.5	127337.6	1
	'12'	634268.6	127325	1
	'13'	634262.4	127338.5	1
	'21'	634286	127356	1
	'22'	634271.5	127309	1
	'23'	634243.6	127346.8	1
	'31'	634297.5	127375.9	1
	'32'	634253.8	127287.1	1
	'33'	634229.9	127308.8	1
	'34'	634231.8	127355.2	1
	'41'	634318.1	127401.1	1
	'42'	634245.8	127237.3	1
	'43'	634179.5	127379.2	1

VIS6	Station	X-coord	Y-coord	ring
	'0 '	634382	126752.5	1+2
ring1: 44min	'11'	634390	126767.5	1
ring2: 49min	'12'	634393.9	126753.5	1
	'13'	634387.4	126742.1	1
	'14'	634373.3	126749.1	1
	'15'	634374.2	126763	1
	'21'	634370.6	126777.9	1
	'22'	634402.8	126757.9	1
	'23'	634391	126732.3	1
	'24'	634359.8	126745.4	1
	'31'	634365.3	126788.6	1+2
	'32'	634418.4	126775.9	1+2
	'33'	634397.8	126713.4	1+2
	'34'	634344.4	126741.7	1+2
	'41'	634346	126828.4	2
	'42'	634469.4	126788.4	2
	'43'	634415.9	126668.5	2
	'44'	634292.9	126738.7	2
VIS7	**Station**	**X-coord**	**Y-coord**	**ring**
	'0 '	634654.6	126972.6	1
ring1: 43min	'11'	634661.8	126986.7	1
	'12'	634672.5	126968.1	1
	'13'	634659.2	126959.8	1
	'21'	634654.4	127000.4	1
	'22'	634685.1	126961.3	1
	'23'	634670.1	126949.6	1
	'24'	634653.8	126947.1	1
	'31'	634632.9	127026	1
	'32'	634711.6	126992.5	1
	'33'	634693.1	126920.8	1
	'34'	634620.6	126929.5	1
VIS8	**Station**	**X-coord**	**Y-coord**	**ring**
	'0 '	635051.1	126997	1
ring1: 57min	'11'	635051	127002.2	1
	'12'	635055.5	126994.5	1
	'13'	635046.6	126994.5	1
	'21'	635051.1	127012.1	1
	'22'	635064.9	127003.5	1
	'23'	635060.2	126984.8	1
	'24'	635041.2	126985.5	1
	'25'	635036.7	127002.1	1
	'31'	635071.7	127025.6	1
	'32'	635085.5	126989	1
	'33'	635052.2	126961.9	1
	'34'	635021.4	126983.9	1
	'35'	635028.7	127024.1	1
StN_Array1	**Station**	**X-coord**	**Y-coord**	**ring**
	Zentrum	628086.8	113989	1+2+3
ring1: 72min	ring1 S1	628092.5	113998	1
ring2: 68min	ring1 S2	628097.4	113983.1	1
ring3: 23min	ring1 S3	628076.9	113986.3	1
	ring1 S4	628104	114012.6	1
	ring1 S5	628111	113983.3	1
	ring1 S6	628089.8	113964.7	1
	ring1 S7	628062.9	113986.3	1
	ring1 S8	628078.2	114011.2	1
	ring2 S1	628115.2	114018	2
	ring2 S2	628119.5	113968.1	2
	ring2 S3	628050.9	113991.3	2
	ring2 S4	628127.8	114046.2	2
	ring2 S5	628146.5	114001.4	2
	ring2 S6	628112.1	113920.2	2
	ring2 S7	628016.2	113959.6	2
	ring2 S8	628070.2	114056.3	2
	ring3 S1	628072.5	114094.4	3
	ring3 S2	628200	114117.1	3

	ring3 S3	628228.6	114018.3	3
	ring3 S4	628200.5	113938.9	3
	ring3 S5	628097.3	113870.9	3
	ring3 S6	627986.7	113906.5	3
	ring3 S7	627968.5	113962.2	3
	ring3 S8	627996.1	114071.8	3
StN_Array2	**Station**	**X-coord**	**Y-coord**	**ring**
	Zentrum	627797.2	113441.2	1+2
ring1: 29min	ring1 S1	627794.3	113450.6	1
ring2: 89min	ring1 S2	627803.9	113434.1	1
	ring1 S3	627793.6	113432.1	1
	ring1 S4	627781.3	113460.3	1
	ring1 S5	627807.1	113459.5	1
	ring1 S6	627821.9	113449.4	1
	ring1 S7	627809.9	113422.1	1
	ring1 S8	627783.3	113418.3	1
	ring2 S1	627824.6	113486.4	2
	ring2 S2	627810.6	113378.2	2
	ring2 S3	627744.1	113455.1	2
	ring2 S4	627863.3	113558.1	2
	ring2 S5	627886	113457.3	2
	ring2 S6	627833	113329.2	2
	ring2 S7	627704.5	113414.2	2
	ring2 S8	627766.3	113498.4	2
StN_Array3	**Station**	**X-coord**	**Y-coord**	**ring**
	Zentrum	630034.1	115669.4	1+2+3
ring1: 31min	ring1 S1	630024.8	115674.8	1
ring2: 83min	ring1 S2	630043.9	115675.6	1
ring3: 51min	ring1 S3	630038.9	115658.7	1
	ring1 S4	630011.2	115682.7	1
	ring1 S5	630046.4	115690.4	1
	ring1 S6	630058.7	115665.4	1
	ring1 S7	630043.3	115647	1
	ring1 S8	630012.2	115652.8	1
	ring2 S1	630001.6	115702.6	2
	ring2 S2	630077.9	115693.8	2
	ring2 S3	630007.7	115630.1	2
	ring2 S4	629940.3	115711.6	2
	ring2 S5	630056.2	115765.3	2
	ring2 S6	630130.8	115706.4	2
	ring2 S7	630106.5	115603.1	2
	ring2 S8	629982.8	115585.1	2
	ring3 S1	629977.7	115809.4	3
	ring3 S2	630068.2	115812.8	3
	ring3 S3	630190.4	115707.7	3
	ring3 S4	630159.9	115584.8	3
	ring3 S5	630107.6	115536.7	3
	ring3 S6	630003	115533.8	3
	ring3 S7	629892.7	115608.4	3
	ring3 S8	629893.2	115734.3	3
STN1	**Station**	**X-coord**	**Y-coord**	**ring**
	'0 '	628563.1	114508.5	1+2
ring1: 44min	'11'	628565	114515.7	1
ring2: 47min	'12'	628563.4	114502.4	1
	'13'	628555.3	114503.6	1
	'21'	628551.6	114524.5	1
	'22'	628585.1	114522.5	1
	'23'	628562.6	114482	1
	'24'	628544.6	114512.2	1
	'31'	628564.4	114565.3	1
	'32'	628614.6	114531.2	1
	'33'	628621.1	114509.2	1
	'34'	628577.1	114451.9	1
	'35'	628502.7	114485	1
	'36'	628522	114537.3	1
	'41'	628568.9	114605.4	2
	'42'	628629.7	114580.1	2
	'43'	628654.7	114529.5	2

	‘44’	628635.8	114451	2
	'45'	628586.5	114412.8	2
	'46'	628489.3	114476.5	2
	'47'	628487.9	114576.4	2
STN2	**Station**	**X-coord**	**Y-coord**	**ring**
	'0 '	629316	115087.3	1
ring1: 46min	'11'	629324.5	115096	1
	'12'	629318	115077.3	1
	'13'	629307.7	115096.4	1
	'21'	629330.8	115111.9	1
	'22'	629331.6	115080.9	1
	'23'	629323.9	115058.8	1
	'24'	629291.9	115079.1	1
	'25'	629299.7	115103.7	1
	'31'	629311.8	115157.4	1
	'32'	629375.9	115125.1	1
	'33'	629350.7	115027.8	1
	'34'	629279.9	115038.5	1
	'35'	629275	115131.2	1
GRA2	**Station**	**X-coord**	**Y-coord**	**ring**
	'00'	631008.8	116692.4	1+2
ring1: 38min	'11'	631018.6	116703.3	1
ring2: 55min	'12'	631018.1	116688.6	1
	'13'	631002.1	116690	1
	'21'	631004.9	116722.2	1+2
	'22'	631027.3	116712.9	1+2
	'23'	631036	116693.8	1+2
	'24'	631004.7	116672.6	1+2
	'25'	630989.5	116696.1	1+2
	'31'	631044.5	116733.4	2
	'32'	631059.8	116668.7	1+2
	'33'	631005.5	116636.5	2
	'34'	630968.5	116651.3	1+2
	'35'	630956.3	116697.5	2
	'36'	630980.6	116743.4	1+2
STNP2	**Station**	**X-coord**	**Y-coord**	**profile**
	'1'	628214.8	114194.2	1
profile1: 118min	'2'	628240.1	114163	1
	'3'	628296.9	114144	1
	'4'	628328.4	114111.7	1
	'5'	628360.5	114076.6	1
	'6'	628399.3	114029.7	1
	'7'	628462.2	113981.9	1
	'8'	628381.8	113759.4	1